Technische Universität München
TUM School of Medicine and Health

Aorta-on-a-chip: a novel tool to gain molecular insight into vascular diseases

Nora Margaux Hummel

Vollständiger Abdruck der von der TUM School of Medicine and Health der Technischen Universität München zur Erlangung einer

Doktorin der Medizin

genehmigten Dissertation.

Vorsitz: apl. Prof. Dr. Ute Reuning

Prüfer*innen der Dissertation:

1. Prof. Dr. Lars Mägdefessel
2. Priv.-Doz. Dr. Johannes Böhm

Die Dissertation wurde am 27.01.2023 bei der Technischen Universität München eingereicht und durch die Fakultät für Medizin am 13.06.2023 angenommen.

TABLE OF CONTENTS

LIST OF FIGURES

LIST OF TABLES

LIST OF ABBREVIATIONS

Abbreviation	Explanation
AA	aortic aneurysm
AAA	abdominal aortic aneurysm

cDNA	complementary desoxyribonucleic acid
cm2	square centimeters
COL1A1	collagen type I alpha 1 chain
COL1A2	collagen type I alpha 2 chain
COL3A1	collagen type III alpha 1 chain
Ct	crossing threshold
CVD	cardiovascular diseases
CRYAB	alpha-crystallin B chain
DEG	differentially expressed genes
DNA	desoxyribonucleic acid
EC	endothelial cells
ECGS/H	endothelial cell growth supplement
ECM	extracellular matrix
Et al.	et alter (and others)
FC	fold change
GWAS	genome-wide association study
H	hour
HUVEC	human umbilical vein endothelial cells
INHBA	inhibin beta A chain
KEGG	Kyoto Encylopedia of Genes and Genomes
KLF2	kruppel-like factor 2

KLF4	kruppel-like factor 4
LRG1	leucine Rich Alpha-2-Glycoprotein 1
Min	minute
Ml	milliliter
Mm	millimeter
NO	nitric oxide
OoC	organ-on-chip
OR	Odds Ratio
PBS	phosphate buffered saline
PCA	principal component analysis
PCR	polymerase chain reaction
PDMS	polydimethylsiloxane
PECAM	platelet endothelial cell adhesion molecule
rAAA	ruptured abdominal aortic aneurysm
Rpm	revolutions perminute
RNA	ribonucleic acid
RPLPO	large ribosomal protein
SMC	smooth muscle cell
SMTN	smoothelin
TGF-β	transforming growth factor-β
VSMC	vascular smooth muscle cells
VWF	von Willebrand factor

WHO	World Health Organization
°C	degree Celsius
Δ	delta (incremental change in a variable)
µl	microliter

SUMMARY

The group of cardiovascular diseases represent the leading causes of death worldwide (Lozano, Naghavi et al. 2012). The understanding of the complex pathomechanisms can benefit significantly from new technologies in the form of organ-on-chip models. In addition, by combining these in vitro models with new sequencing techniques, relevant genes in pathogenesis can be detected, providing new targets for potential drug development.

The aorta-on-a-chip (AoOC) is a micro-engineered in vitro model which aims to mimic the *in vivo* complexity of a human aorta in terms of cell-cell interaction, tissue architecture and hemodynamic conditions, i.e., the wall shear stress force that the blood exerts on the vessel luminal surface in the direction of blood flow. The device used to generate the AoOC consists of a resealable glass chip with an intermediate semi-permeable membrane dividing the chip into two distinct chambers. This enables the flow of different fluids under varying dynamic conditions through the respective chambers. Primary aortic endothelial cells are cultivated on a thin layer of collagen on the flat-side of the membrane, whereas primary aortic smooth muscle cells are cultured on a fibronectin layer on the well-side of the same membrane. Once cells are confluent, the glass chip is assembled and connected to a microfluidic pressure controller. The chamber containing the ECs is subjected to a high flow rate of 1.2ml/min, equivalent to 10dynes/cm², mimicking the shear stress of the aortic wall. In contrast, the SMCs are exposed to a slow flow rate of 10µl/min, corresponding to 0.0021 dynes/cm², that simulates the physiological diffusion rate between the intima and the media layer (of the aorta), ensuring an adequate supply of nutrients to the cells. In order to confirm specific cell identity, the cells were carefully collected from the membrane, and the gene expression of a panel of genes was measured. In general, the ECs and SMCs growing in our co-culture had a similar expression pattern profile of cells growing in single culture on regular culture flask. To evaluate transcriptomic changes under different flow conditions (static vs 10dyne/cm2) cells were subjected to RNA sequencing analysis. These analyses showed significant up-regulation of KLF 2 and 4, and of CRYAB, by flow exposure, and down-regulation of LRG1. Furthermore, a KEGG pathway enrichment was performed, which showed increased enrichment in pathways involved in processes that control angiogenesis, proliferation, differentiation and vasodilation, validating this model as an *in-vitro* tool of an artery. Furthermore, an interesting aspect of this device will be the observation of SMC functionalities such as contractility.

In subsequent experiments, the model will be used as a drug testing device, with direct application of potential therapeutic drugs to investigate their effect on EC and underlying SMCs.

1. INTRODUCTION

1.1. Epidemiology and pathogenesis of atherosclerosis

1.1.1.1. Epidemiology of Atherosclerosis

Atherosclerosis is the primary cause of the majority of cardiovascular diseases (CVD), such as stroke and myocardial infarction, which are responsible for about 50% of all deaths in the developed countries (Lusis 2000). According to the WHO, approximately 17.9 million people worldwide have died from CVDs in the year 2016, which accounts for 31% of global deaths (WHO 2017). For this reason, the WHO, in cooperation with the U.S. Centers for Disease Control and Prevention, launched a major prevention program for cardiovascular diseases in 2016 aiming to reduce the mortality of CVDs (WHO 2018). Epidemiological studies, which predict an increase in cardiovascular deaths to approximately 23.6 million people per year by 2030, highlight the urgent need for research on atherosclerotic diseases, their potential therapies and the implementation of preventive measures (Song, Fang et al. 2020), (WHO 2020).

1.1.1.2. Disease stages in atherosclerosis

Atherosclerosis is a chronic disease of the medium-sized and large arteries, which leads to a stiffening and narrowing of the arteries as a result of plaques accumulating between the intima and the media layer in the artery wall (Ross 1999). The formation of plaques is developing over time and underlies a complex pathophysiology. This pathomechanism can be divided into three stages, which are pictured in Figure 1 and described in detail in the following chapter. In summary, chronic stress causes damage to the endothelium, resulting in activation of macrophages (Stage I). The macrophages are promoting the foam cell formation and are generating the formation of an atherosclerotic plaque (Stage II). The major complication of atherosclerosis is rupture of the atherosclerotic plaque leading to the formation of a thrombus (Stage III).

1.1.1.3. Pathological mechanism for each stage

The internal layer of the muscular arteries consists of endothelial cells (ECs) which are in direct contact with blood. As mentioned above, the endothelium may develop endothelial dysfunction through exposure to chronic stress, in form of hyperlipidemia, diabetes mellitus, proinflammatory mediators or hypertension (Tabas and Bornfeldt 2016), (Vaziri 2008).

This endothelial dysfunction occurs particularly at predilection sites in the vessels, including branches, curved sections and bifurcations. This is due to the fact that the physiological flow profile is disturbed at these sites. Instead of a physiological pulsatile flow with a well-defined direction, a disturbed flow occurs, which exhibits an oscillating flow profile dominated by turbulence (Zhou 2014). A laminar and pulsatile flow, as it is present in healthy vessels, plays an important role in maintaining a homeostasis with the vessel. Disturbed flow favors endothelial dysfunction. This dysfunction leads to endothelial permeability, enabling inflammatory cells such as monocytes and leucocytes to migrate into the intimal layer (Ross 1993), (Davignon 2004). After their migration the monocytes differentiate into macrophages, which then absorb cholesterol from oxidized low-density lipoprotein (LDL) and transform into so-called foam cells (Glass 2001).

After the initial phase, there is a progression of the lesion, as shown in Figure 1b. As a response to the inflammatory processes, taking place in the intima, the vascular smooth muscle cells (VSMCs) proliferate and migrate from the media to the intima resulting in a reactive thickening of the vascular layers (Tedgui 2006). This leads to an increased production of extracellular matrix (ECM) which then forms a fibrous cap covering the plaque (Libby, Ridker et al. 2011). In advanced lesions, there is increased cell death of macrophages and SMCs induced by apoptosis (Tabas and Bornfeldt 2016), (Falk 2006). Simultaneously, the debris can no longer be effectively phagocytosed by the remaining macrophages, which is referred to as efferocytosis. Thus, the released lipids accumulate and form the so-called lipid or necrotic core. As shown in Fig.1, further rupture of the plaque may result in the contact of prothrombotic material from the bloodstream with the exposed tissue of the plaque. This interaction can lead to the formation of a thrombus. To assess the risk of rupture, the stability of the plaque, rather than its absolute size, is the most important determinant (Sakakura, Nakano et al. 2013). While a thick fibrous cap consisting of SMCs in a proteoglycan-collagen matrix stabilizes the plaque, a high number of metalloproteases released by macrophages, along with an enlarging size of the necrotic core and fewer SMCs, promotes the risk of rupture (Sakakura, Nakano et al. 2013), (Childs, Baker et al. 2016), (Libby, Ridker et al. 2011).

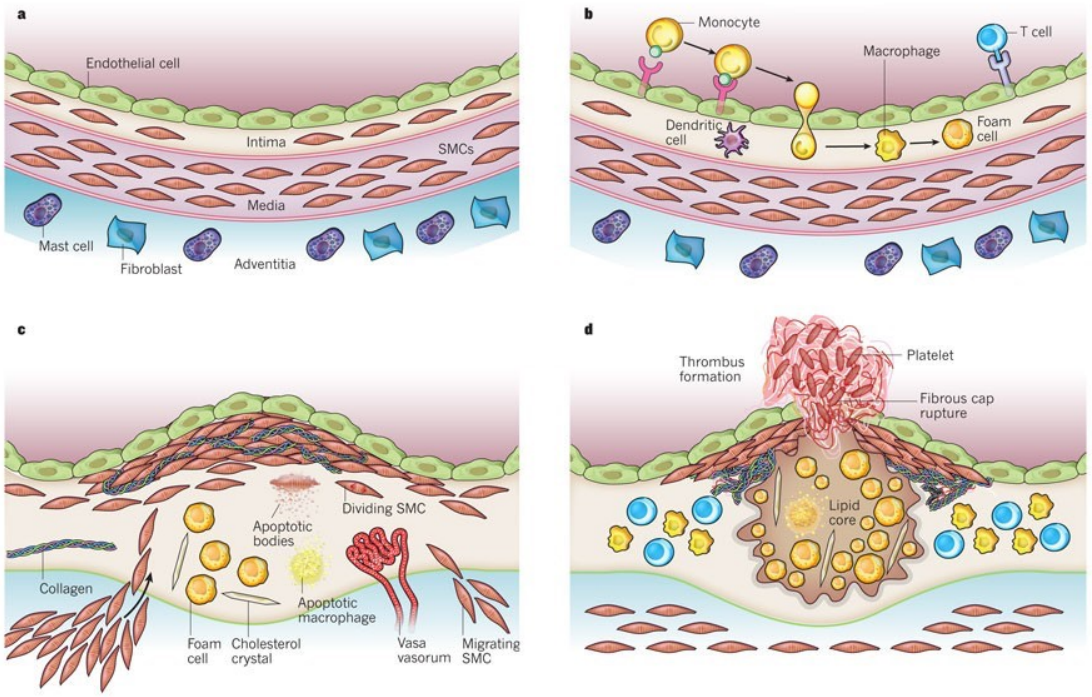

Figure 1. Development of atherosclerotic lesions. Based on (Libby, Ridker et al. 2011) **a** Normal muscular artery with a three-layered wall structure. **b** The initial steps of atherosclerosis include adhesion of blood leukocytes to the activated endothelial monolayer. Leukocytes migrate into the endothelium and differentiate to macrophages. With the uptake of cholesterol, they transform into so-called foam cells. **c** Inflammatory mediators lead to a migration of SMCs, which secrete collagen, glycosaminoglycans and elastin. The cholesterol released from apostolic cells accumulates and forms a lipid core. **d** Rupture of the fibrous cap resulting in the formation of a thrombus.

1.1.1.4. Atherosclerotic-related secondary diseases

Atherosclerosis remains asymptomatic for a relatively long time, however, the chronic growth leads to an increasing stenosis of the arteries resulting in a reduced perfusion and tissue hypoxia (Libby 2002). The most common secondary diseases are coronary heart disease and ischemic stroke caused by superimposed thrombosis that often lead to devastating health consequences and death (Falk 2006). Moreover, depending on the area of the affected artery, distinct clinical manifestations can occur, such as peripheral arterial occlusive disease, aneurysm formation, and renal failure due to stenosis or occlusion of the renal artery (Bennett 2016), (Kasper 2015), (Singh 2003).

1.1.1.5. Life style risk factor and genome-wide association studies on risk predisposition

A variety of risk factors have been identified in relation to atherosclerosis. Among the major risk factors are dyslipidemia, hypertension, smoking, diabetes mellitus, obesity, male gender and genetic predisposition (Rafieian-Kopaei 2014), (Libby 2019). However, the molecular genetic processes that are causative for the development and progression of atherosclerosis remain largely unexplained. To gain a better understanding of this complex pathomechanism, which is also significantly influenced by hereditary components, genome-wide association studies (GWAS) represent a promising approach. Within GWAS, a comprehensive genomic analysis of a great number of individuals is used to identify genetic polymorphisms, which in turn are associated with specific diseases (Insull 2009). Especially for clinically prevalent diseases, such as diseases of the cardiovascular system, this study design offers a powerful tool for the exploration of therapeutic targets (Holdt and Teupser 2013). With the help of GWAS, as of 2013, fifty-eight novel gene loci have been discovered known to increase the risk of developing atherosclerosis-associated disease (Holdt and Teupser 2013). The precise involvement of these genes in the development of atherosclerosis is the subject of further research.

1.1.1.6. Intervention and therapies

Lifestyle modifications play a decisive role in the prevention of atherosclerosis and in the risk reduction of cardiovascular events. Smoking cessation, weight loss, moderate exercise and a balanced diet significantly lower the risk of atherosclerosis (Carson 2019), (Arnett 2019), (Hadi, Carr et al. 2005), (Manson, Greenland et al. 2002). The primary goals of medicationbased prevention are the treatment of hyperlipidemia, hypertension and diabetes mellitus (Piper 2013). Frontline drugs in the treatment of atherosclerosis and associated diseases include statins to lower LDL levels, ß-blockers, ACE inhibitors or sartans, and diuretics to treat hypertension, as well as antidiabetic drugs (Mills, Rachlis et al. 2008). However, lifestyle changes remain the first-line therapeutic approach because they are easy to implement but show a high impact and have no side effects.

1.2. Epidemiology and classification of Aortic aneurysms

After atherosclerosis, aortic aneurysms (AAs) are the second most common disease affecting the aorta (Erbel 2015). In Germany alone, approximately 1200 people succumb annually to the consequences of ruptured aortic aneurysms (Zylka-Menhorn 2018). The prevalence of aortic

aneurysms increases considerably with age (Wanhainen, Verzini et al. 2019). In 2010, the global prevalence per 100,000 individuals is estimated at 7.9 in the age group 40 to 44 years and 2274.8 in the age group 75 to 79 years (Schmitz-Rixen, Debus et al. 2017). Depending on the affected segment of the aorta, one can distinguish between thoracic and abdominal aortic aneurysm. Thoracic AAs, which affect 0.1-0.3% of the global population (annually), are significantly less common than abdominal AAs, which have a prevalence of approximately 3.5 % (Baumann 2013), (Debus 2018). Therefore, I will focus on abdominal aortic aneurysms (AAA) in the following chapter.

1.2.1.1. Definition and risk factors for the rupture of aortic aneurysms

Aortic aneurysms (AA) are pathological dilatations of the aorta caused by pulsatile blood flow, leading to an interaction of degenerative, proteolytic and inflammatory processes (Baumann 2013). Not all dilatations of abdominal aorta are an aneurysm. According to the most common definition, an aneurysm is an enlargement of the diameter to at least 30mm (Erbel 2015). A less frequent definition of AAA is the enlargement of the expected healthy vessel diameter by 1.5 times (Kent 2014).

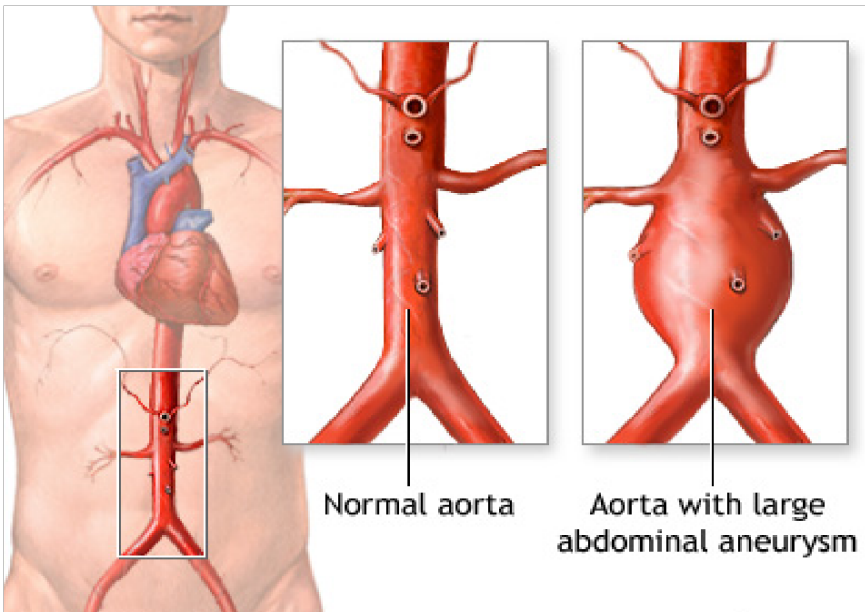

Figure 2. Illustration of an abdominal aortic aneurysm.
Based on (National Institue of Health n.d.)

The major threat of an AAA is its rupture, leading to a life-threatening condition associated with a high lethality rate. More than 40% of patients with cases of ruptured AAA (rAAA), who make it to the hospital in time for treatment, die. Due to additional pre-hospitalization deaths the

estimated total lethality is about 60-80% (Lederle, Johnson et al. 2002). The same study revealed that the diameter has the greatest influence on the likelihood of rupture; the larger the diameter, the higher the risk of rupture. Accordingly, the annual rupture rate for patients with a diameter of AAA < 5 cm is ≥ 1 %. For a diameter of AAA > 6 cm the 1-year rupture risk is already above 10%. Other factors that favor the rupture of AAA are active smoking and being female (Brown and Powell 1999).

1.2.1.2. Risk factors and therapeutic approaches for aneurysms

In fact, smoking is not only a risk factor for rupture, but also for the development of aneurysms (Brady, Thompson et al. 2004). There is a variety of risk factors, in addition to smoking, that may contribute to the development of aortic aneurysms. According to a comprehensive metaanalysis, the strongest association of AAA was found to be with male gender, with males being affected more frequently than females, by a ratio of 6:1 (Cornuz 2004), (Fezoulidis 2019). Further risk factors include atherosclerosis, advanced age, hypertension, family history and ethnicity (Moll 2011), (Vardulaki 2000).

Aortic aneurysms can remain undiagnosed as they often do not cause any symptoms (Sakalihasan, Limet et al. 2005). The rupture of AAAs are mostly followed by classic symptom triad: sudden onset of severe abdominal or back pain, pulsatile abdominal mass and hypotension or acute drop in blood pressure up to shock (Gawenda 2012). In the event of a rupture, emergency surgery is the only way to prevent death. To date, the only treatment option of AAA consists of either an endovascular aneurysm repair (EVAR), or an open-surgery repair. However, according to data from the DGG (Deutsche Gesellschaft für Gefäßchirurgie), the mortality risk is rather high at 5.4% in open surgery and 0.9% in EVAR (Zylka-Menhorn 2018). The only conservative treatments currently available are regular ultrasound screening for surveillance and smoking cessation, which lowers the risk of rupture (Sweeting 2012).

Due to the high prevalence of aortic aneurysms, along with the risk of rupture leading to catastrophic consequences, this disease has been the focus of clinical research for decades. Numerous studies have been conducted using different groups of drugs such as doxycylin, beta blocker, and ACE-Inhibitors with the goal of reducing the growth of small aneurysms (Rughani 2012), (Kiru 2016). Unfortunately, up to now no effect of these drugs has been proven. Overall, the development of novel therapeutic approaches is of great social relevance and will continue to be the medical focus in the future.

1.3. Organ-on-chip Technology

The organ-on-chip (OoC) technology is considered to be a promising technology with great potential to revolutionize drug development and personalized medicine (Klak 2020)It was listed in the top 10 emerging technologies in 2016 (by the World Economic Forum), and has been the focus of scientific research since the early 2000s (Cann 2016).

Organs-on-chips (OoCs) aim at recapitulate the physiological microarchitecture of organs through a combination of cell biology, tissue engineering and microfluidic technology (Mastrangeli 2019), (Wu 2020). OoCs are built on microfluidic chips that are connected to tubing enabling a continuous perfusion with medium, which supplies the cells with nutrients and oxygen and at the same time eliminates cell-waste (Lee 2017), (Mastrangeli 2019). These dynamic cell culturing systems emerged from the necessity of developing a suitable model that mimics human physiology as accurately as possible, since discoveries in animal models often cannot be transferred to human species (Ramadan and Zourob 2020). This necessity is mirrored in the fact that despite increasing investments in the pharmaceutical development and testing of new drugs, the number of successful trials is declining (Pammolli 2011), (Scannell 2012). Initially, drugs undergo preclinical testing on cells and two different animals, before being approved for the clinical trial on patients. Even if novel drugs successfully pass preclinical testing, about 85% of early clinical trials fail; and only half of the drugs passing phase III are eventually approved for clinical application (Mak 2014), (Ledford 2011). This indicates that there is a need for innovative models, providing a more accurate view on physiological processes in the human body and helping to reduce the transitional gap from scientific research into practical clinical application (Mak 2014). The possibility with OoCs is to gain insights into disease physiology, metabolic profiling and drug discovery and testing (Jensen 2020).

1.3.1.1. Set-up of Organ-on-Chip devices

Organ-on-chips form small functional units that reflect structural characteristics and functional complexity of a tissue (Bhatia and Ingber 2014), (Huh, Torisawa et al. 2012). In order to create these functional units, a number of individual components have to be integrated into the chip and the perfusion set-up. Besides the co-cultivation of several cell types, the establishment of a physiological scaffold composed of ECM as well as the exposure of the cells to chemical and mechanical stimuli are essential to reflect the physiological environment (Jackson and Lu 2016). The most important components are summarized in Figure 3.

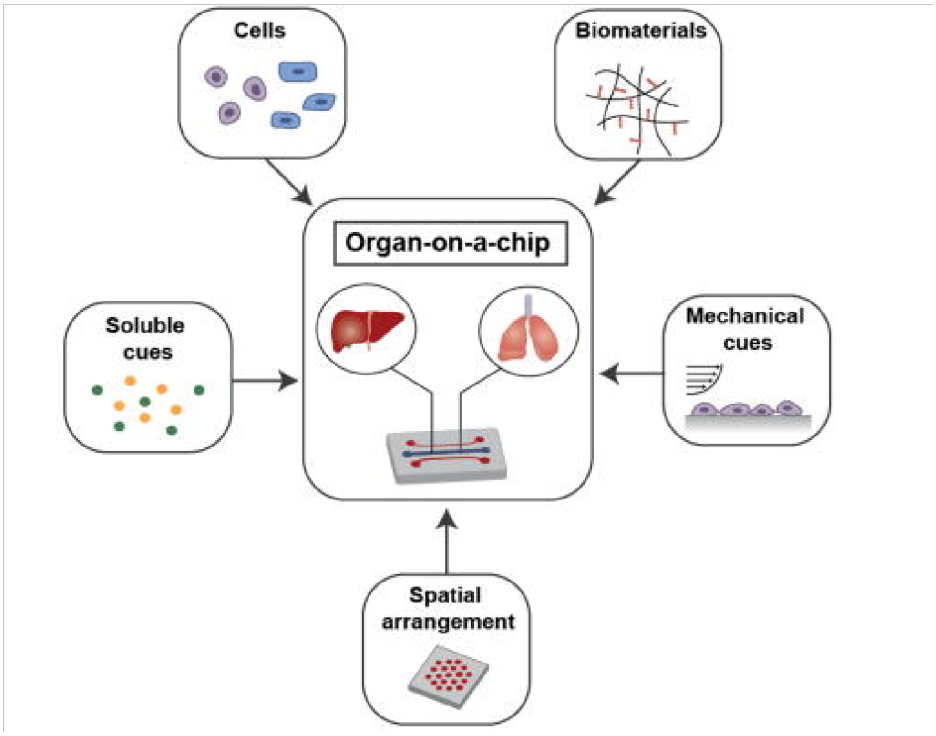

Figure 3. Presentation of the different components to be considered for the implementation of a valid OoC model.

Modified from (Jackson and Lu 2016)

These components include the incorporation of different cell types, the use of different biomaterials such as collagen, and the integration of mechanical stimuli into the model. In addition, the supply of the cells with soluble components, e.g. in the form of medium perfusion, as well as a spatial arrangement, which is crucial for the polarity of the cells and the supply via diffusion, is important to recreate a physiological microenvironment.

A co-culture of two or more cell types can be obtained by separating the chip into different vertical compartments (or chambers) using semi-permeable barriers between the different cell layers. For example, ECs can be grown on the upper side of the porous membrane (apical chamber), while other parenchymal cells are cultured in the bottom (basolateral) chamber (Ramadan and Zourob 2020). The membrane is permeable to nutrients, fluids and oxygen and allows close cell-cell communication despite the physical barrier between the chambers.

By connecting the devices to microfluidic tubes, a continuous perfusion of the chambers and the cells can be provided, mimicking the vascular perfusion. Thereby the cells are exposed to biomechanical forces such as fluid shear stress, compression or tension, while a physiological turnover of influx of nutrients and efflux of waste is guaranteed (Mammoto, Mammoto et al. 2013). Microfluidics enable the application of small amounts of volume in the micro- to picoliter range (10^{-9} to 10^{-18}), making it possible to create an accurate chemical microenvironment (Mastrangeli 2019), (Ravi, Paramesh et al. 2015), (Gravesen, Branebjerg et

al. 1993). The microfluidic technology also enables a laminar volume flow and a low Reynolds number, which also constitutes to a dynamic mechanical set-up as present in the human body (Jackson and Lu 2016), (Perestrelo, Águas et al. 2015). These mechanical forces, through further processing into biochemical signals, have a significant impact on the proliferation, gene expression, adhesion and migration of cells, and are therefore crucial for an organ-specific function (Wang and Li 2010).

Even with the constant development and improvement, it remains a challenge to integrate all physiologically relevant parameters into the model. In particular, the interactions between different organs and tissues are extremely complex and therefore difficult to reproduce (Jackson and Lu 2016) . Holistic chips, so-called body-on-chip models, attempt to address this challenge. Despite these existing limitations, microfluidic platforms enable a highly realistic imitation of the complex human physiology in terms of morphology, differentiation, proliferation, migration, apoptosis, response to stimuli, protein synthesis and drug metabolism (Antoni, Burckel et al. 2015).

1.3.1.2. Material and fabrication of Organ-on-chips

To address all the above mentioned aspects that are relevant for creating a valid model, the microfluidic devices have been designed based on fabrication techniques that were originally developed in the microelectrode industry (Duffy, McDonald et al. 1998). These techniques are capable of creating individual compartments and channels ranging in size from a few micrometers (µm) to a several millimeters (mm), corresponding with the real size of arteries. The use of modern technologies such as 3D printing enable the rapid and relatively simple fabrication of these microfluidic devices (Ho, Ng et al. 2015). Most of the techniques can be summarized as soft lithography, since the materials used are soft materials such as polymers, gels and organic monolayers (Ahmed, Iqbal et al. 2018). Soft lithography replicates the surface structure of a mold (so-called master) by pressing it into a deformable material. The replica of the stamp is solidified by thermal curing, for example by means of applied UV radiation. The mold can then be detached from the replica, leaving the desired fine structure in the latter. The most commonly used material for this purpose is polydimethylsiloxane (PDMS) (Ramadan, Gourikutty et al. 2020). The production of channels for the perfusion is based on the same principle as described above, but the microchannels created by soft lithography are then bonded to a glass slide to form a sealed channel. Subsequently, in and outlet holes can be punched in the channels for connecting them to the perfusion tubing (Paloschi, Sabater-Lleal et al. 2021). To replicate the intima, the channels can then be coated with ECs. For an even more precise

model, SMCs can additionally be integrated into the chip. For the fabrication of the chip, glass is an advantageous alternative to PDMS. On the one hand, glass is optically completely transparent, making it particularly suitable for imaging, and on the other hand, it exhibits higher cell adhesion than PDMS chips (Hirama, Satoh et al. 2019). The main advantage of glass chips over PDMS chips is that glass restricts the absorption of smaller molecules, whereas PDMS can absorb them easily due to its biological structure (Sugiura, Hattori et al. 2010). This feature plays aminor role for the absorption of compounds from the medium but is of major advantage when chips are used for drug testing.

Overall, these advanced manufacturing techniques and materials have enabled the fabrication of several different organs on chips, such as lungs, liver, brain, kidney, heart or skin (Azizipour, Avazpour et al. 2020). The following section reviews the vessel-on-chips technology, in order to introduce the aorta-on-a-chip model.

1.4. Vessel-on-chip models

1.4.1.1. Physiological vessel wall structure

The human arterial blood vessels are responsible for the blood transport and consequently for supplying the cells with nutrients and oxygen. To supply the cells with these substances, the capillaries, which are the terminal part of the arterial system, have relatively thin single-layered walls. The major arterial vessels, such as the aorta, are primarily responsible for the transport of blood and a continuous blood flow. Due to the high volumes of blood transported by these vessels, they require a more robust wall structure. Accordingly, they feature a three-layer wall structure whereby each layer serves a different function.

The innermost layer, lining the vessel lumen, is the intima. Between the outermost layer, the adventitia and the intima, lies the media. The intima is composed of ECs (Sato and Sato 2018). A healthy endothelium controls the vascular tone, suppresses thrombotic processes as well as inflammatory reactions (Juonala, Viikari et al. 2004), (Deanfield, Halcox et al. 2007). The inflammatory reactions are regulated by the adhesion of immune cells. On the other hand, unhealthy endothelium can lead to endothelial dysfunction, which is a major contributing factor for the development of atherosclerosis and is associated with cardiovascular diseases (Endemann and Schiffrin 2004), (Hadi, Carr et al. 2005). The middle layer, the media, is composed of elastic fibers and SMCs, which regulate the lumen diameter and thus the resistance of the blood vessels by contraction or relaxation (Sato and Sato 2018). This allows adjustment

of organ perfusion according to nutrient and oxygen demand. The outermost layer, the adventitia, connects the vessel to the surrounding tissue.

1.4.1.2. Existing vessel-on-chip platforms

The currently existing models attempt to mimic physiological processes within the vascular system as closely as possible and, on the other hand, aim to imitate pathological conditions occurring in the context of vascular disease (Paloschi, Sabater-Lleal et al. 2021). Thereby, organ-on-chip technology allows tight control of mechanical and biomolecular stimuli, which contributes substantially to the comprehension of flow-based effects on cells. Processes such as vasculogenic and angiogenic vessel formation, interaction of the blood cells with the endothelium as well as the influence of mechanical stimuli e.g., by perfusion of the chip can be mimicked and investigated with current models (Young 2013), (Kim, Lee et al. 2013), (Zheng, Chen et al. 2012). These microfluidic devices are particularly useful for mimicking thrombosis, since crucial factors for thrombus formation and platelet aggregation, such as the interaction between blood cells and the endothelium, as well as the impact of blood flow properties on the endothelium, can be integrated into these models. By direct microscopic monitoring of platelet aggregation within the organ-on-chip models, several triggering factors for thrombus formation have previously been detected. Thus, platelet adhesion was shown to occur only at damaged sites in the endothelium or at sites where the endothelium was activated, exposing long vonWillebrand-Factor fibers on the surface of the ECs (Zheng, Chen et al. 2012). Apart from the thrombosis models, further vessel-on-chip devices have been created whose central research goal is a comprehensive understanding of the complex pathophysiology of atherosclerosis. One approach to address this objective are the models of Westein et al. and Tovar-Lopez et al Lopez, in which an engineered atherosclerotic plaque was incorporated into a square micro-channel to simulate the stenotic flow characteristics of a partially occluded artery (Westein, van der Meer et al. 2013), (Tovar-Lopez, Rosengarten et al. 2010). Besides these models, there are other organ-on-chip systems, that allow the analysis of the inflammatory response and the immune cell recruitment.

2. OBJECTIVE / AIM OF THE STUDY

The main objective of the present PhD thesis was to create a more valid in vivo model of a human artery. This model aims to mimic the in vivo complexity of a human aorta in terms of cell-cell interaction, tissue architecture and hemodynamic conditions, i.e., the wall shear stress force exerted by blood on the vessel luminal surface in the direction of blood flow. To achieve

this, a micro-engineered 3D in vitro model of the aorta was designed in the form of an aortaon-chip. In vivo conditions were then created by application of a wall shear stress of 10 dyne/cm2 and co-cultivation of ECs and SMCs within the chip. The implementation of aortaon-chip requires sequential steps:

- obtain a culture device in which cells can grow and be subjected to physiologically relevant shear stresses
- identify optimal plating conditions of ECs and SMCs to achieve confluent monolayers
- integrate the EC and SMC co-culture with a flow-through system and provide a userfriendly interface

In addition to establishing a precise model of the aorta, this study aims to identify transcriptomic changes under different flow conditions (static vs 10 dyne/cm2). Prospectively, the identification of differentially expressed genes (DEGs) provides potential targets for further investigation of flow-triggered signaling pathways, endothelial integrity, and cell-cell communication between the endothelium and SMC.

3. MATERIAL AND METHODS

3.1. Material List

3.1.1.1. Chemicals and Reagents

Table 1. Used chemicals and reagents.

Chemicals and Reagents	**Supplier**	**Charge/ Reference Nr.**
Ethanol 70%-99,8% (v/v)	Carl Roth GmbH + Co KG 76185 Karlsruhe, Germany	Charge: 306247495
QIAzol Lysis Reagent (50ml)	Qiagen Sciences, Maryland 20874, USA	79306 Lot: 56308422
Isopropanol	Klinikum rechts der Isar, Krankenhausapotheke, Munich, Germany	Ch. b. 3-164
Chloroform	Sigma-Aldrich Chemie GmbH, 82024 Taufkirchen, Germany	32211-1L-M

Trypsin-EDTA (0.25%), phenol red	Life Technologies by Thermo Fisher Scientific Inc. Waltham, Massachusetts, USA	Lot: 1945359 Ref: 25200-056 (100ml) 25200-114 (20x100ml)
Lipofectamine™ RNAiMAX Transfection Reagent	Thermo Fisher Scientific Inc. Waltham, Massachusetts, USA	13778150
Fibronectin	Qiagen, 40724 Hilden, Germany	
RNAse free water	Qiagen, 40724 Hilden, Germany	163050321
High Sensitivity RNA Screen Tape	Agilent Technologies Inc., 76337 Waldbronn, Germany	5067-5579
High Sensitivity RNA Screen Tape Ladder	Agilent Technologies Inc., 76337 Waldbronn, Germany	5067-5581
High Sensitivity RNA Screen Tape Sample Buffer	Agilent Technologies Inc., 76337 Waldbronn, Germany	5067-5580
Collagen I, Rat Tail, 100mg	VWR International LLC, Fontenot-Sous-Bois, France	734-1097

3.1.1.2. Cell line

Table 2. Used cell lines.

Cell Type	**Cell application**
Smooth Muscle Cells	Cell culture
Endothelial Cells	Cell culture

3.1.1.3. Instruments and Equipment

Table 3. Used instruments and equipment.

Instruments and Equipment	**Supplier**
Master Cycler Nexus Gradient	Eppendorf AG, 22339 Hamburg, Germany
QuantStudio 3 Real-Time PCR Instrument	Thermo Fisher Scientific Inc. Waltham, Massachusetts, USA
Microscope	Carl Zeiss AG, 73447 Oberkochen, Germany
Incubator	Klaus Binder Labortechnik, 85241 Hebertshausen, Germany
NanoDrop 2000c	Thermo Fisher Scientific Inc. Waltham, Massachusetts, USA

Water Bath	Memmert GmbH + Co.KG, 91126 Schwabach, Germany
Centrifuge big, Multifuge X3R (Heraeus)	Thermo Fisher Scientific Inc. Waltham, Massachusetts, USA
Centrifuge small, Fresco 21 (Heraeus)	Thermo Fisher Scientific Inc. Waltham, Massachusetts, USA
Agilent 2200 TapeStation instrument	Agilent Technologies Inc., 76337 Waldbronn, Germany
MCFS TM – EX: Extended Flow Control	Fluigent Smart Microfluidics, 07743 Jena, Germany
LineUp Flow EZ TM	Fluigent Smart Microfluidics, 07743 Jena, Germany

3.1.1.4. Commercial reagent kits

Table 4. Commercially available kits that were used in this work.

Commercial reagent kits	Charge/ Reference Nr.	Supplier
High Capacity RNA-to-cDNA Kit	4387406	Applied Biosystems by Thermo Fisher Scientific Inc. Waltham, Massachusetts, USA
miRNeasy Kit	217084	Qiagen, 40724 Hilden, Germany
TaqMan™ MicroRNA Reverse Transcription Kit	4366596	Thermo Fisher Scientific Inc. Waltham, Massachusetts, USA

3.1.1.5. Consumables

Table 5. Used consumables.

Consumables	Charge/ Reference Nr.	Supplier
Millex-GP Syringe Filter Unit, 0,22µm	SLGP033RS	Merck KGaA, 64293 Darmstadt, Germany
Falcon tubes (15ml)	Lot: E16093MJ 188271	Greiner Bio-One, 4550 Kremsmünster, Austria
75cm^2 C/N Flask	Lot: 14118011 Ref: 3290	Corning Incorporated Corning, NY 14831, USA
25cm^2 C/N Flask	Lot: 33817016 Ref: 3289	Corning Incorporated Corning, NY 14831, USA
Petri dishes	633181	Greiner Bio-One, 4550 Kremsmünster, Austria

Falcon tubes (50ml)	Ref: 352070	Corning Incorporated Corning, NY 14831, USA
96- well PCR Plate	FG-200250	Nippon Genetics Europe, 52349 Düren, Germany
384-well PCR Plate	FG-300150	Nippon Genetics Europe, 52349 Düren, Germany
Mini Cell Scrapers, Biotium	10018-388	VWR International LLC, Fontenot-Sous-Bois, France
Membrane	14120102	Micronit Micro Technologies B.V., 7521 PV Enschede, Netherland
Fluiwell 4C	-	Fluigent Smart Microfluidics, 07743 Jena, Germany
P-CAP 50ml	-	Fluigent Smart Microfluidics, 07743 Jena, Germany
Red peek tubing (ID 0.127mm)	-	Fluigent Smart Microfluidics, 07743 Jena, Germany
High flow rate tubing (ID 1mm)	-	Fluigent Smart Microfluidics, 07743 Jena, Germany
Outlet tubing (OD 4mm)	-	Fluigent Smart Microfluidics, 07743 Jena, Germany
Inlet tubing (OD: 6mm)	-	Fluigent Smart Microfluidics, 07743 Jena, Germany
Soft tubing (OD: 3mm)	11758705	Thermo Fisher Scientific Inc. Waltham, Massachusetts, USA
Reservoir 50ml	-	Fluigent Smart Microfluidics, 07743 Jena, Germany

3.1.1.6. Primers for qRT-PCR

Table 6. Primers used for PCR in this work.

Primers for qRT-PCR	**Charge/ Reference Nr.**	**Supplier**
FBNI	Hs00171191_m1	Thermo Fisher Scientific Inc. Waltham, Massachusetts, USA
RPLPO	HS00420895_gH	Thermo Fisher Scientific Inc. Waltham, Massachusetts, USA
Col1A1	HS00943809_m1	Thermo Fisher Scientific Inc. Waltham, Massachusetts, USA

Col1A2	HS01028970_M1	Thermo Fisher Scientific Inc. Waltham, Massachusetts, USA
Col3A1	Hs00943809_m1	Thermo Fisher Scientific Inc. Waltham, Massachusetts, USA
KLF 2	Hs00360439_g1	Thermo Fisher Scientific Inc. Waltham, Massachusetts, USA
PECAM1	Hs01065279_m1	Thermo Fisher Scientific Inc. Waltham, Massachusetts, USA
SMTN	Hs01022255_g1	Thermo Fisher Scientific Inc. Waltham, Massachusetts, USA
VWF	HS01109446_M1	Thermo Fisher Scientific Inc. Waltham, Massachusetts, USA

3.1.1.7. Buffers and Solutions

Table 7. Used buffers and solutions.

Buffers and Solutions	**Charge/ Reference Nr.**	**Supplier**
Smooth Muscle Cell Growth Medium	PB-MH-100-2100	PeloBiotech GmbH, 82152 Planegg, Germany
Endothelial Cell Growth Medium	PB-MH-100-2190	PeloBiotech GmbH, 82152 Planegg, Germany
OptiMEM	11058-021	Thermo Fisher Scientific Inc. Waltham, Massachusetts, USA
High Sensitivity RNA Screen Tape Sample Buffer	5067-5580	Agilent Technologies Inc., 76337 Waldbronn, Germany
IO-Biofilm-Remover	Ch-B: 17140217	Ingenieurbüro Oetzel, 34212 Meisungen, Germany

3.1.2. Software

Table 8. Used software.

Software	**Supplier**
NanoDrop 3.1.0.	NanoDrop Technologies, Wilmington, Delaware, USA

Graph PadPrism	GraphPad Software, La Jolla, California, USA
Microsoft Excel	Microsoft Corporation, Redmond, Washington, USA

3.2. Methods

3.2.1.1. Cell Culture

Both human aortic smooth muscle cells and human aortic endothelial cells used are derived from healthy tissue of a transplant donor (and are commercially available). ECs were cultivated using the standardized culture medium Cellovations Endothelial Cell Growth Medium Kit classic (by PELOBiotech) with glutamine, basic fibroblast growth factor (bFGF), hydrocortisone, fetal calf serum (FCS), epidermal growth factor (EGF) and endothelial cell growth supplement (ECGS/H). SMCs were cultivated with Cellovations Smooth Muscle Cell Growth Medium Kit classic, containing basic fibroblast growth factor (bFGF), epidermal growth factor (EGF), Insulin, 5 % fetal calf serum (FCS) and glutamine. The cultivation was performed in 75cm^2 culture flasks under standard conditions at 37°C and 5% CO2 saturation. The cell culture work was carried out under sterile S1 safety level conditions. The cultured cells were transferred to the membranes once a confluence of approximately 70% was reached, as shown in Figure 4. For this purpose, the cells were inspected daily by light microscopy and a medium change was carried out in case of lower confluence.

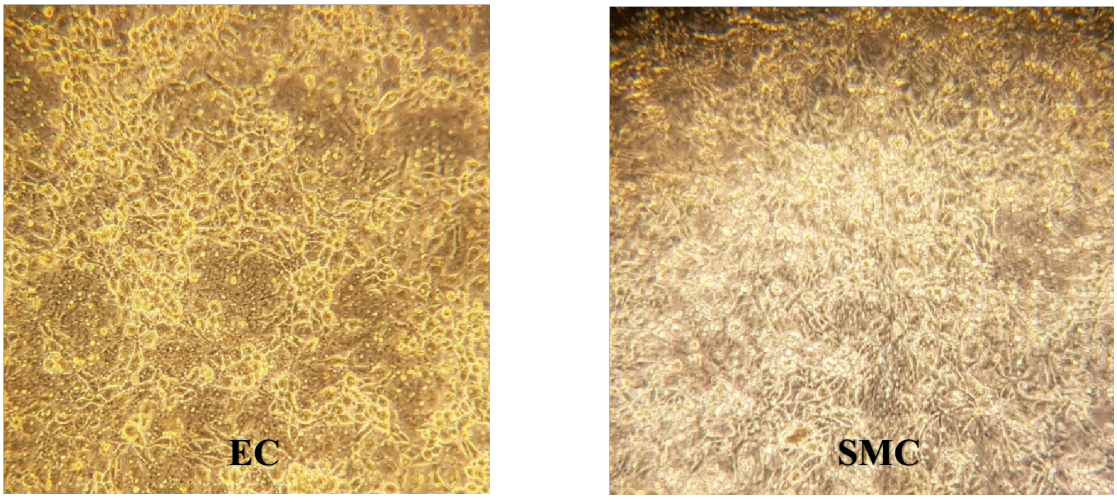

Figure 4. Light microscope image of confluent monolayers of EC (left) and SMC (right) Own illustration

To prepare the cells for the transfer onto the membrane, following steps were conducted, starting with the SMCs:

The culture medium was aspirated, and the cells were washed with 10ml of PBS solution. After aspiration of the PBS, 2ml of Trypsin 0.25% was added to the cells and they were incubated for two minutes. Once the microscopic picture showed that the vast majority of cells were no longer attached to the flask, 5ml of medium was added to terminate the effect of trypsin. After gentle back-and-forth pipetting, the cells were transferred into a 15ml falcon and centrifuged at 500 G for five minutes. The residual medium was aspirated, and 1ml of new medium was added to the remaining cell pellet. After thorough mixing, the cells were counted using the Neubauer counting chamber. Since the experiment consists of two conditions, static and flow, two different membranes were used, plastic for the former and glass for the latter. The size of the membrane used was 1 cm^2.

Prior to placing the cells (100,000 cells/cm^2) on the respective side of the membrane, first the bottom layer (EC side) was coated with 0.1mg/ml collagen rat tail and then the top layer (SMC side) was coated with a 20 µg/ml fibronectin solution (30µl fibronectin were diluted with 1.5ml PBS solution), to ensure cell attachment. For coating, 400µl of this solution were pipetted onto the bottom of a small Petri dish (100mm x 15mm) and the membrane was placed onto the solution. Further, its flat, downward facing side was covered with 200µl coating solution and the membrane was incubated for 2 hours. After aspiration of the collagen solution and subsequent rinsing with water, the ECs were seeded on the membrane's flat side. For the next 24 hours the membranes were kept in the incubator and then the same procedure as described above, except with fibronectin instead of collagen, was carried out on the SMCs in order to place them on the concave side of the membranes. For both SMCs and ECs, the same concentration of cells and the same coating solution were used. The cell-coated membranes were reincubated for the next 24 hours, and then the plastic membrane was enclosed in the chip device. The glass membrane remained in the incubator.

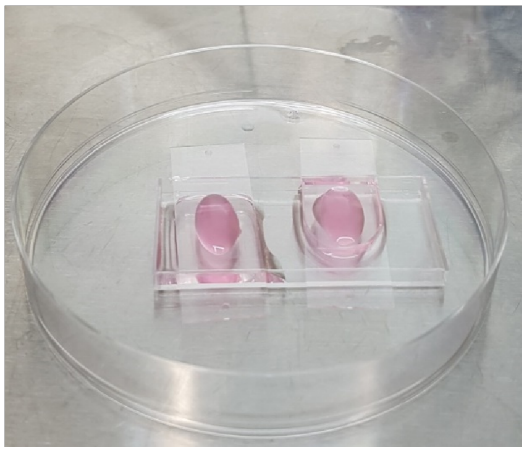

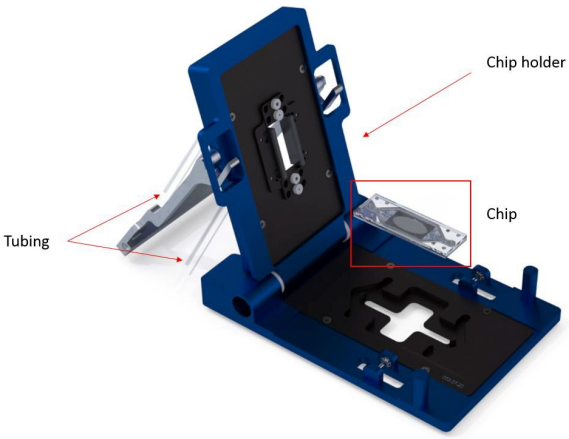

Figure 5. Cell seeding onto membranes and insertion of membranes into chip-holder.

Own illustration

Two aorta-on-chip membranes are shown on the left, demonstrating co-culturing of ECs and SMCs on opposite sides. The right image shows the insertion of the membrane into the chip holder (obtained from Micronit Technologies).

3.2.1.2. Chip Structure

The device used to obtain the aorta-on-chip was developed by Micronit Microtechnologies (Enschede, The Netherlands). It consists of a resealable glass chip with an intermediate porous cell culture membrane, dividing the chip into two different chambers and enabling the flow of different liquids in the chambers. Once the cells are confluent, the flow chamber is assembled and sealed by applying slight pressure with the chip holder. The membrane consists of two layers; a top and a bottom layer. The top layer of the membrane forms a concave surface on which the smooth vascular muscle cells are located. The fluid passing through this chamber flows at a low flow rate. The ECs are placed on the bottom layer of the membrane. In comparison to the top chamber, the liquid in the bottom chamber flows at a considerably higher speed. The low flow rate in the top layer resembles the diffusion between the intima and the media in the aorta wall, whereas the high flow rate in the bottom layer mimics the shear stress in the aortic wall.

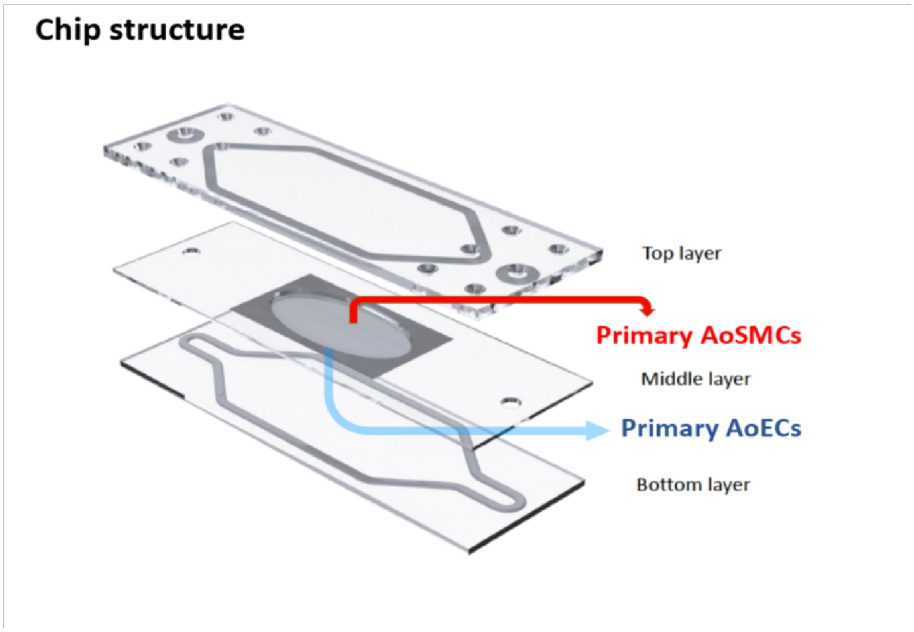

Figure 6. Structure of the chip.

Modified from (Micronit GmbH n.d.)

Primary aortic ECs are placed on the flat side of the porous membrane, which is integrated into the middle layer of the chip. After an incubation period of 24 hours the SMCs should be attached to the membrane. The middle layer can be flipped over in order to place the primary aortic SMCs on the other side of the membrane. Once both cell types are attached to the membrane, two glass layers are placed on both sides of the middle layer. Thus, two chamber systems are installed: one between the middle and the top layer for the SMCs, the other one between the middle and the bottom layers containing the ECs.

3.2.1.3. Flow set -up

The system that was used to provide a physiological microenvironment and a dynamic perfusion condition consists of the Micronit chip and chip holder, a pressure controller (MFCS™-EZ), a flow sensor (Flow Unit), a flow-rate platform (Flow Board) and Reservoirs (Fluiwell), all produced by Fluigent (Villejuif, France). The whole set-up was installed in an incubator, as shown in the Figure 7 below:

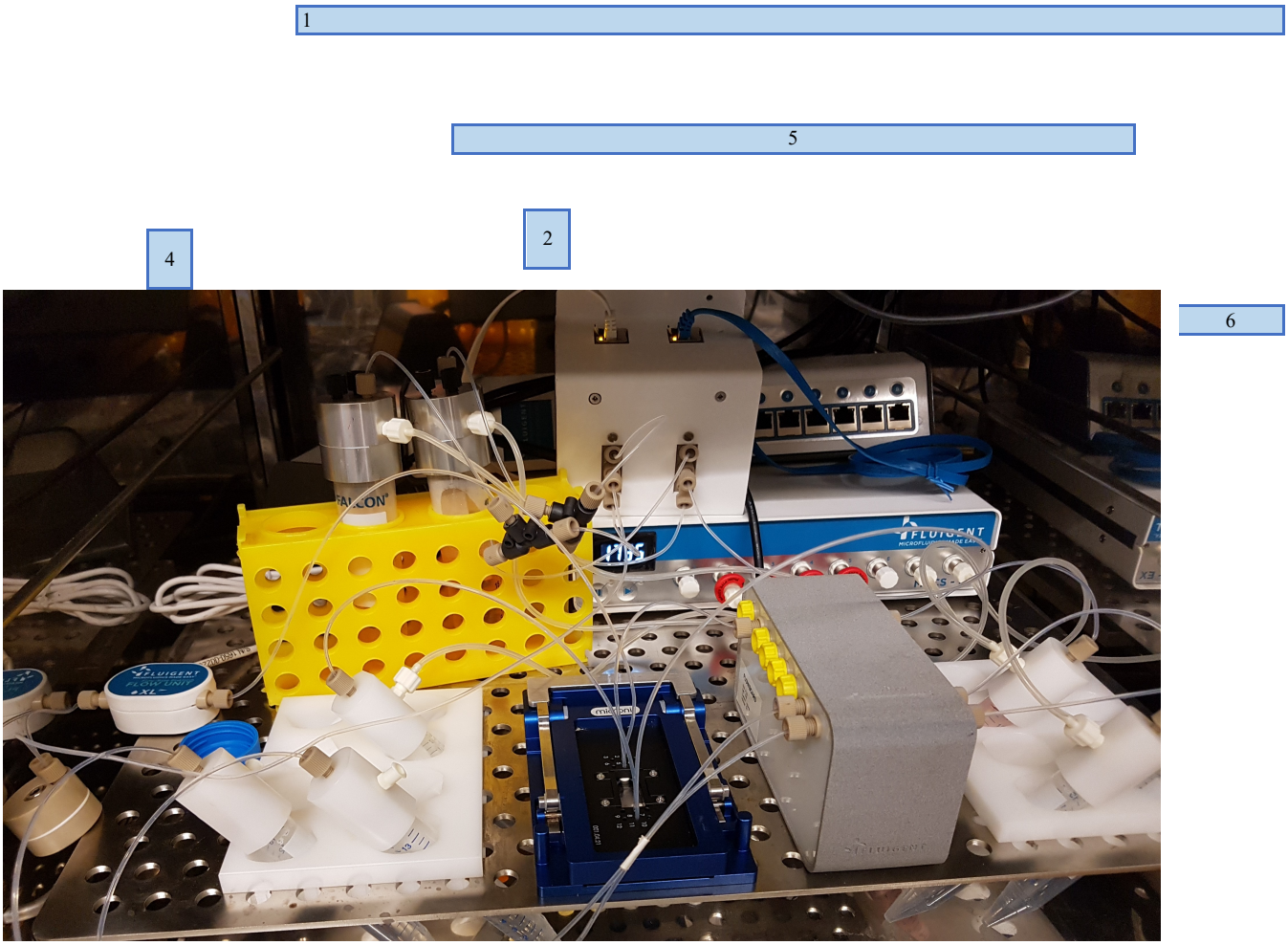

3

Figure 7. Installation of the Aorta-on-chip.

Own illustration

The reservoirs containing the medium (1) are connected to the chip (3) via microfluidic tubing (2). The pressure for the medium circulation is controlled by the MFCS™-EZ (5) and the flow unit sensors (4, 6) ensures that the flow rate is stable and constant in the two channels. Silicone tubing leads from the MFCS™-EZ to the reservoir, which exerts air pressure to allow circulation.

Prior to the chip assembly, all the tubes and reservoirs were rinsed with biofilm remover according to the cleaning protocol provided by Fluigent. The cleaning solution was purified through a filter with the pore size 0.22µm and then transferred into the respective reservoirs (SMC / EC). The system was then cleaned for four minutes with a pressure of 10mbar. Once the solution in the reservoir was used up, the flow unit was disconnected from the output tubing and pressurized again for a few seconds at maximum pressure until air came out of the tubing. The system was flushed with filtered isopropanol at maximum pressure for four minutes and dried afterwards.

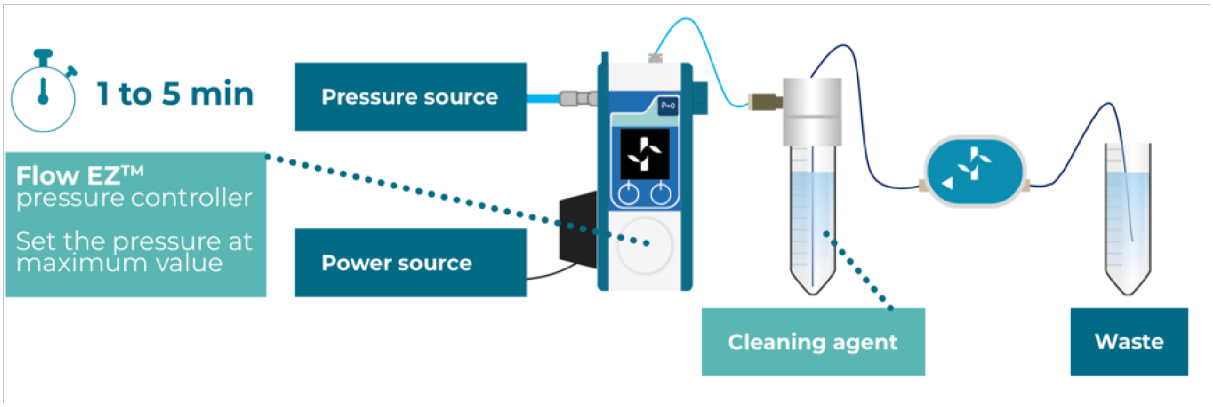

Figure 8. Schematic representation of the cleaning process.

Modified from (Fluigent)

As soon as the cleaning protocol was finished, the two chambers of the chip were connected via fluidic tubing to two different channel systems as shown in figure 9, so that the SMCs and ECs could be exposed to different flow rates. To supply the cells with nutrients and oxygen as well

as to allow the removal of waste, vials containing medium were placed in the incubator and connected to the chip station via the fluidic tubing. The medium-reservoirs are pressurized by the MFCS™-EZ to enable the flow of the fluids through the tubing into the microfluidic setup. For this purpose, soft tubing made of silicone with an OD of 3mm and an ID of 1mm connect the MFCS™-EZ with the reservoirs. The upper chamber, where the SMCs are located, has a low flow rate of 10µl/min corresponding to 0.0021dyne/cm^2. To generate such a low flow rate, a red polyether ether ketone (PEEK) tubing with a very small inner diameter of only 0.127mm (= 0.005") was used. This flow condition allows influx of nutrients and elimination of waste. Due to the low flow velocity, and consequently the small volume of liquid flowing through the upper channel, a unilateral flow from reservoir 1 to reservoir 2 could be ensured for the entire 24h experiment. The lower chamber with the ECs was exposed to a significantly higher flow rate of 1.2ml/min, corresponding to 10dyne/ cm^2, in order to mimic the physiologically relevant shear stress of 8-12dyne/ cm^2. The medium was transferred from the reservoir to the ECs via a fluorinated ethylene-propylene (FEB) tubing with 1.587mm (= 0.063") outer diameter and 1mm (= 0.039") inner diameter. To ensure a unidirectional flow, the L-SWITCH™ valve (Fluigent, Villejuif, France) was integrated in the system. This allowed recirculation of the fluid over several hours to days.

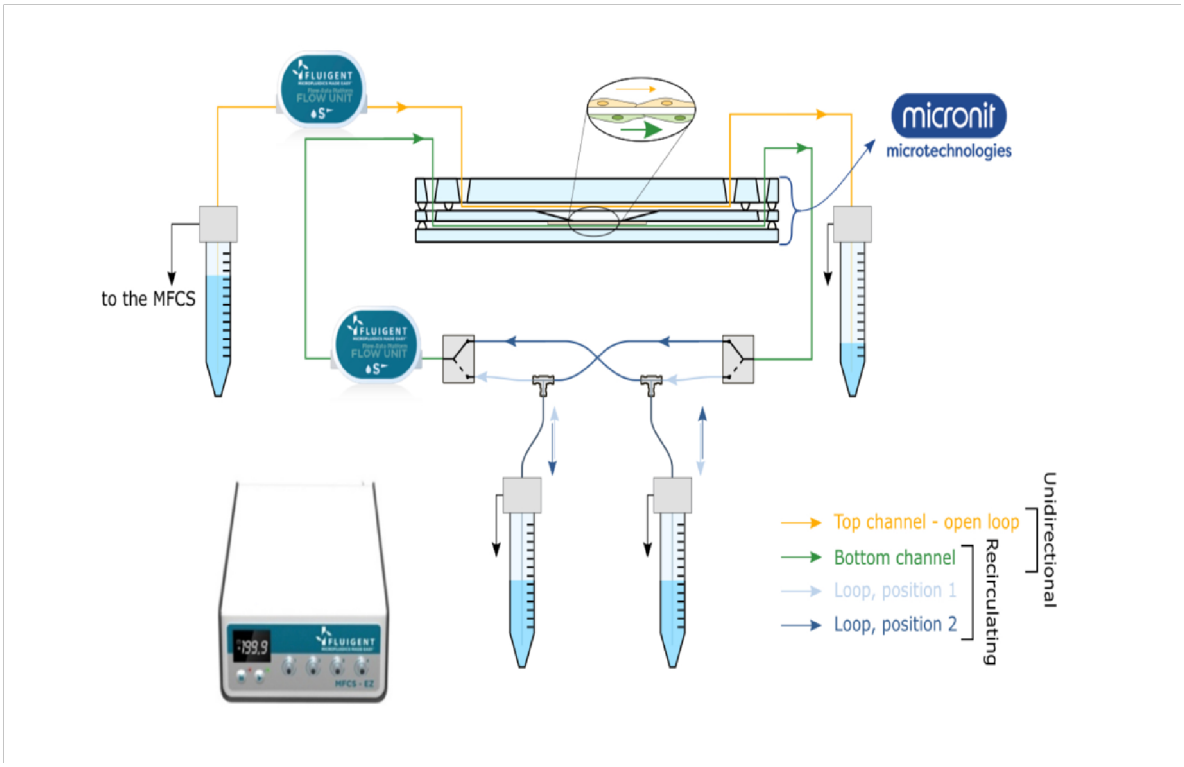

Figure 9. Schematic illustration of the aorta-on-chip set-up showing the chip developed by Micronit connected to the pump system with valves enabling a flow recirculation.

Own illustration

To maintain the desired flow rate at a constant level along the experiment, continuous adjustment of the pressure is essential. Such control is provided by a MFCS-EZ ™, which is capable of detecting alterations in the pressure profile and adjusting the pressure according to the fluctuations present. Cell death and the clogging of the adjacent tubing resulting therefrom can be a potential cause for fluctuations in the usual laminar flow profile (Hoeng, Bovard et al. 2019). Leakages are another potential reason for alterations in pressure and flow rate. In order to constantly monitor and control the flow rate a flow sensor is installed between the reservoir and the chip station. As soon as the chip station is connected to the tubes, the MAESFLO™ software starts a protocol that allows a constant pulsatile flow to be maintained for the next 24 hours. The interconnection between the MAESFLO™ software and the flow sensors was provided by the Flowboard, which was mentioned in the beginning of the chapter.

While the plastic membrane was exposed to flow, the static membrane was placed in the incubator under equal environmental conditions. Once the chip is disassembled, it is possible to isolate the membrane layer from the top and bottom flow chamber and harvest the two different cell types for further analysis of the co-culture. After a short rinsing with PBS, 100µl trypsin 0.25% were pipetted onto the concave side of the membrane. Then, after a two minute exposure time, the SMCs were transferred into an Eppendorf tube and centrifuged at 11.2rpm at 4°C for six minutes followed by pellet resuspension with 200µl of QIAzol. The membrane was flipped in order to harvest the ECs from the bottom layer with directly using 200µl of QIAzol and a scraper to collect as many cells as possible. Both tubes were stored at -80°C. After completion of the experiment, all tubes and the flow sensors were cleaned according to the manufacture's protocol. For that purpose, the chip was removed, and the tubes were connected using adapters. The system was cleaned with an IO- Biofilm remover over a period of approximately 12 hours at a flow rate of 3.5µl/min. Prior to this, the Biofilm Remover was diluted 1:20 with sterile water. Ensuing, a short cleaning was run with sterile water for 10 minutes. at a higher flow rate of around 7µl/min. This was followed by a flushing with isopropanol at a lower flow rate of 3.5µl/min. for five minutes.

3.2.1.4. RNA Isolation

The isolation of the RNA was performed using the Qiagen RNeasymini Kit. For the majority of the samples, RNA isolation was not performed immediately after completion of the chip experiment; instead, the cells were stored in the -80°C freezer (after adding 200µl of QIAzol). Subsequently thawing the sample, 40µl of chloroform were added and the sample was thoroughly mixed for 15 seconds. After a short incubation period at room temperature, the

sample was centrifuged for 15 minutes at ≥ 12,000G at 4°C. The aqueous upper phase was transferred to a new collection tube and, after adding 1.5 times the volume of ethanol, the solution was mixed properly. Up to 700µl of this solution were transferred into a RNeasymini column in a 2-ml collection tube and again centrifuged at ≥ 8000G for 15 seconds. Afterwards the flow-through was discarded. Now 700µl of RWT Buffer were added to the column and centrifuged at ≥ 8000G for 15 seconds. After discarding the flow-through, two further washing steps were performed using 500µl of RPE Buffer. For the first step, the kit was centrifuged for 15 seconds at 8000G and the flow-through was discarded. The second rinse with RPE buffer was centrifuged for two minutes at ≥ 8000G, with the flow-through also discarded afterwards. Next, the RNeasymini column was transferred to a new 1.5ml collection tube. 30–50µl of RNase-free water were pipetted directly onto the RNeasymini column membrane, followed by centrifugation for one minute at ≥ 8000G to elute. After discarding the run, the spin column was placed on a RNase-free microreactor tube to precipitate the RNA. The RNA was processed directly or stored at -20°C until further use.

3.2.1.5. Measurement of RNA-Concentration

The RNA-Concentration and purity of the samples were measured with the Nanodrop 2000c. First, the measuring surfaces of the device had to be carefully cleaned, then the blank value was determined by using RNAse-free water. From the respective samples stored on ice, 1µl sample was taken for each measurement and pipetted onto the measuring surface. Between the measurement of the several samples, the measuring surfaces were cleaned with distilled water to avoid contamination. The principle of concentration measurement is based on the fact that the nucleic acids have an absorption maximum at 260nm wavelength (Desjardins and Conklin 2010). The concentration can then be calculated using a specific factor. To prevent falsifications due to contamination by proteins as well as other organic particles, additional measurements were performed at 230nm, 280nm and 320nm. From the ratio of the absorption at the wavelengths at 260nm and 280nm, it is possible to obtain information about the purity of a nucleic acid sample (Armbrecht and Eppendorf 2013).

3.2.1.6. cDNA Synthesis

By using the enzyme reverse transcriptase, a complementary DNA (cDNA) strand was synthesized from the RNA template. The cDNA Synthesis was performed using the High-capacity RNA-to-cDNA Kit from Applied Biosystems by Thermo Fisher. Due to the instability of RNA, all surfaces were cleaned with RNAse free water, prior to starting the cDNA synthesis. It is crucial to keep the samples on ice during the whole working process. Since a total volume

of 9µl RNA solution is required, the maximal achievable RNA concentration is calculated by measuring each concentration diluted with sterile water to an amount of 9µl, starting from the sample with the lowest RNA concentration. Subsequently, the dilution ratio with sterile distilled water was calculated for all further RNA samples in order to obtain the desired RNA concentration in a total volume of 9µl. Samples with a very low RNA concentration were discarded. After vortexing shortly, the samples were pipetted into micro reaction tubes. 10µl RT Buffer Mix and 1µl RT Enzyme Mix were added to the 9µl RNA of each sample, resulting in a total volume of 20µl. After a short centrifugation the samples were placed in the Thermal Cycler and the following program was selected:

Step 1: 37°C for 60 minutes
Step 2: 95°C for 5 minutes
Step 3: 4°C -
Once the cDNA Synthesis was completed the samples were either stored at the -20 freezer or were directly used for amplification.

3.2.1.7. RNA quantification and gene expression via qRT-PCR

To amplify the cDNA via PCR the TaqMan Fast Master Mix and various TaqMan Assay Primers were utilized. The aim of the PCR was to determine the differences in the expression level of specific EC and SMC marker genes with regards to the two different condition flow and static. The primers used for the gene amplification were SMTN, A1, A2, A1, KLF2, PECAM and VWF (Thermo Fisher). As an internal control the reference gene RPLPO was used. The PCR reaction set-up was prepared according to the manufacturer's protocol (Thermo Fisher). All reagents and the cDNA templates were thawed on ice and thoroughly mixed. Next,
10µl TaqMan Fast Advanced Master Mix, 1µl TaqMan Assay Primer and 7µl Nuclease-Free Water were pipetted into a 96 well plate. After adding 2µl of cDNA template into each well, the plate was sealed and briefly centrifuged. Once the plate has been placed into the Quant Studio PCR Instrument, following steps were conducted:
The initial step was to denature the double-stranded cDNA at 95 degrees for five minutes, followed by a series of cyclical reactions. Each cycle consisted of a denaturation step, followed by a primer and probe annealing step and a polymerization step, where the Taq DNA polymerase synthesizes new strands. Once the Polymerase reached the probe, a fluorescent signal was emitted and detected by the device. Each cycle again generated fluorescent signals proportional to the amount of the created amplicon. The cycle of threshold (CT) value detects the cycle

number at which the fluorescence exceeds the threshold line, (which resembles the background fluorescence), the for the first time (Schefe, Lehmann et al. 2006). The CT value reacts inversely to the quantity of the target sequence. This implies that the more of a particular DNA sequence is present in the investigated sample, the faster the fluorescence threshold is exceeded. Accordingly, a low number of mRNA copies results in a high CT value. For illustrative purposes, the $2^{-\Delta CT}$ value was calculated as it does not relate inversely with expression level like CT value but shows a proportional correlation. For further analysis and calculation, the qPCR results were converted into an Excel file and transferred to a computer. In order to control the variations in loading, extraction, RNA integrity, and RT-efficiency, the qPCR results were normalized to a housekeeping gene (RPLPO), that shows cell non-specific and relatively stable expression (Stahlberg, Aman et al. 2003), (Bustin, Benes et al. 2009).

3.2.1.8. Statistical analysis of the qPCR Data

The evaluation of the qRT-PCR data was performed using Microsoft® Excel 2011. The statistical analysis and the creation of line and bar graphs was performed with the software GraphPad Prism (GraphPad Software, Inc). For each condition (flow vs. static), four independent replicates were performed and the respective mean values were determined for statistical analysis. Outliers were excluded from the statistical analysis. Two-sided t-tests were used to test statistical significance, whereas values of $p < 0.05$ were considered statistically significant.

3.2.1.9. Determination of the RNA integrity number

In order to estimate the integrity of the RNA samples an electrophoresis was performed, using the Agilent 2200 TapeStation. The reagents were held at room temperature for 30 minutes and then thoroughly mixed. In the meantime, the RNA samples were thawn on ice. Next, the High Sensitivity RNA (ScreenTape) Ladder was diluted with 10µl RNase-free water and then 2µl of this solution were mixed with 1µl High Sensitivity RNA Sample Buffer. In the following step, 1µl of the buffer was mixed with 2µl RNA sample. The vials containing the RNA and buffer mixture were spun down and vortexed at 2000rpm for one minute. The next step consisted of sample denaturation by exposing the sample to 72°C for three minutes. Subsequently the samples were placed on ice for two minutes, before being loaded into the 2200 TapeStation. Once the program is completed a number between 1 and 10 defines the quality of each sample. A number of 10 stands for a non-degraded, intact and non-fragmented RNA of very high quality,

whereas 1 stands for completely degraded and fragmented RNA of lowest quality (Schroeder, Mueller et al. 2006).

3.2.1.10. RNA-Sequencing

ECs and SMCs were exposed to different conditions (flow vs. static) leading to changes in the gene expression profile. These transcriptomic changes can be detected by Next Generation Sequencing (NGS), which is a technology that enables the sequencing of a complete genome in shortest time. In order to do this, we selected a total of 16 samples from 8 membranes (there are two cell types on each membrane) for next generation sequencing. The samples were split into following groups:

- Four EC samples cultured under static conditions
- Four EC samples cultured under flow conditions
- Four SMC samples cultured under static conditions
- Four SMC samples cultured under flow conditions

For the sequencing, the choice of membrane was based upon the RNA amount, the expression of lineage genes and the RNA Quality. The RNAseq Data was generated using the IonTorrent Chef System. The sequencing method consists of three general steps, starting with the library preparation, followed by an DNA amplification and subsequent sequencing.
In the first step libraries are created by random fragmentation of the genomic strand, followed by ligation with specialized adapters to both ends of the fragment (atdbio n.d.). The DNA amplification is a mandatory procedure required to ensure that the fragment is detectable. In our case the DNA was amplified using Emulsion-PCR. Therefore, the fragmented and ligated DNA was denatured and then mixed with multiple beads. Each bead contained thousands of copies of an oligonucleotides with a complementary sequence to one of the adapters, as shown in figure 9. The beads were then incorporated into an emulsion, consisting of a single DNA fragment, primer and PCR reagents (Xu, Aragon et al. 2010). This droplet provided a micro reaction space for the clonal amplification of a DNA fragment (Van Dijk, Auger et al. 2014), (Kanagal-Shamanna 2016). Once the PCR was completed, the bead was covered with thousands of identical copies of this specific DNA fragment (Merriman, D Team et al. 2012), (Diehl, Li et al. 2006).

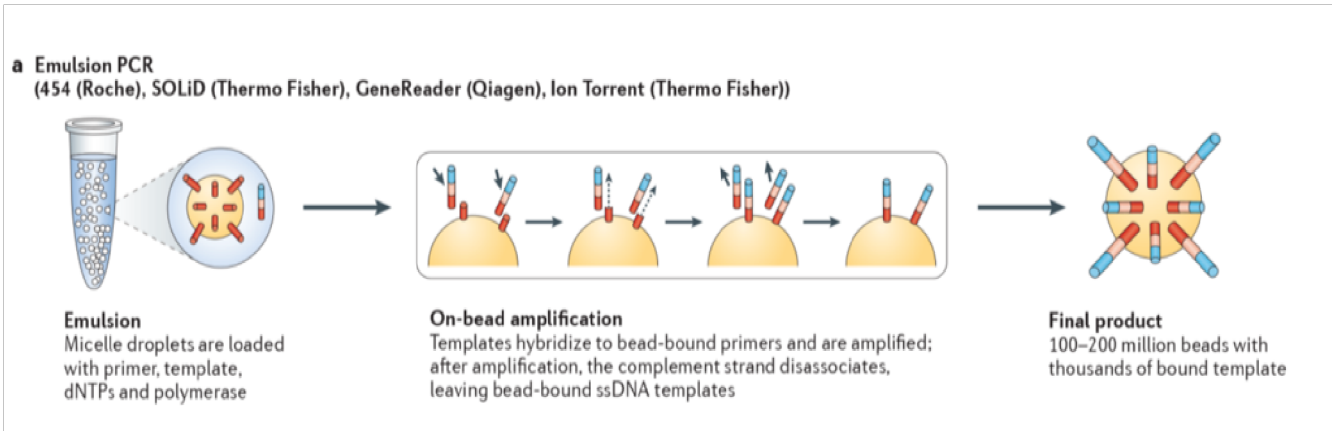

Figure 10. Schematic procedure of an emulsion PCR.
Modified from (Goodwin, McPherson et al. 2016).

For the last step the with DNA covered beads are deposited into micro reaction chambers (one bead into one chamber) of a complementary metal-oxide semiconductor (CMOS) chip. Unlike many other sequencing techniques, Ion Torrent is not based on optical methods. Instead, the incorporation of nucleotides on the growing DNA strand causes the release of an H+ ion, leading to a slight pH value shift (Rothberg, Hinz et al. 2011). This shift is detected and converted into a digital signal by a sensor layer underneath the chambers (ibid). The four different dNTPs are added to the reaction chamber one after the other. Once a nucleotide is incorporated, the pH value in the chamber changes and a digital signal is generated (Merriman, D Team et al. 2012). This, with the help of software calculations, enables the identification of the DNA sequence.

The first step of our sequencing experiment, prior to the library preparation, was the dilution and transcription of the RNA samples into cDNA. The following steps were performed according to the Thermo Fisher protocol. Initially, the RNA samples were diluted with nuclease free water to maintain a RNA concentration of 0.833 ng/µl in a volume of 12µl (when using Super Script IV VILO Master Mix or Con. 0.95 ng/µl in a volume of 10.5µl when using super script VILO cDNA Synthesis Kit). Next, 3µl of SuperScript IV VILO Master Mix were pipetted into the wells A1 to H1 on a 96 well PCR plate. 12µl of each RNA sample were added to these 3µl, so that in the end each well contains a total volume of 15µl. Every well in Column 4 contained a dried down barcode. Finally, after sealing and brief centrifugation, the PCR plate was placed in the thermal cycler and the following program was run:

Step 1: 25°C for 10 minutes

Step 2: 50°C for 10 minutes

Step 3: 85°C for 5 minutes

Step 4: 10°C

Subsequently to the cDNA synthesis the library and template preparation was performed. Therefore, after short vortexing and centrifugation, two primer tubes were inserted into the marked positions of the AmpliSeqTM Chef. Furthermore, the Solutions DL8 cartridge was placed into the Solutions station, the reagents DL8 cartridge into the reagents station and the Tip Cartridge L8 into the Pipette Tip Station. The 96 well PCR plate with the previously synthesized cDNA was placed in the thermal cycler sample block. Finally, the Enrichment Cartridge was placed in the Enrichment Station.

Once everything was installed in the Ion Chef System, the settings for the run were selected as follows: the number of primers chosen was 1, the number of target amplification cycles was set to 13 and the anneal and extension time selected was 16 minutes. Eventually the library preparation run started. After completion of the library preparation, the Ion Chef™ was unloaded and the two chips for the sequencing step were placed in the chip clamp. Finally, the automated run based on the technology described above was started. The generated sequencing data was saved and transferred to a USB stick.

3.2.1.11. Bioinformatic and Statistical analysis of the RNA-sequencing data

The bioinformatical and statistical analysis of the RNA-sequencing Data was performed by the company Fios Genomics. The quality of the raw expression data was evaluated using several automated outlier tests, namely the sum of Euclidean distance to other samples, KolmogorovSmirnov (test statistic), (mean Pearson) correlation and Hoeffding's D. Further the quality was checked manually inspecting the density plot, PCA plots and correlation heatmap. A total of 16 samples were checked for quality issues, of which one sample was identified as an outlier based on two or more of the four quality metrics used. Normalization was carried out using trimmed mean of M-values normalization and expression values were transformed using voom. Principal component analysis (PCA) was performed on the normalized dataset to determine which of the study factors were significantly associated with variation. PCA is used to structure or simplify large data sets by reducing the total number of measured variables via grouping into a few principal components. The principal components are constructed one after the other in descending importance. This means that the first principal component is constructed to be responsible for most of the variation within the data set. Variables for ‘Cell type’, ‘Intronic’ and ‘Treatment Group’ were significantly associated with the first principal component, accounting for over 50% of the variation within the data. The factors that were taken into account were “Exposure” (flow vs. static for each cell type) and “Chip”. Quality control and

exploratory data analysis were subsequently performed using this moralized dataset subsetted by ‘Cell type’ as shown in Figure 11.

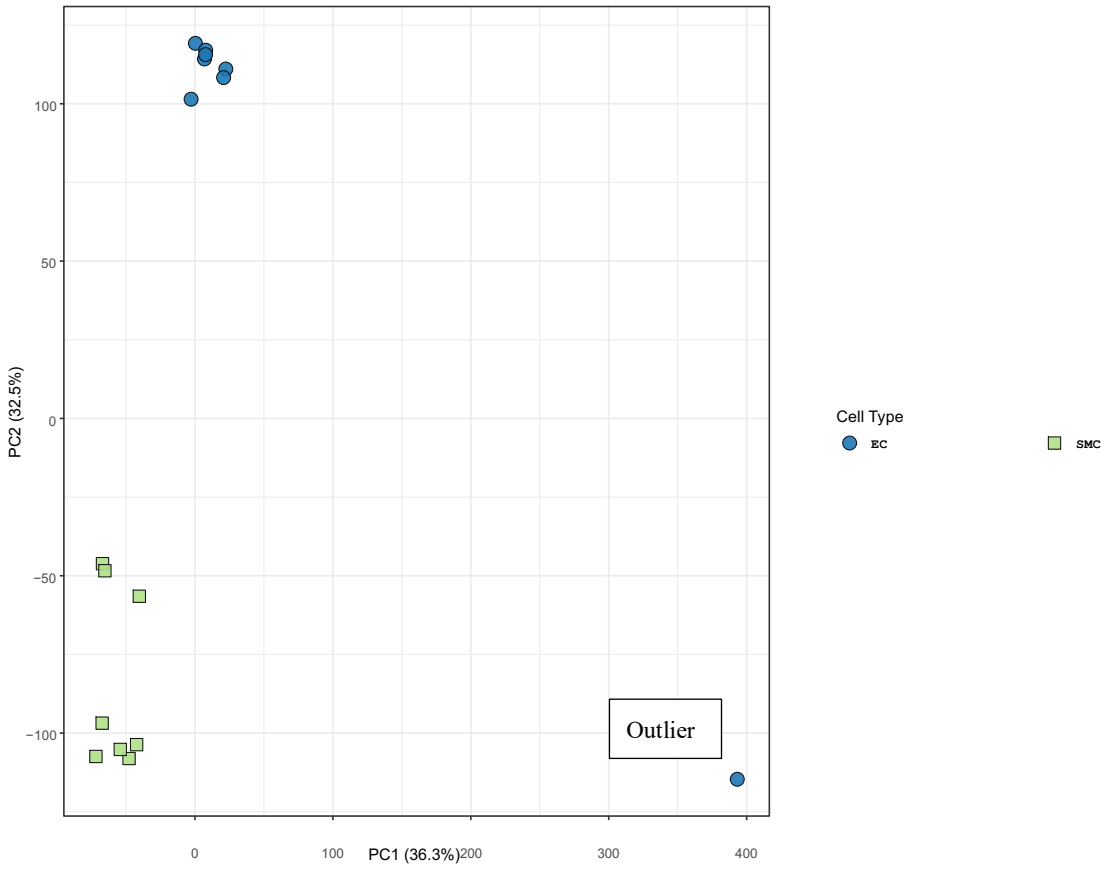

Figure 11. PCA scatterplot for the first two principal components from the raw data set. Modified from (Fios Genomics)

Shown are all samples for EC and SMC separated by the first principal component. Abbreviations: PCA1 = First principal component; PCA2 = Second principal component.

The scatterplot shows clustering for the different cell types. As expected, the main part of the total dispersion lies between the two clusters, while the respective internal dispersion is minor. Within the EC group one sample did not pass the quality control and is therefore marked as an outlier. This was carried out to identify study factors that were significantly associated with variation within a cell type. The entire normalized dataset was subsequently batch effect corrected for technical variables using the ComBat method (QC section). To determine differentially expressed genes (DEGs) between the groups, the following statistical contrasts were performed using the batch corrected normalized datasets:

- ECs (Flow vs. Static)
- SMCs (Flow vs. Static)

DEGs were identified using a statistical threshold of $P < 0.01$ with fold change ≥ 2.

A functional enrichment analysis was performed using the DEGs identified in the association tests (at the $P < 0.01$, fold change ≥ 2 threshold). In order to control the false positive rate in significant results an adjusted p-value was calculated using the Benjamini-Hochberg method. For these analyses, DEGs were assigned to pathway information from the KEGG (Kyoto Encyclopedia of Genes and Genomes) database. This is a database that stores information on biochemical reactions and signaling pathways, as well as enzymes and substrates that are involved in them. This information is largely generated by discoveries from scientific literature or whole genome sequencing. Manually generated pathway maps can summarize thousands of genes into a few hundred signaling pathways (Du, Li et al. 2016). Significant enrichment within specific KEGG pathways was assessed by evaluating whether the number (S) of significantly differentially expressed genes within a pathway was more than expected by chance, given the total number (N) of genes. A hypergeometric test was used to determine the p-value (P), followed by correction for tests across multiple pathways using the Benjamini-Hochberg procedure to obtain an adjusted p-value (P (adj.)). The Odds ratio (OR) was calculated as the number of significant genes observed versus expected. The KEGG Pathways are shown in the result part.

4. RESULTS

4.1. Co-Cultivation under static and flow condition

In order to make sure that during the cell harvest at the end point of the experiment there was no contamination between the two cell types we used a panel of genes that are typically expressed from either EC or SMC.

4.1.1.1. Selected marker genes for endothelial cells and smooth muscle cells

Von Willebrand factor (vWF), a large glycoprotein, that circulates in human plasma, is exclusively produced by ECs and megakaryocytes and therefore widely used as a marker gene for ECs (Zanetta, Marcus et al. 2000), (Mannucci 1998). VWF has two main functions: It forms a complex with coagulation factor VIII and protects the latter from proteolysis (Federici 2003). In addition, it contributes significantly to platelet aggregation by functioning as a 'bridge' between platelets and the injured vessel wall (Meyer, Pietu et al. 1991), (Luxembourg 2007). As a further EC marker gene, the transcription factor Kruppel-like factors (KLFs), was used. KLFs are a subclass of the zinc finger family and are involved in the regulation of cell differentiation and development (Bieker 2001). The subtype KLF2 is, with referring to the vascular system, exclusively expressed in ECs (Kuo, Veselits et al. 1997). It plays a decisive role in maintaining an antithrombotic endothelial surface by inhibiting both the cytokineinduced release of adhesion molecules and the adhesion of immune cells (Lin 2005). It was discovered that exposure to laminar shear stress induces overexpression of KLF2 and KLF4 in ECs (Dekker, van Soest et al. 2002), (White, Hayes et al. 2011).

Due to its high expression in ECs, platelet endothelial cell adhesion molecule-1 (PECAM) qualified as an endothelial marker gene for the experiments. PECAM-1 is a member of the immunoglobulin (Ig) superfamily and is expressed on the surface on the majority of cell types within the vascular compartment (Newman 1997), (DeLisser, Newman et al. 1994). The molecule is involved in a variety of signaling pathways. These pathways include angiogenesis, platelet function, thrombosis, the regulation of leukocyte migration and the control of integrity and permeability of the adherent junction (Ilan and Madri 2003), (Woodfin, Voisin et al. 2007).

We have selected the human large ribosomal protein (RPLPO) as reference gene, as it has proven to be highly stable and reliable in terms of its expression profile (Stern-Straeter, Bonaterra et al. 2009).

As a marker gene for SMCs, smoothelin was used, because it is exclusively expressed in differentiated contractile SMCs (NCBI n.d.). Studies have shown that smoothelin, which

encodes a structural protein, plays a crucial role in the contractility level of SMCs (van Eys, Niessen et al. 2007). Accordingly, in diseases of the vascular tissue, such as atherosclerosis or restenosis, a significant decrease in expression of smoothelin was observed (Tharp, Wamhoff et al. 2006), (Verhamme, Quarck et al. 2002). It is therefore assumed that this gene constitutes part of the contractile apparatus and the cytoskeleton (van Eys, Niessen et al. 2007).

In a preliminary series of experiments, in our laboratory, it was found that the three collagen genes; COL1A1, COL1A2, COL3A1, are expressed considerably higher in SMCs than in ECs, hence we selected these genes as SMC specific markers. Collagen type I is one of the most abundant of the collagen fibrils and consists of two a1 (I) chains and one a2 (I) chain, encoded by COL1A1 and COL1A2 genes, forming a characteristic triple helix structure (Karsenty and de Crombrugghe 1991). The protein provides structure to tissues and organs of the body, thus contributing to strength and stability (Ponticos, Partridge et al. 2004). Furthermore, collagen I is an important component in homeostasis and wound healing - as well as growth and morphogenesis (Pan 2013). It is found in all three layers of the vessel wall and particularly around the SMCs of the media, providing the required mechanical strength and contractility (Ponticos, Partridge et al. 2004). Collagen alpha-1 (III) also contributes an essential component to the ECM and is particularly present in more extensible connective tissue, such as skin, uterus and large blood vessels (Kuivaniemi and Tromp 2019), (Miller and Gay 1987).

4.1.1. Marker gene expression profile under flow condition

The gene expression levels under flow condition that were measured to confirm specific cell identity are summed up in figure 10a. As seen from the plot, the genes we selected as SMC marker genes, namely COL1A1, COL1A2, COL3A1 are expressed at high levels by SMCs, whereas they are barely present in ECs. This was detected for both conditions, flow and static. Inversely, VWF and PECAM, are specifically expressed in ECs and are only present at very low levels in SMCs (Figure 10a). Significant changes in gene expression between cell types were found in PECAM ($p = 0.000239$), in VWF ($p = 0.000001$), COL1A1 ($p = 0.000020$), COL1A2 ($p = 0.000001$) and COL3A1 ($p = 0.000453$). SMTN and KLF2 display a similar expression profile is EC and SMC and therefore do not serve as discriminating genes for our purpose.

These results demonstrate that under flow condition and in co-cultivation the respective cell types show a cell-specific gene expression.

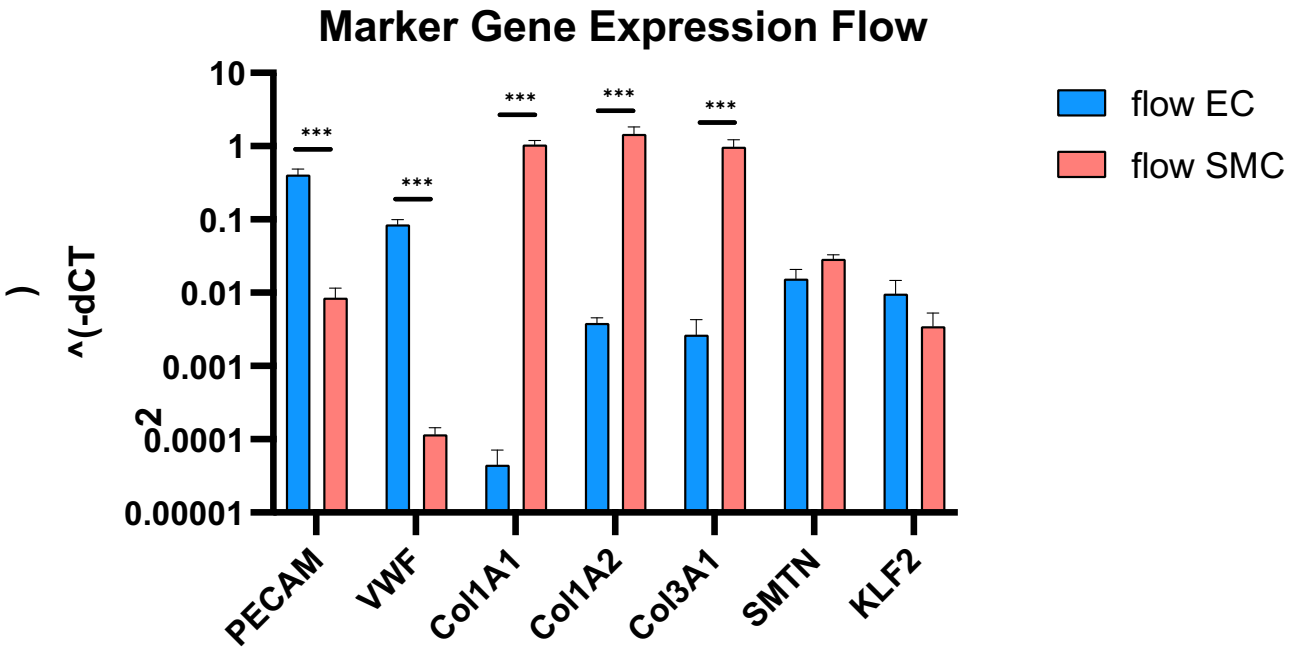

Figure 12. Expression of Marker Genes in ECs and SMCs under flow condition.

Own illustration

Expression levels are normalized by RPLP0 housekeeping gene. The higher the 2^-dCT value, the higher the gene expression Shown are means +/- standard errors of the 2-deltaCT values compared to the control (static). Abbreviations: * $p < 0.05$; **$p < 0.01$; ***$p < 0.001$.

4.1.1.1. Marker gene expression profile under static condition

The control experiments, where the EC and SMC colonized membranes were maintained under static conditions, showed a similar expression pattern as compared to the cells exposed to the flow experiment. EC marker genes exhibit a higher expression level in EC, similarly SMC marker genes are more highly expressed in SMCs. Significant gene expression changes between both cell types were detected in PECAM ($p = 0.002270$), VWF ($p = 0.000348$), COL1A1 ($p = 0.000054$), COL1A2 ($p = 0.000013$) and COL3A1 ($p = 0.000145$).

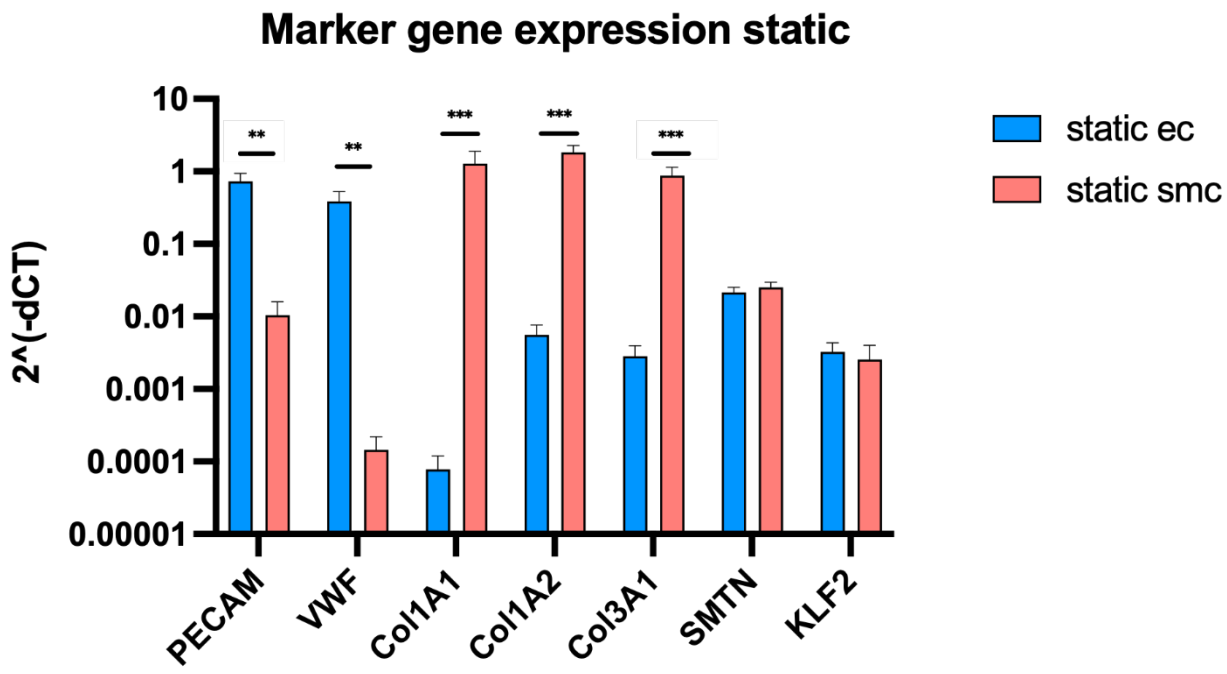

Figure 13. Expression of Marker Genes in ECs and SMCs under static condition.

Own illustration

Expression levels are normalized by RPLP0 housekeeping gene. The higher the 2^-dCT value, the higher the gene expression. Shown are means +/- standard errors of the 2-deltaCT values compared to the control (static).

Abbreviations: * $p < 0.05$; ** $p < 0.01$; *** $p < 0.001$

4.2. RNA concentration and RNA Integrity Number for quality control

After successful co-cultivation, the RNA concentrations of the 8 selected membranes were determined using the Nanodrop 2000c. The results of the RNA concentration measurements ranged from 14.2 at membrane 26 as the lowest value and 84.2 at membrane 4 as the highest value. The concentrations are summarized in the following two tables.

Table 9. RNA concentration of cells exposed to flow condition as quantity control.

Flow		Celltype	Membrane	RNA Conc.
Chip 3	17	EC	Membrane 2	23.2
	18	EC	Membrane 6	29.2
	19	EC	Membrane 20	43.2

	20	EC	Membrane 26	14.2
	21	SMC	Membrane 2	67.9
	22	SMC	Membrane 6	72.2
	23	SMC	Membrane 20	18.3
	24	SMC	Membrane 26	34.3

Table 10. RNA concentration of cells exposed to static condition as quantity control.

Static		**Celltype**	**Membrane**	**RNA Conc.**
Chip 4	25	EC	Membrane 4	29.8
	26	EC	Membrane 14	29.6
	27	EC	Membrane 18	28.2
	28	EC	Membrane 28	21.5
	29	SMC	Membrane 4	84.2
	30	SMC	Membrane 14	52.5
	31	SMC	Membrane 18	45.2
	31	SMC	Membrane 28	31.6

Besides adequate quantity (RNA concentration), the RNA quality (RIN) is a crucial criterion for the selection of suitable membranes for the sequencing step. The results of the RIN are illustrated in the table below. There are ten integrity categories, with 10 being the highest quality

and 1 representing total degradation. The measured RIN ranged from 7.0 to 9.8 for the different membranes.

Table 11. RIN measurement of cells exposed to flow condition as quality control.

Celltype	Membrane	RIN	Membrane	RIN
EC	Membrane 2	8.60	Membrane 4	9.8
EC	Membrane 6	9.7	Membrane 14	9.4
EC	Membrane 20	9.4	Membrane 18	9.7
EC	Membrane 26	9.0	Membrane 28	9.4

Table 12. RIN measurement of cells exposed to static condition as quality control.

Celltype	Membrane	RIN	Membrane	RIN
SMC	Membrane 2	7.9	Membrane 4	7.0
SMC	Membrane 6	9.4	Membrane 14	8.9
SMC	Membrane 20	7.0	Membrane 18	9.1
SMC	Membrane 26	9.3	Membrane 28	8.6

4.3. Quality control of the RNA Sequencing exploratory data analysis

As already described in chapter 3.2.11, a principal component analysis was performed after evaluation of the RNA sequencing data. After subsetting the data set according to the factor "cell type", scatter plots were created for the respective factors "chip" (Fig. 14), "exposure EC" (Fig. 15) and "exposure SMC" (Fig. 16).

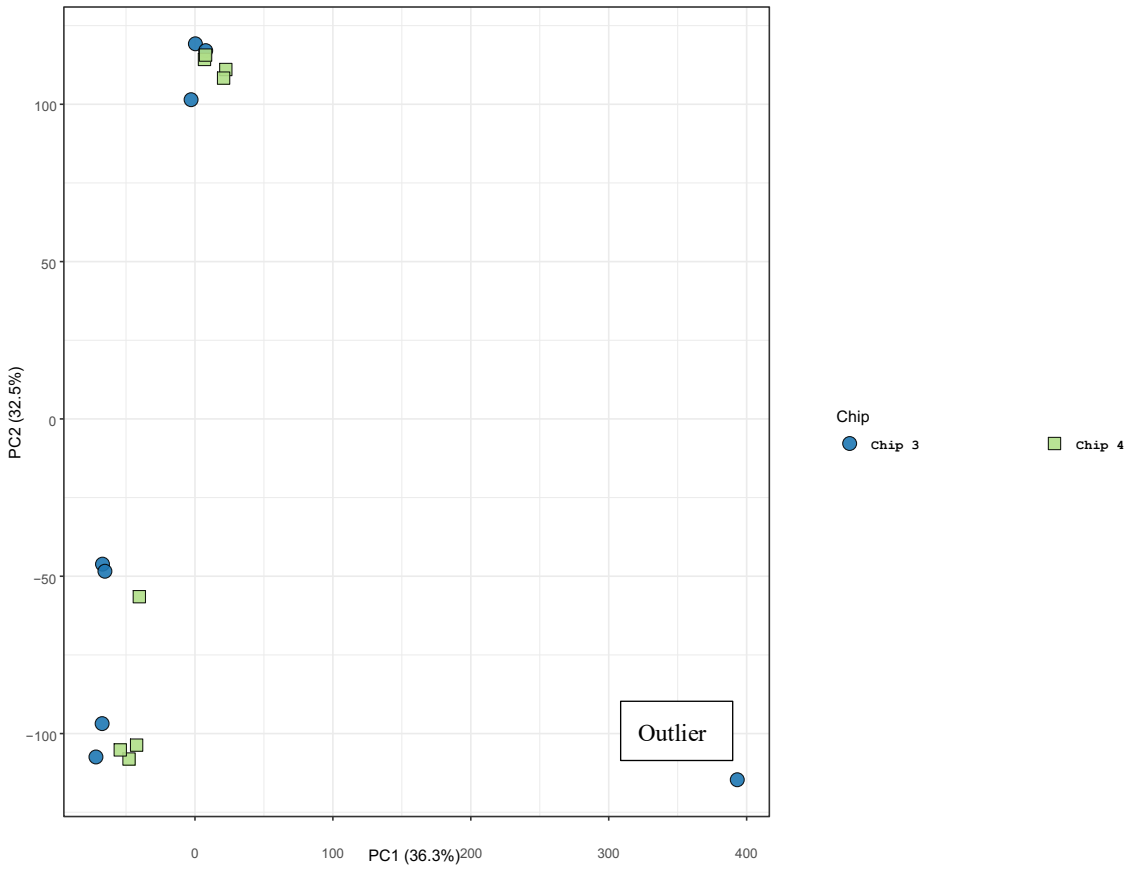

Figure 14. PCA scatterplot for the first two principal components from the raw data set.
Modified from (Fios Genomics)

Shown are all samples for EC and SMC separated by the first two principal component. Abbreviations: PCA1 = First principal component; PCA2 = Second principal component.

Applying the variable chip as a principal component, the plot displays a higher dispersion within each cluster than between the clusters. This indicates a balanced distribution across the different chips and thus using two different chips do not play a considerable role in the variability of the data. The EC sample, which did not pass quality control, is marked as an outlier.

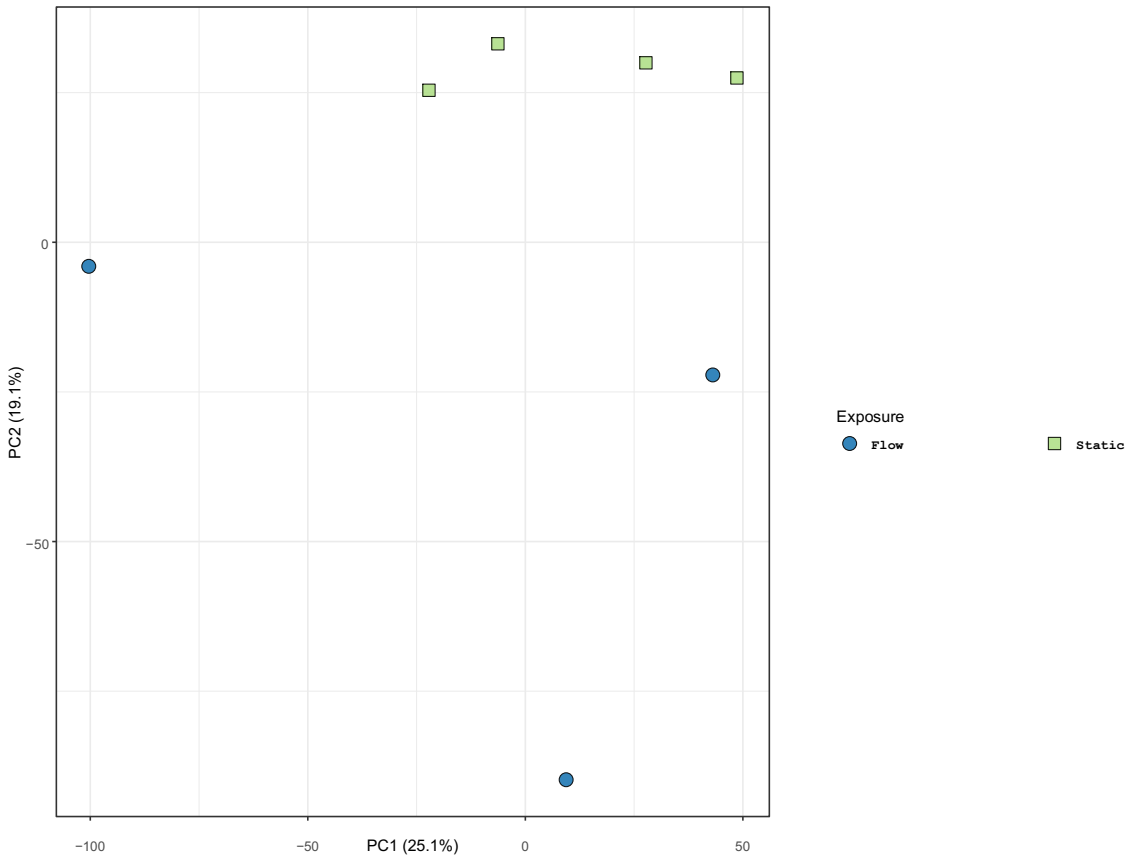

Figure 15. PCA scatterplot of normalized EC data.

Modified from (Fios Genomics)

Shown are all samples for EC separated on the first two principal component by exposure group. Abbreviations: PCA1 = First principal component; PCA2 = Second principal component.

The figure represents a scatterplot for the first two principal components from the normalized EC dataset. This PCA showed that samples were generally separated by the factor ‘Exposure’, with samples from the static exposure group forming a tighter cluster than samples from the flow exposure group. The plot only displays three samples for the flow exposure in ECs as one of the samples was identified as an outlier.

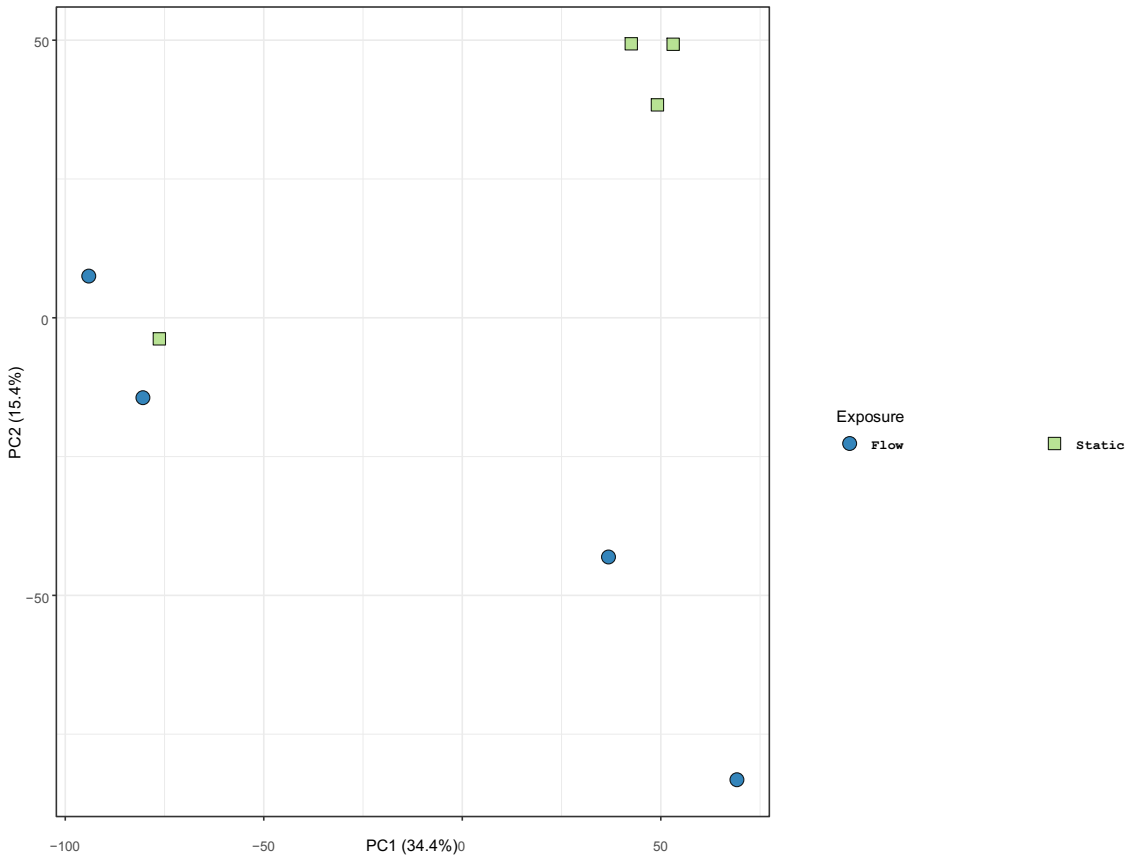

Figure 16. PCA scatterplot of normalized SMC data.

Modified from (Fios Genomics)

Shown are all samples for SMC separated on the first two principal component by exposure. Abbreviations: PCA1 = First principal component; PCA2 = Second principal component.

The figure represents a scatterplot for the first two principal components from the normalized SMC dataset. The plot shows dispersion between the clusters formed by the factor 'Exposure'. Three static samples form a tight cluster, while one static sample clusters with the flow samples.

4.4. Evaluation of transcriptomic changes using RNA sequencing technology

The following chapter aims to assess the transcriptomic changes within a cell type in relation to the two different conditions, flow and static, to which the cells were exposed. Using a statistical cut-off with a threshold of $P < 0.01$ and fold change ≥ 2, we identified 224 and 233 differentially expressed genes (DEGs) in EC and SMC respectively. First the transcriptional changes within the ECs are shown; then the effects in the VSMCs are investigated.

4.4.1.1. Significant genes for comparison Endothelial Cells (Flow vs. Static)

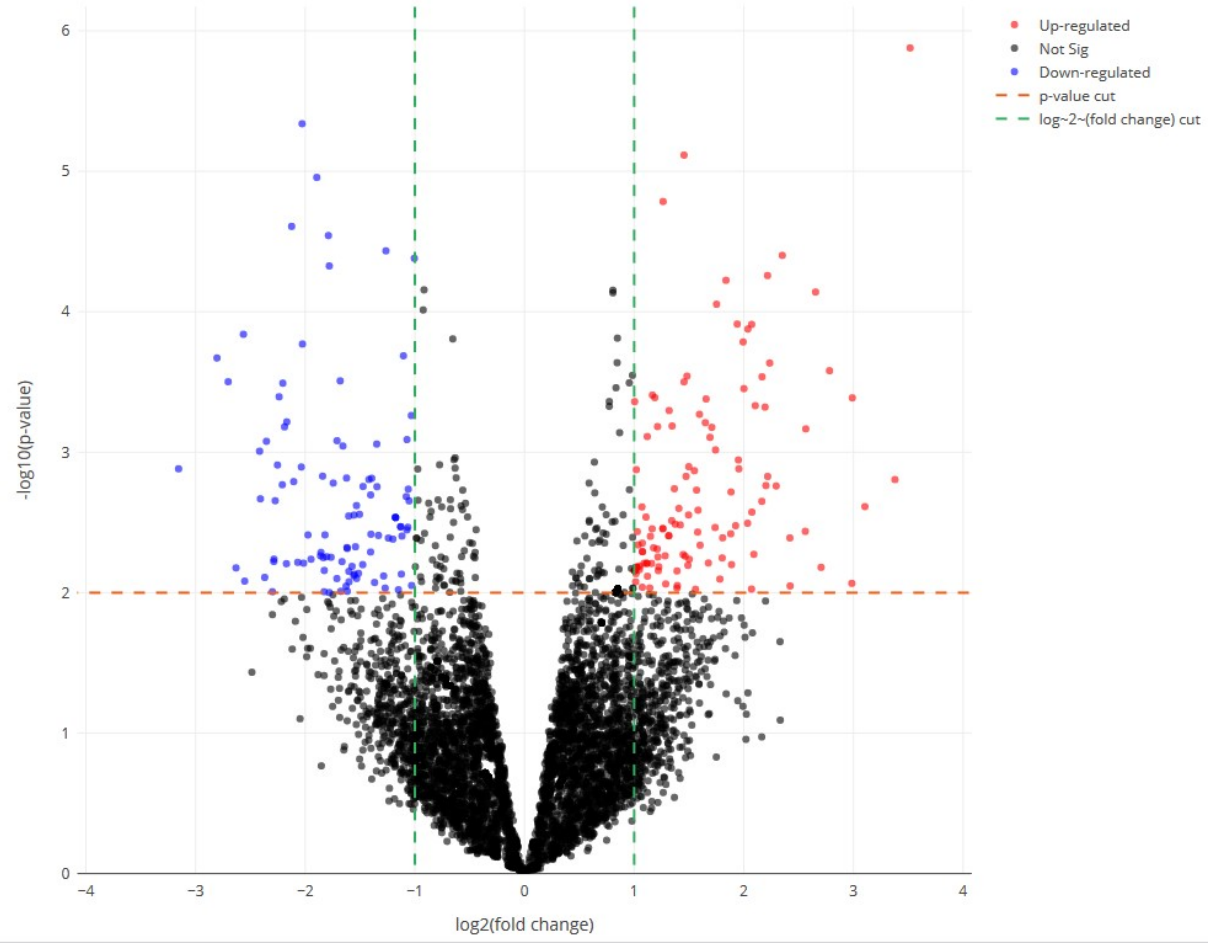

Figure 17. Volcano Plot for comparison of endothelial cell gene expression (flow vs. static). Modified from (Fios Genomics)

Volcano plot showing statistical significance (as -log10 transformed p-values) versus magnitude of change (log2(fold change)). Red dots resemble up-regulated genes, while blue dots stand for down-regulated. The most statistically significant genes positioned towards the top. The black dots stand for genes not showing a significant change in their expression. Vertical green and horizontal red lines mark the respective thresholds for the fold change and the p-value.

The Volcano plot illustrates the altered gene expression of ECs under flow exposure. Under the setting of a fold change ≥ 2, different numbers of significantly altered gene expressions could be evaluated for different statistical p-values. The data shows that at a defined p-value of < 0.05, significant changes in the expression were found in 548 genes, while at a lower p-value of <0.01, we detected 224 DEGs. At a p-value = < 0.001 the number of differentially expressed genes was 59, whereas at p < 0.0001, gene expression was found to be significantly altered only in 15 genes.

Table 13. Significance profile of differentially expressed genes in endothelial cells.

This table lists the number of genes significant at the different statistical thresholds for comparison between static and flow condition. The profiles are assessed while also defining a fold change ≥ 2.

P < 0.05	**P < 0.01**	**P < 0.001**	**P < 0.0001**
548 genes	224 genes	59 genes	15 genes

Based on a p-value of < 0.01 the number of differentially expressed genes for a range of fold change magnitudes were evaluated and summarized in the table below. Under a set fold change of 1.3, we identified 216 up-regulated and 164 down-regulated genes. With a fold change value of 2, the number of up-regulated genes was 123 and the number of down-regulated genes was 101. At a fold change of 4 we detected 29 overexpressed genes and 28 downregulated genes, whereas with a fold change of 8, only 3 genes showed increased expression and one gene showed decreased expression.

Table 14. Fold change profile of differentially expressed genes in endothelial cells.

The table below lists the number of genes for the static vs. flow comparison for a range of fold change sizes. Profiles are evaluated while also setting raw p-value < 0.01.

Fold Change Direction	**1.3x**	**2x**	**4x**	**8x**
Up-regulated	216	123	29	3
Down-regulated	164	101	28	1

The 13 most significant DEGs are listed in the following table in descending order according to the lowest p-value. Table 15 also shows the KEGG pathways associated with the respective genes and the fold change value. The small heat shock protein CRYAB shows the most significant change in expression with an adjusted p-value of 0.0296. As our data show, the gene LRG1 is significantly lower expressed under flow conditions with an adjusted p-value of 0.0917 than in the static control group. In turn, the gene KLF4 showed a significantly increased expression after flow exposure with an adjusted p-values of 0.0933. The abovementioned genes are highlighted in the table. These three genes were selected as genes of interest given that they are known to be involved in cellular processes in the ECs such as inflammatory reaction, response to stress, and angiogenesis. These are processes that, as our data show, are influenced by the exposure of the endothelium to wall shear stress.

Table 15. Differential gene expression in endothelial cells (flow vs. static).

The 13 most significant differentially expressed genes with the smallest p-value are given. The FC-Value describes the ratio of quantity change in gene expression between EC flow and EC static. Log 2(FC), the logarithmic fold change, is also used as a parameter to assess the expression levels of genes, whereas negative Log2(FC) means that the respective gene is downregulated. KEGG pathways link specific genes to cellular signaling pathways and molecular interactions.

ID	Description	KEGG-Pathway	FC	Log2(FC)	P	P(adj.)
CRYAB	Crystallin, alpha B	Protein processing in endoplasmic reticulum, Longevity regulating pathway	11.442	3.516	1.32e-6	0.0296
AC100852.2	-	-	-4.080	-2.028	4.58e-6	0.0513
TRAPPC2P1	Trafficking protein particle complex 2 pseudogene 1	-	2.741	1.455	7.67e-6	0.0573
NPFFR2	Neuropeptide FF receptor 2	Neuroactive ligandreceptor interaction	-3.718	-1.895	1.1e-5	0.0619
TPTE2P1	Transmembrane phosphoinositide 3phosphatase and tensin homolog 2 pseudogene 1	-	-2.401	1.264	1.64e-5	0.0735
GPRIN3	GPRIN family member 3	-	-4.360	-2.124	2.47e-5	0.0917
LRG1	Leucine-rich alpha-2glycoprotein 1	-	-3.455	-1.789	2.87e-5	0.0917
SLAIN2	SLAIN motif family, member 2	-	-2.402	-1.264	3.68e-5	0.0933
KLF4	Kruppel-like factor 4 (gut)	Signaling pathways regulating pluripotency of stem cells	5.102	2.351	3.96e-5	0.0933
ASPHD2	Aspartate betahydroxylase domain containing 2	-	-2.007	-1.005	4.16e-5	0.0933

TMEM30B	Transmembrane protein 30B	-	-3.436	-1.781	4.72e-5	0.0961
SNAI2	Snail family zinc finger 2	Hippo signaling pathway, Adherens junction	4.646	2.216	5.52e-5	0.0966
INHBA	Inhibin, beta A	Cytokine-cytokine receptor interaction, TGF-beta signaling pathway, signaling pathways regulating pluripotency of stem cells	3.573	1.837	5.97e-5	0.0966

4.4.1.2. CRYAB expression under the influence of flow in endothelial cells

The boxplot below shows significantly (p= 0.0296) increased expression of CRYAB in ECs exposed to flow compared to static ECs. Comparing the median for CRYAB expression in ECflow shows a $\log_2$ of 3.927, whereas it is significantly lower in EC static with a $\log_2$ value of 0.55.

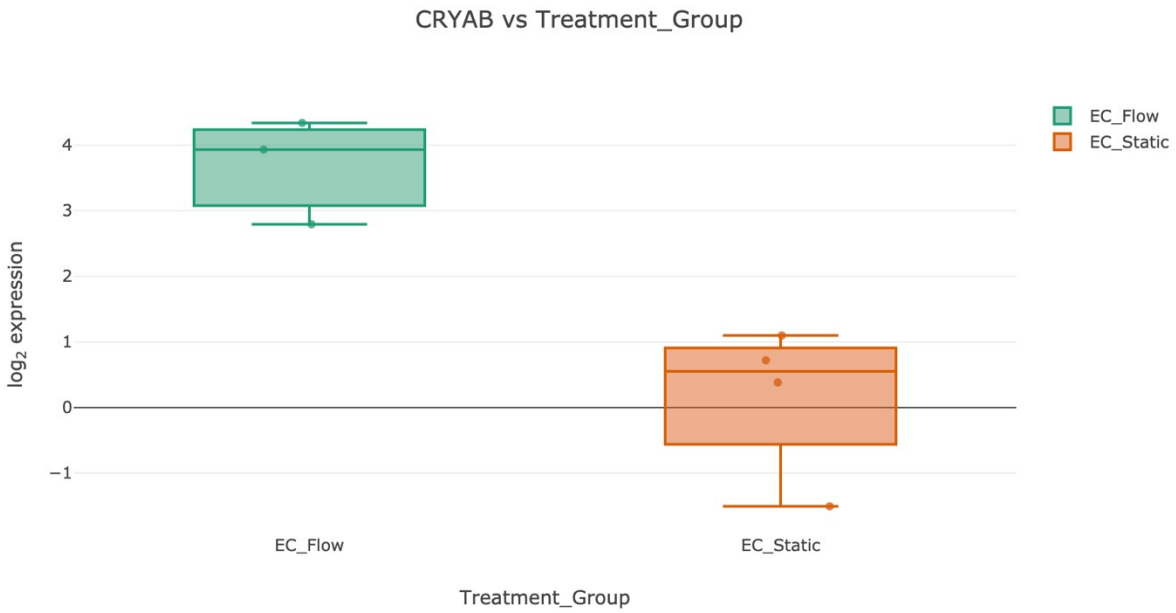

Figure 18. CRYAB expression in endothelial cells under flow conditions (green box) and after static conditions (orange box).

Modified from (Fios Genomics)

The box plot shows the median, the interquartile range (Q3-Q1), and the whiskers, which represent the lower 25% and the upper 25% of the values excluding the outliers.

4.4.1.3. LRG1 expression under the influence of flow in endothelial cells

The boxplot shows significantly (p= 0.0917) decreased expression of LRG1 in ECs exposed to flow versus static ECs. Comparing the medians, the values for the EC flow group are $\log_2$= 3.116 and those for the EC flow group are $\log_2$= -1.396.

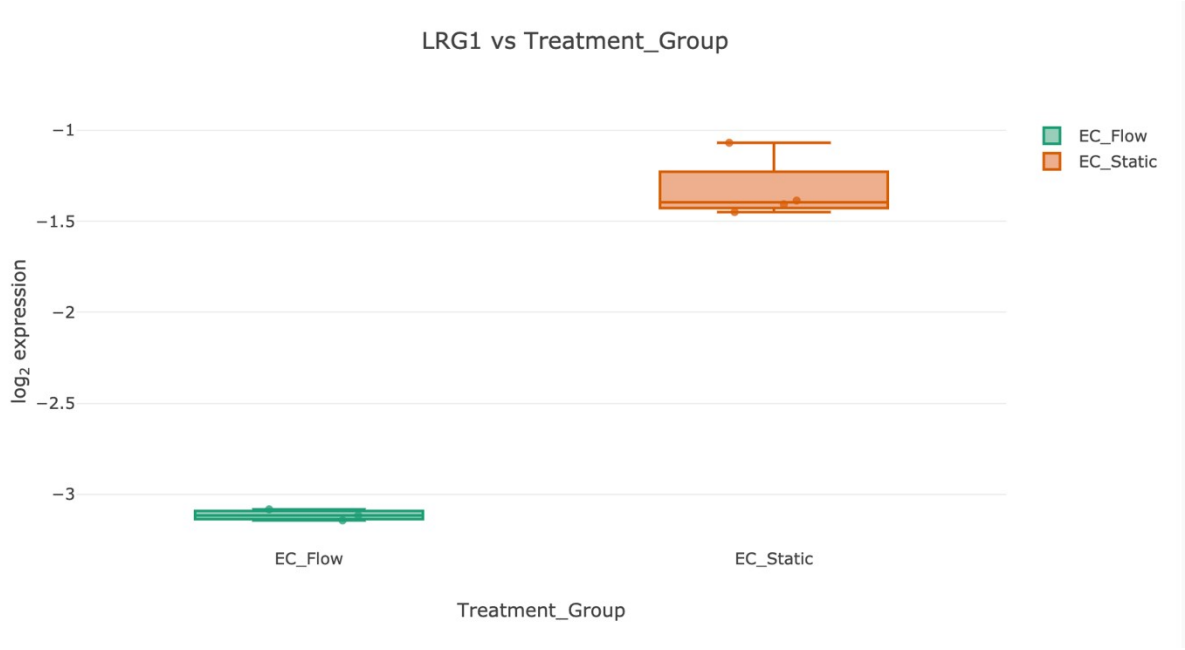

Figure 19. LRG1 expression in endothelial cells under flow conditions (green box) and after static conditions (orange box).

Modified from (Fios Genomics)

The box plot shows the median, the interquartile range (Q3-Q1), and the whiskers, which represent the lower 25% and the upper 25% of the values excluding the outliers.

4.4.1. KLF4 expression under the influence of flow in endothelial cells

With a significance of $p = 0.0933$ the transcription factor KLF4 showed an increased expression in ECs exposed to flow versus static ECs. The median of X in the EC flow group is higher compared to the median value $\log_2 = 4.44$ in the EC static group $\log_2 = 2.089$.

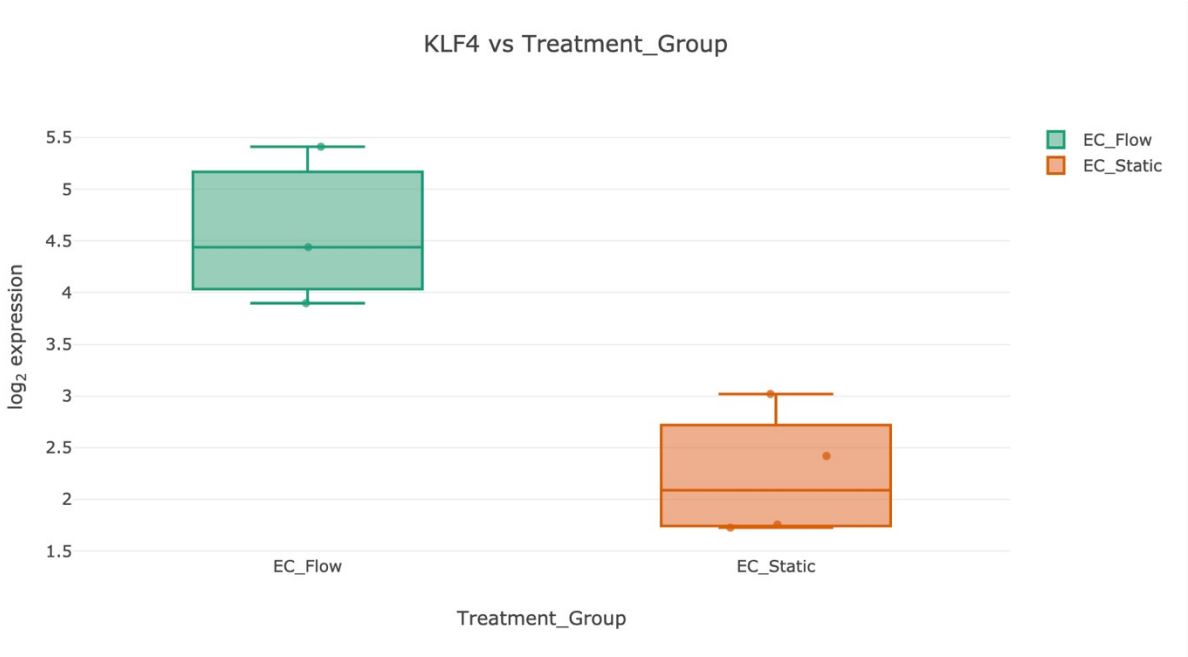

Figure 20. KLF4 expression in endothelial cells under flow conditions (green box) and after static conditions (orange box).

Modified from (Fios Genomics)

The box plot shows the median, the interquartile range (Q3-Q1), and the whiskers, which represent the lower 25% and the upper 25% of the values excluding the outliers.

4.4.1.1. KEGG-pathways for endothelial cells

Significantly up- and down-regulated genes (at p-value < 0.01 and fold change ≥ 2) in the comparison 'ECs (Flow vs. Static)' were assigned to 182 genes and analyzed for KEGG pathway enrichment. For clarity, only KEGG pathways with an enrichment P value of less than 0.05 and 2 or more involved genes are shown in figure 16.

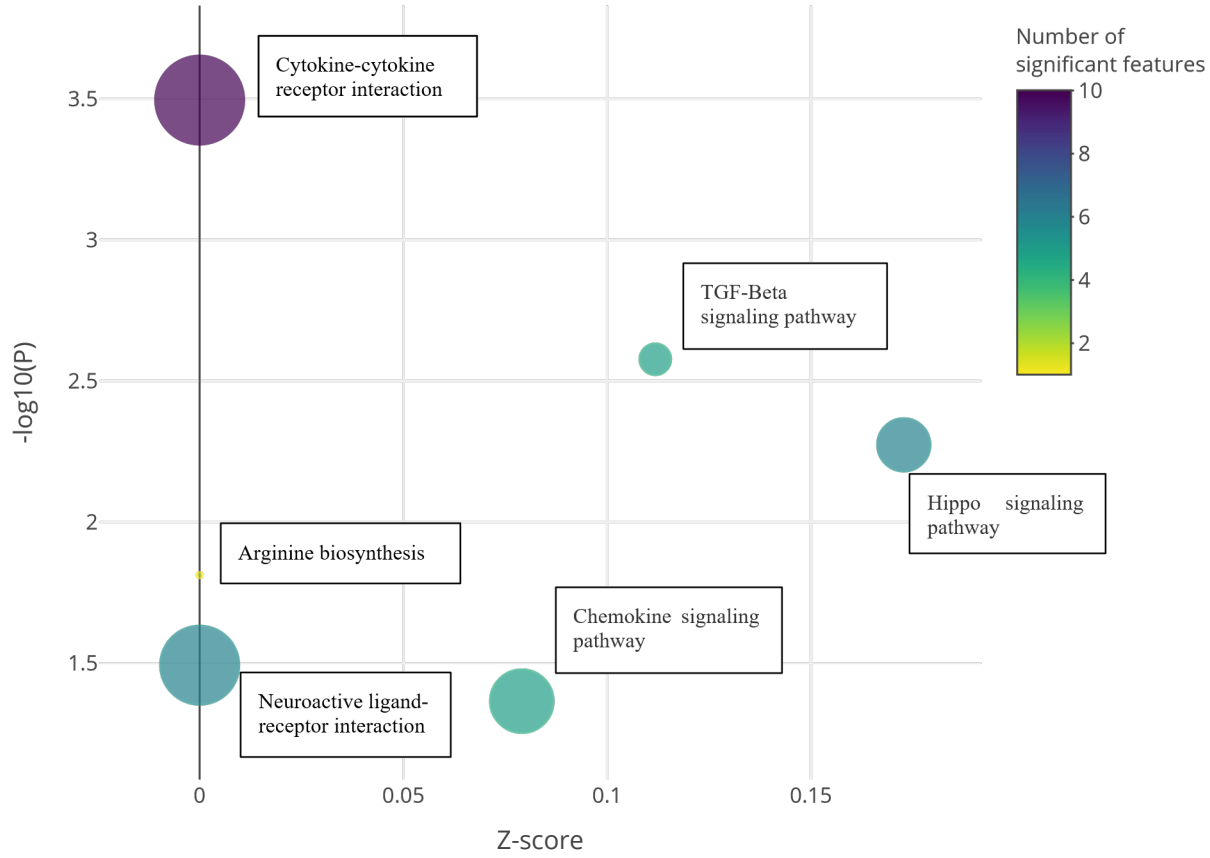

Figure 21. Bubble plot of enriched pathways.

Modified from (Fios Genomics)

The bubble plot illustrates enrichment analysis with enrichment Z-score on the X-axis and -log10(p-value) on the Y-axis. The Z-axis determines the size of the bubble, which in turn is proportional to the number of genes associated with the pathway. The point color is determined by the total number of genes N in the pathway.

The pathway with the lowest adjusted p-value (1.277e-2) is the cytokine-cytokine receptor interaction pathway. Out of a total number of 224 genes (N) involved in this pathway, 10 are significant (S), corresponding to a ratio of S/N= 4.46% (10/224). The second lowest adjusted p-value (p = 5.298e-2) was found for TGF-beta signaling pathway (S/N= 6.25%, 5/80), followed by Hippo signaling pathway (4.48%, 6/134) with an adjusted p-value of 7.101e-2. The arginine biosynthesis pathway showed an adjusted p-value of 1.542e-1 and a S/N ratio of 12.50% (2/16). The adjusted p-value of the neuroactive-ligand receptor interaction pathway was 2.574e-1 with a S/N ratio of 3.02% (6/199). The sixth point in the bubble plot represents the chemokine signaling pathway, which had a p-value of 2.877e-1 and a S/N ratio of 3.12% (5/160).

4.4.1.2. Significant genes for comparison Smooth Muscle Cells (Flow vs. Static)

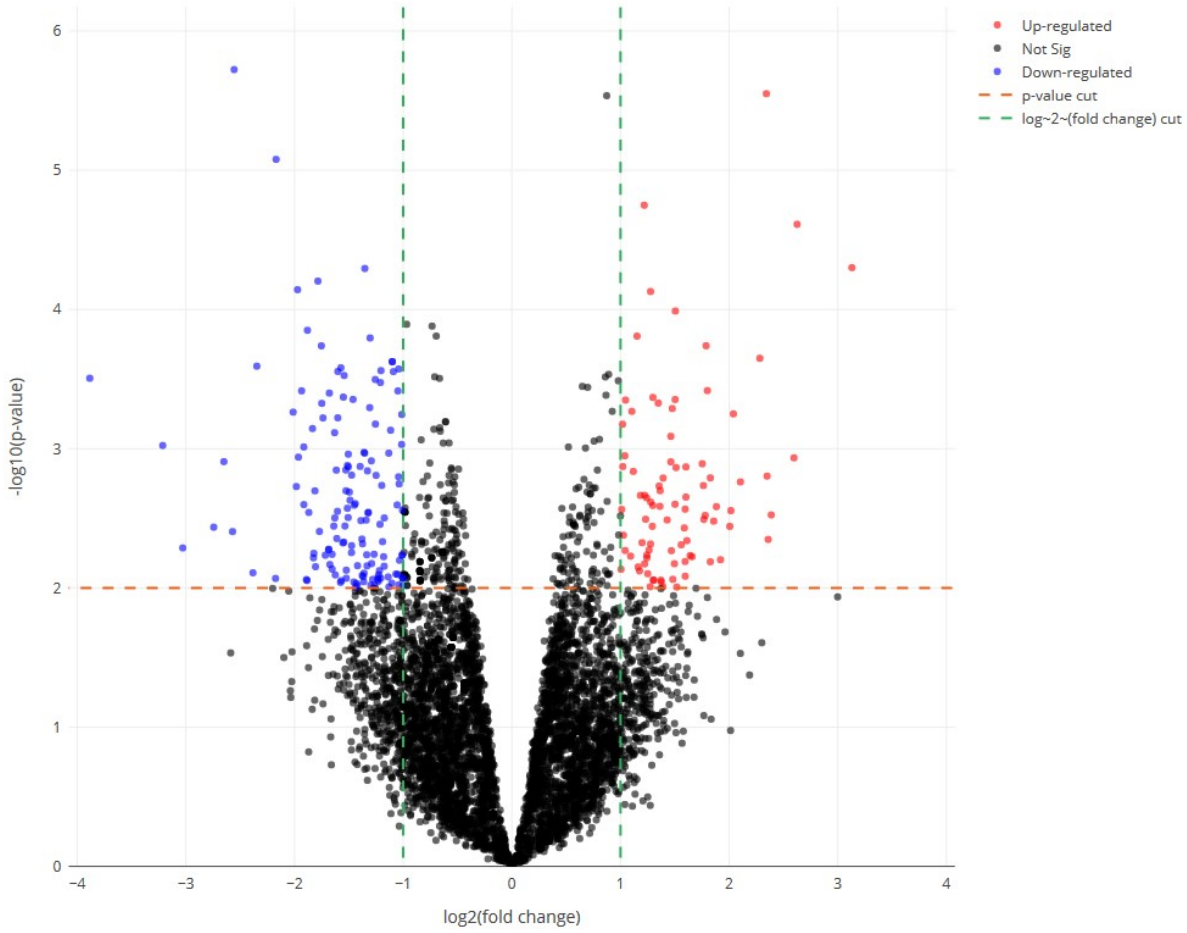

Figure 22. Volcano Plot for comparison of smooth muscle cell gene expression (flow vs. static).

Modified from Fios Genomics

Volcano plot showing statistical significance (as -log10 transformed p-values) versus magnitude of change (log2(fold change)). Red dots resemble up-regulated genes, while blue dots stand for down-regulated. The most statistically significant genes positioned towards the top. The black dots stand for genes not showing a significant change in their expression. Vertical green and horizontal red lines mark the respective thresholds for the fold change and the p-value.

The Volcano plot illustrates the altered gene expression of SMCs under flow exposure. Under the setting of a fold change ≥ 2, different numbers of significantly altered gene expressions could be evaluated for different statistical p-values.

At a defined p-value of < 0.05, significant changes in the level of expression were found for 606 genes. The number of DEGs at a lower P value of < 0.01 was only 233 and at p value < 0.001 just 57 DEGs. At P < 0.0001, significantly altered gene expression was found in 10 genes.

Table 16. Significance profile of differentially expressed genes in smooth muscle cells.

This table lists the number of genes significant at the different statistical thresholds for comparison between static and flow condition. The profiles are assessed while also defining a fold change ≥ 2.

P < 0.05	**P < 0.01**	**P < 0.001**	**P < 0.0001**
606 genes	233 genes	57 genes	10 genes

Based on a p-value of < 0.01 the number of differentially expressed genes for a range of fold change magnitudes were evaluated and are summarized in the table below. Under a fold change of 1.3 we identified 187 up-regulated and 327 down-regulated genes. The number of upregulated genes was 87 and the number of down-regulated genes 146 at a fold change value of 2. With a fold change of 4, increased and decreased expression was observed for 12 genes, respectively. At a fold change of 8, only one gene was up-regulated and three genes was downregulated.

Table 17. Fold change profile of differentially expressed genes in smooth muscle cells.

The table below lists the number of genes for the static vs. flow comparison for a range of fold change sizes. Profiles are evaluated while also setting raw p-value < 0.01.

Fold Change Direction	**1.3x**	**2x**	**4x**	**8x**
Up-regulated	187	87	12	1
Down-regulated	327	146	12	3

The following table lists the 13 most significant DEGs in SMCs in descending order according to the lowest p-value. Also shown in the table are the KEGG pathways, that could be mapped to the respective genes and the fold change value to indicate the magnitude of the expression changes. LRFN5 and HHEX were highlighted in the table as they were selected as genes of interest. LRFN5 is a stiffness regulator in SMCs and was up-regulated with an adjusted p-value of 0.142. HHEX promotes SMC proliferation and showed an up-regulation with an adjusted pvalue of 0.0933.

Table 18. Differential gene expression in smooth muscle cells (flow vs. static).

The 13 most significant differentially expressed genes with the smallest p-value are given. The FC-Value describes the ratio of quantity change in gene expression between EC flow and EC static. Log 2(FC), the logarithmic fold change, is also used as a parameter to assess the expression levels of genes, whereas negative Log2(FC) means that the respective gene is downregulated. KEGG pathways link specific genes to cellular signaling pathways and molecular interactions.

ID	Description	KEGG-Pathway	FC	Log2(FC)	P	P(adj.)
PTPRR	protein tyrosine phosphatase, receptor type, R	MAPK signaling pathway	-5.882	-2.556	1.89e-6	0.0217
SHE	Src homology 2 domain containing E	-	5.072	2.343	2.82e-6	0.0217
RCC2	regulator of chromosome condensation 2	-	1.831	0.873	2.91e-6	0.0217
CAMK1G	calcium/calmodulindependent protein kinase IG	Calcium signaling pathway Oxytocin signaling pathway, Aldosterone synthesis and secr., glioma	-4.499	-2.169	8.35e-6	0.0468
LYZ	lysozyme	Salivary secretion	2.327	1.218	1.78e-5	0.0798
PCDHB7	protocadherin beta 7	-	6.169	2.625	2.44e-5	0.0912
LRFN5	leucine rich repeat and fibronectin type III domain containing 5	-	8.751	3.129	5.0e-5	0.142
HHEX	hematopoietically expressed homeobox	Maturity onset diabetes of the young, Transcriptional	-2.402	-1.264	3.68e-5	0.0933

		misregulation in cancer				
FTH1P5	ferritin, heavy polypeptide 1 pseudogene 5		-3.447	-1.785	6.25e-5	0.151
GLDCP1	glycine dehydrogenase (decarboxylase) pseudogene 1	-	-3.924	-1.972	7.2e-5	0.151
RP11-111F5.5		-	2.423	1.277	7.43e-5	0.151
HIST2H2AB	histone cluster 2, H2ab	Necroptosis Alcoholism Systemic lupus erythematosus	2.838	1.505	0.000102	0.191
BNIP3P1	BCL2/adenovirus E1B 19kDa interacting protein 3 pseudogene 1	-	-1.956	-0.968	0.000128	0.197

4.4.1.3. LRFN5 expression under the influence of flow in smooth muscle cells

The boxplot shows significantly ($p= 0.142$) increased expression of LRG1 in SMCs exposed to flow versus static SMCs. Comparing the medians, the values for the SMC flow group are $\log_2 = 0.328$ and those for the SMC static group are $\log_2 = -2.778$.

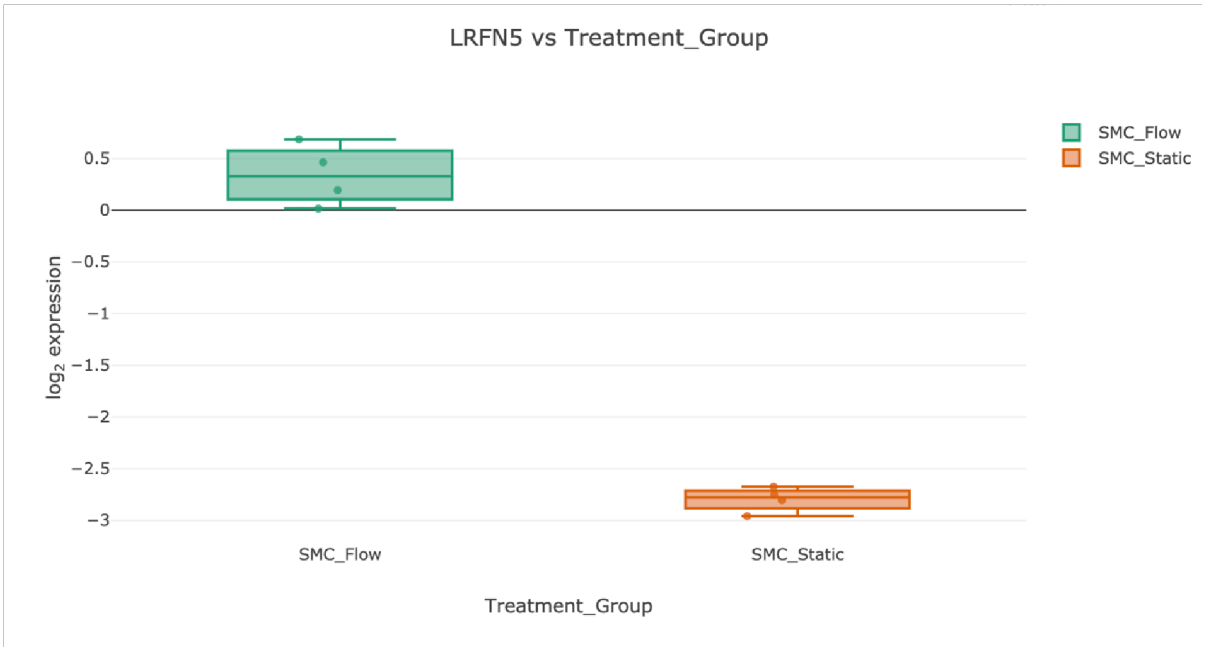

Figure 23. LRFN5 expression in smooth muscle cells under flow conditions (green box) and after static conditions (orange box).

Modified from Fios Genomics

The box plot shows the median, the interquartile range (Q3-Q1), and the whiskers, which represent the lower 25% and the upper 25% of the values excluding the outliers.

4.4.1.4. HHEX expression under the influence of flow in smooth muscle cells

The boxplot below shows significantly (p= 0.0933) decreased expression of HHEX in SMCs exposed to flow compared to static SMCs. Comparing the median for HHEX expression in SMC flow shows a $\log_2$ of 3.548, whereas it is significantly higher in SMC static with a $\log_2$ value of 5.024.

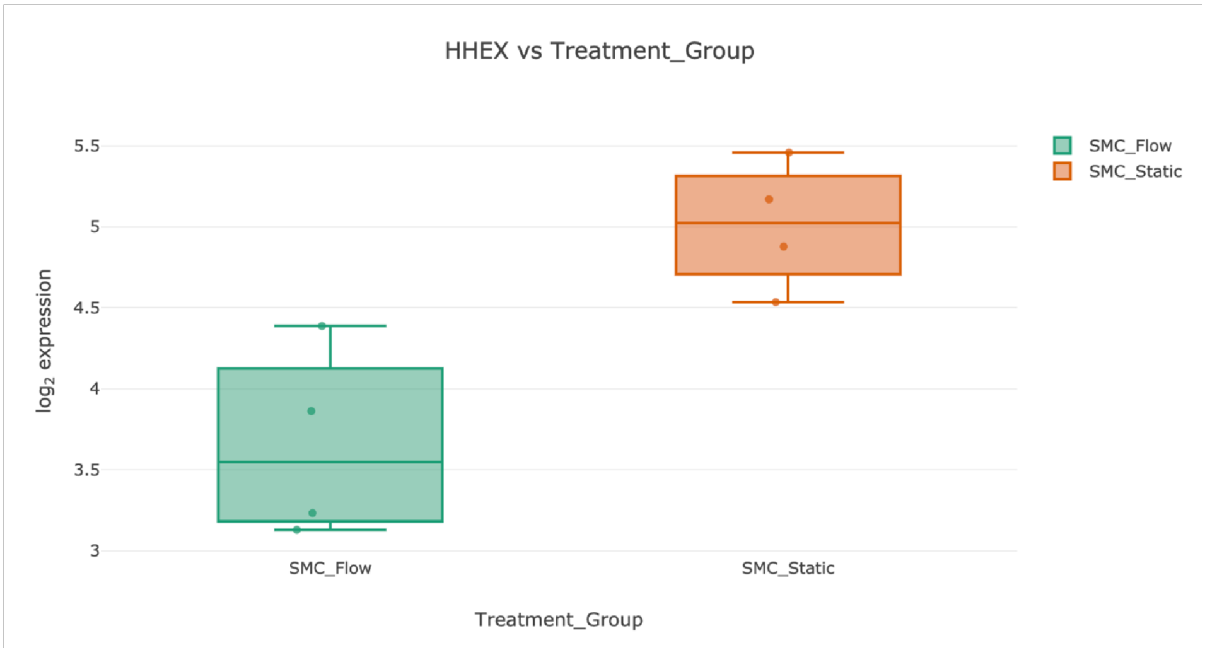

Figure 24. HHEX expression in smooth muscle cells under flow conditions (green box) and after static conditions (orange box).

Modified from Fios Genomics

The box plot shows the median, the interquartile range (Q3-Q1), and the whiskers, which represent the lower 25% and the upper 25% of the values excluding the outliers.

5. DISCUSSION

5.1. Overview of the results

In this work, we were able to show that the co-cultivation of different cell types, EC and SMC, is possible within the aorta-on-chip model. Furthermore, we were able to analyze the flowbased transcriptomic changes within the respective cells. In order to demonstrate the functioning co-culture, marker genes were selected for characterization of the respective cell type, which are either cell-specific or at least expressed with a high constancy by the respective cell types in their physiological state. The marker genes showed higher expression in each of the corresponding cell types. Based on these results, the transcriptomes of selected membranes were analyzed to assess flow-based changes in gene expression of ECs and SMCs. This method allowed us to prove that the expression of certain genes changed as a result of the exposure of cells to a defined wall shear stress. ECs in particular showed stronger flow-related changes, whereas the changes in SMCs were less prominent. The flow-based changes in the ECs were also reflected in the KEGG pathway analysis. In particular, genes showed increased expression

after flow exposure whose functions include one or more of the following: Promotion of physiological vessel growth, inhibition of immune cell adhesion, and support of a protective cell response to stress stimuli. Genes such as LRG1 which are involved in pathogenic neovascularization and increased circulation of immune cells, showed decreased expression after exposure to flow. Genes with a vasoprotective property, such as CRYAB and KLF2/4, exhibited higher expression induced by flow. These findings support the hypothesis that wall shear stress maintains a vasoprotective function and is essential for the integrity of the endothelium.

5.2. Discussion of methods part

5.2.1.1. Co-Cultivation of endothelial cells and smooth muscle cells

To expose the cells to a defined laminar flow rate it was necessary to establish a co-culture of EC and SMC. For this purpose commercially available primary aortic cells were cultivated. The use of these cells is special, as in the majority of studies on the human vascular system embryonic cells from the umbilical vein (HUVECs) are used. HUVECs are widely used for several reasons: the isolation from the umbilical vein is well established and highly successfull, they are easy to handle and they have remarkable capacity for growth (Heiss, Hellstrom et al. 2015), (Medina-Leyte, Domínguez-Pérez et al. 2020), (Maciag, Hoover et al. 1981). However, they originate from a venous and not from an arterial vessel. The aortic cells we have used are derived directly from the aorta and are therefore better suited to simulate the physiology of the blood vessel for the aorta-on-chip model.

The molecules used for coating the AoC membrane are also natural components of the human aorta. The subendothelial membrane of the human aorta separates the intima from the media. It is formed of ECM, which in turn is composed of a variety of molecules. The most relevant are collagen, proteoglycans and glycoproteins such as fibronectin (Kefalides 1978), (Gordon and Bernfield 1980). The ECM not only fulfills a structure-giving function, but also affects key cellular processes such as cell differentiation, cellular growth and cell adhesion (Carlsson, Engvall et al. 1981), (Wagenseil and Mecham 2009). The latter is an essential prerequisite for the assembly and functionality of the aorta on a chip. As the cells, through exposure to wall shear stress, are subjected to mechanical forces, it is necessary to ensure strong cell attachment to the surface of membrane. ECM molecules such as fibronectin and collagen, serve this function in the aorta in vivo and studies have proved their superiority as surface solutions for cell adhesion over other molecules such as laminin (Ramalanjaona, Kempczinski et al. 1986),

(Palotie, Tryggvason et al. 1983). Fibronectin exhibits the ability of strong attachment even at low concentrations of only 10 to 20 ~g/ml in vitro (Gordon, Levitt et al. 1984).

Although the use of fibronectin and collagen as coating solutions creates a certain interaction and spatial relationship between ECM and cells, the three-dimensionality of the structure is limited by the fact that the cells and the coating solutions are arranged in contiguous layers. The complex construct of different cell types embedded in ECM can only be imitated to a limited extent. An advanced approach to replicate more complex organ-specific tissues are organoids. These 3D cell culturing systems grow pluripotent stem cells and adult stem cells. By using growth factors and other biochemical factors, the natural differentiation process of stem cells is stimulated, resulting in the production of different cell types. Together, these different cell types shape an organ-specific tissue through self-assembly (Yin, Mead et al. 2016). This morphogenesis is based on cultivation over a period of time up to 30 days and is therefore very time-consuming (Takebe and Wells 2019). Since our experiments require a high number of replicates, organoids are not suitable for our experimental set-up due to time constraints. Another limitation of organoids is their restricted ability to integrate mechanical properties such as flow, shear stress and pressure into their self-organized tissue structures (Hofer and Lutolf 2021). Yet, the exposure of cells towards these stimuli influences fundamental biological processes such as differentiation, proliferation and regeneration (Vining and Mooney 2017). Our experiments aim to comprehend transcription changes of EC and SMC caused by flow exposure; therefore, integration of flow, shear stress and pressure into the aortaon-chip is indispensable.

5.2.1.2. Exposure to flow

Although the co-cultivation of the two cell types described above is indeed challenging, the groundbreaking step is rather the exposure of the ECs to such high laminar wall shear stress of 10dyne/cm^2. Determining a suitable wall shear stress value was very difficult, since there are large deviations between measured or estimated values in the literature. This is because the wall shear stress value depends on complex factors such as vessel geometry, blood composition, and flow velocity. These interactions collectively render the measurement of wall shear stress exceedingly difficult, which is why values are often based on approximations and assumptions rather than precise measurements (Papaioannou and Stefanadis 2005). Extensive research has indicated that the mean wall shear stress (time-averaged over the cardiac cycle) in the suprarenal aorta ranges from 8.6 to 10.4dyne/cm^2 (Oshinski, Ku et al. 1995). Meanwhile, the mean values

measured in the common carotid artery are approximately 8.0yne/cm^2 (Oshinski, Curtin et al. 2006). Thus, 10dyne/cm^2 is the closest to a physiologically relevant wall shear stress.

Alongside the wall shear stress, the flow behavior of the blood influences the cellular response decisively. Basically, two different flow behaviors exist within the vessels, laminar and turbulent flow. In the physiological state, there is laminar flow, which is characterized by the fact that the flow direction of all particles is aligned parallel to the vessel wall. However, laminar flow usually exists only under ideal conditions as it can be easily modified by a number of parameters. For example, the composition of the blood, the flow velocity, and the geometry of the vessels can modify the flow behavior in a sense that the particles are no longer aligned parallel in their motion (Peskin 1977). Instead, the motions overlap, creating vortices and thus turbulent flow (Biasetti, Hussain et al. 2011). This leads to a deceleration of the flow velocity, whereby the kinetic energy released in the process is transferred to the ECs. This transfer of energy to the adjacent vessel wall, places a strain on the cells that is assumed to promote the development of atherosclerosis (Giddens, Zarins et al. 1993). In the AoC model, only steady laminar flow could be generated by the Fluigent pump. As described above, hemodynamics in vivo is extremely complex and therefore steady laminar flow is rarely present. Generating flow irregularities in the form of turbulent flow within the model would be an interesting possibility to study how endothelial cell gene expression is altered by turbulent flow. The cardiac cycle, which creates pulsatile flow within human blood vessels, was also not incorporated into the model. Previous studies demonstrated that cell morphology and fiber arrangement of the cytoskeleton were altered by exposure of EC cells to pulsatile flow (Helmlinger, Geiger et al. 1991). The cells exhibited an elongated shape and the fibers of the cytoskeleton thickened (Helmlinger, Geiger et al. 1991), (Levesque, Sprague et al. 1989). It was also shown that the formation of vascular relaxing factors such as nitric oxide (NO) produced by the endothelium was more strongly stimulated by pulsatility than by steady laminar flow (Nakano, Tominaga et al. 2000). Although exposure of the co-culture to laminar shear stress already provides a comprehensive approach to detect flow-induced responses and signaling pathways, some important physiological counterparts such as pulsatility are missing in the model.

5.2.1.3. Aorta-on-chip set-up in comparison to other existing models

Most of the existing vessel-on-chip models were developed with the objective to study the pathogenesis of thrombosis and, in this context, the interaction between flow and endothelium. These chips usually consist only of a perfused EC layer and lack the integration of SMC. Models that provide perfused co-culture of EC and SMC are rare but essential for many research

questions such as structural changes occurring within the vessel wall due to flow exposure (Paloschi, Sabater-Lleal et al. 2021). Apart from our model, there are two interesting models for such in vitro arteries. One from (Cho and Park 2020), which was published just recently, and one from (Gunther, Yasotharan et al. 2010).

In the model by Cho and Parks, 3D printing was used to form a circular PDMS channel, in whose surface wrinkles were subsequently imprinted. SMCs were then seeded on the circumferential surface of the channel. The wrinkles on the surface serve as a directional guide for cellular arrangement and allow for a contractile morphology of the SMCs. After 48h incubation time, HUVECs were seeded on top of the SMCs forming directly adjacent layers of the two cell types. Subsequently, the ECs were exposed to a laminar shear stress of 1.8 dyn/ cm^2 (Cho and Park 2020).

The main differences of this model and ours are the materials and fabrication of the chip, the arrangement of the cell layers, and the applied wall shear stress. Cho and Park used a 3D-printed microfluidic platform made of PDMS, while our chip was fabricated from glass and channels were made of polyetheretherketone or fluorinated ethylene-propylene. The advantages and disadvantages of the respective materials were already discussed in chapter 1.3.2.

Besides the materials, cell arrangement and morphology play a crucial role in mimicking the in vivo structure and function of the arteries. In Cho and Park's model, the channel is circular in shape so that the cells arrange themselves circumferentially according to the channel geometry. In our model, the cells attach to the semi-permeable membrane in a linear arrangement. Although the circumferential alignment of the cells is a more accurate approximation of the physiological architecture of the vessels, the cell layers in Cho and Park's model are directly adjacent to each other without being spatially compartmentalized by or embedded in a scaffold of ECM. However, as ECM molecules have an impact on key cellular processes, their absence in the model limits the representation of physiological conditions. In our model, the cells are also not embedded in a self-organized scaffold of ECM, but by coating the membrane with important ECM molecules such as fibronectin and collagen, the ECM is incorporated into the model, thus ensuring cell-ECM communication. In addition, the semipermeable membrane between ECs and SMCs creates a spatial separation similar to the physiological wall structure, where the basal lamina demarcates the endothelial layer from the VSMCs in the tunica media. The wall shear stress subjected to the ECs in our model was 10dyne/cm^2, which is considerably higher than the value chosen by Cho and Parks, which was only 1.8dyne/cm^2. As already described in chapter 6.2.2., the determination of a suitable wall shear stress value is challenging; nevertheless, a shear stress of 10dyne /cm^2 is a more suitable value for the investigation of

flowbased changes compared to a lower value. This is due to the assumption that cells exhibit stronger changes in their gene expression and morphology when the applied wall shear stress is higher.

Günther et al demonstrate quite a different approach in establishing an in vitro artery than we did in our model. For their in-vitro artery model, small resistance vessels were obtained ex vivo from mice and integrated into a microfluidic platform fabricated by soft lithography, where they were immobilized by applying negative pressure. The platform enabled cultivation of the cells under physiological conditions by generating and maintaining a transmural pressure of 45mmHG and a physiological temperature of 37 C. By connecting the isolated arteries with microfluidic channels the cells were exposed to perfusion. The response of the cells and the changes in the vascular wall induced by vasoconstrictive drugs such as phenyephrines or acetylcholine was then measured and analyzed. The exciting aspect of this model is that the physiological structure of the vessel wall remains intact, since the vessels are removed as a complete segment and inserted into the model (Gunther, Yasotharan et al. 2010). However, the limitation of this approach is that the arteries are not derived from humans, but from mice. Therefore, the extent to which the results can be transferred to the human organism initially remains uncertain. The transferability of the results to the human organism is considerably higher in our model due to the use of human donor-derived aortic cells.

5.2.1.4. RNA Sequencing via IonTorrent

To analyze flow-based changes in gene expression, RNA sequencing was performed using Thermo Fisher's IonChef system. Synthesizing the RNA template in cDNA via reverse transcription increases the stability of the molecules. Subsequently, RNASeq enables the simultaneous sequencing of millions of cDNA molecules. Thus, in a remarkably short time, it is possible to not only analyze which genes are being expressed at a given moment, but also to measure the level of expression (Ekblom and Galindo 2011). This high productivity and sensitivity, combined with the low cost of the analysis make RNASeq a widely used technology. In contrast to qPCR and DNA microarrays, where predefined templates are used to search for target sequences, RNASeq provides an unbiased approach to analyzing the entire transcriptome (Mantione, Kream et al. 2014). This enables the detection of known as well as unknown transcripts and variants (Thermo Fisher n.d.). Therefore, RNASeq is a suitable method to address our research question: which alterations caused by the exposure of cells to flow can be detected in the whole transcriptome. Compared to microarrays, RNA Seq has a lower detection limit and thus an increased power to detect unknown genes, rare splice variants and polymorphisms (Zhao, Fung-Leung et al. 2014), (Howard, Hu et al. 2013).

Apart from this project's sequencing model, which entered the market in 2010, there are several other different NGS platforms, such as HiSeq 2000 by Illumina, and SOLiD by Applied Biosystems. The sequencing in these models is performed by incorporating fluorescently labeled oligonucleotides (Siqueira, Fouad et al. 2012). These fluorescent light signals generated by this process are then captured by imaging and displayed as a peak in a pyrogramm (Siqueira, Fouad et al. 2012). The sequencing of the IonTorrent platform is not based on the detection of fluorescent signals, but rather on change in the pH-value. This change is caused by the incorporation of a nucleotide into a DNA strand, which then releases a pyrophosphate and a positively charged hydrogen ion (Martinsried n.d.). This change of the pH value is detected by an ionic sensor and stored by means of semiconductor technology (Bragg, Stone et al. 2013). The selection of membranes, that were used for the RNA sequencing, was based on the measured RNA concentration, the RNA quality, and the expression of the marker genes. In order to process the large amount of data two different sequencing chips were required. The PCA scatterplot (Fig 14.) proved that, even though the samples were compared across two different sequencing chips, this technical variation does not contribute to the differential expression profiles.

The PCA plot of the ECs (Fig. 15) showed that the cells could be separated on the first two principal components forming two clusters according to the different conditions of flow and static. Clusters of the static condition are tighter compared to those of the flow condition. A possible explanation is the higher reproducibility of the static condition due to a smaller number of relevant variables compared to the flow condition. Looking at the PCA plot of the SMCs for the two first principal components, the cells cannot be separated according to the technical factor 'Exposure'. SMC samples appeared to be influenced by the technical component coating. The different coating solutions were documented for each membrane and a retrospective batch correction for the technical variable coating could be performed. However, batch correction did not completely resolve the technical variation associated with the variable 'Coating'. This may therefore impact the capacity to fully infer the true biological variation between contrasts. One major limitation that was noted in the analysis of our RNA sequencing data was the low sample number. A total of 16 membranes was used for analysis, with 4 samples of EC or SMC flow each compared to 4 samples of EC or SMC static. One sample failed two of these outlier tests and was therefore excluded from further analysis. In order to obtain a higher statistical power, it would have been advantageous to perform RNA sequencing for several samples.

5.2.1.5. Detecting alterations in signaling pathways via KEGG PATHWAY Analysis

Increasing amounts of genetic data are being generated using next generation sequencing and other sequencing methods, providing a tremendous source of information. Structuring and mapping this information is crucial for identifying complex cellular processes and signaling pathways. To achieve this, different platforms for data collection have been developed. The database used to downscale the complex flow-based changes in gene expression to a small number of pathways is called KEGG. The KEGG database consists of 18 different interconnected databases (Kanehisa and Sato 2020). These link information from multiple scientific fields, including data on human diseases, biochemical reaction, genes, functional analysis and drugs (Kanehisa, Goto et al. 2012). The pathways were curated manually based on published scientific data, thus illustrating the complex interrelationships of current research (Aoki-Kinoshita and Kanehisa 2007). However, the knowledge consists of humanly produced associations and interpretations, i.e. the accuracy of the created pathways is based on human intelligence (Chowdhury and Sarkar 2015). The drawback of these manually curated pathways is that the information has to be compiled from countless different sources. This requires a tremendous effort and leads to heterogeneity between the different genetic databases, as not every database uses the same sources (Bauer-Mehren, Furlong et al. 2009). KEGG is a database that covers a broad range of pathways, whereas other databases, such as BioModel or SPAD, focus on smaller, more specific pathways (Chowdhury and Sarkar 2015). Since our research question involves a wide range of pathways, it made sense to use a broader database with information on a wide range of cellular processes and signaling pathways for the creation of the pathways instead of using a database specialized in specific signaling pathways.

5.3. Discussion of results

5.3.1.1. Differentially expressed genes after flow exposure in endothelial cells

5.3.1.2. Upregulation of CRYAB in endothelial cells

The most significantly up-regulated gene in the ECs after flow exposure was CRYAB. CRYAB or HSPB5 is a small heat shock protein (sHSP) expressed in a variety of tissues and organs, including ECs (Klemenz, Frohli et al. 1991). By modulating different cellular regulatory processes, HSPB5 contributes to the protective response of cells to stress stimuli by stabilizing the cytoskeleton (especially the microtubules) and protecting cells from protein degradation and ischemia-induced cell death (Dimauro, Antonioni et al. 2018), (Morrison, Hoover et al. 2003),

(Bluhm, Martin et al. 1998). Furthermore, it has been shown that upregulation of aB crystallin results in increased stability and secretion of vascular endothelial growth factor A, thus promoting angiogenesis. Simultaneously aB crystallin protects ECs from apoptosis via inhibition of pro-caspase 3 (Dimberg, Rylova et al. 2008), (Kase, He et al. 2010), (Wang, Abraham et al. 2013).

The relatively increased expression of CRYAB observed in our experiments could be interpreted as a protective, cytoskeleton-stabilizing response of ECs to wall shear stress. This may support our hypothesis that the selected wall shear stress of 10dyne/cm^2 shows a vasoprotective effect on ECs by cytoskeletal rearrangement.

5.3.1.3. Downregulation of LRG1 in endothelial cells

Leucine-rich α-2-glycoprotein 1 (LRG1) showed a significant down-regulation after flow exposure. The gene belongs to the family of leucine-rich repeats (LRR), many of which are involved in cellular processes such as protein-protein interactions, signal transduction, cell adhesion, along with cell survival and apoptosis (Wang, Abraham et al. 2013), (Meng, Song et al. 2016). Recent studies have demonstrated that LRG1 promotes pathogenic neovascularization and angiogenesis through activation of the transforming growth factor (TGF)-β1 signaling pathway in ECs (Wang, Abraham et al. 2013), (Zhang, Zhu et al. 2016). TGF-ß1 itself, is known to be crucial in stimulating endothelial proliferation, tubular formation and vascular outgrowth. Given its broad interfering effects in many cellular domains, it seems reasonable to assume that a comprehensive inhibition of TGF-ß1 in order to influence pathological angiogenesis could be accompanied by a wide spectrum of side effects (Song and Wang 2015). For this reason, LRG1 as a more selective therapeutic target represents a potentially promising approach (Meng, Song et al. 2016).

Since LRG1 is thought to be a contributor to pathological neovascularization, its downregulation after flow strengthens the hypothesis that the applied wall shear stress has a protective effect on ECs. Furthermore, elevated LRG1 levels in ECs are associated with elevated hsCRP and IL-6 expression, as well as increased T-lymphocyte numbers (Wang, Abraham et al. 2013). This analysis, along with the concomitant observation of higher LRG1 levels in the presence of systemic inflammation, cardiovascular disease and peripheral arterial occlusive disease suggest that LRG1 may be involved in the inflammation-induced progression of atherosclerosis (ibid). The precise link between the increased risk of cardiovascular disease such as atherosclerosis and elevated LRG1 levels, is still poorly understood and requires further research in order to identify novel therapeutic targets.

5.3.1.3. Upregulation of KLF4 and KLF2 in endothelial cells

A significant upregulation after flow exposure was also found in KLF 2 and KLF4. Both belong to the Kruppel-like family of transcription factors (KLFs). KLF 2 is much better studied than KLF 4, however, based on the close relationship and recent findings from studies, KLF4 is thought to play a similar role as a key regulator of endothelial integrity and functionality (Bieker 2001). Genome-wide transcriptional profiling for KLF 2 and 4 overexpression showed functional overlap for both transcription factors, with 42.4% of genes controlled by KLF 2 also controlled by KLF 4 (Villarreal, Zhang et al. 2010). The results of our RNA sequencing showed stronger changes in gene expression under the flow condition for KLF4 than for KLF2. In addition, they have an anti-adhesive function by downregulating the expression of the adhesion molecule VCAM1 via a decreased expression of TNF (Ohnesorge, Viemann et al. 2010). This anti-adhesive effect is crucial for the prevention of both the development of thrombosis, along with prevention a hyperinflammatory response, and contributes decisively to a vasoprotective phenotype. Given that both genes are known as flow inducible factors, the upregulation proved that the artery on a chip has the ability to reproduce flow-mediated effects (White, Hayes et al. 2011).

5.3.1.4. Differentially expressed genes in smooth muscle cells

5.3.1.5. Upregulation of LRFN5 in smooth muscle cells

One significantly up-regulated gene in SMCs was the cell adhesion molecule leucine-rich repeat and fibronectin type-III domain-containing protein 5 (LRFN5). There is hardly any data available about its role in SMCs so far. One of the few studies in which LRFN5 has been investigated in the context of SMCs, addresses the cellular response of SMCs to physiological and pathological stiffness of ECM. For this purpose, aortic and cardiac VSMCs were cultured on either ECM with physiological or pathological stiffness, followed by transcriptome analysis. The analysis aimed to detect the long non-coding RNAs and their neighboring genes that were most significantly altered by different ECM stiffness. LRFN5, together with the lncRNA CTD2298J14.2, is one of the top10 most correlating stiffness-sensitive lncRNAs gene pairs and showed a decreased expression caused by stiffness with an FC of 1.37. In our sequencing, LRFN5 showed increased expression under flow condition compared to static condition. This might indicate that flow prevents the ECM and the SMCs from stiffening, but whether there is a causal association between flow condition and altered matrix stiffness cannot be answered based on these data. However, this association, and the question what role LRFN5 plays in vascular stiffening or in sensing VSMC stiffness, poses an exciting question for further research.

5.3.1.6. Downregulation of HHEX in smooth muscle cells

Hematopoietically expressed homeobox (HHEX), also known as proline rich homeodomain (prh), is a highly conserved transcription factor (Ho, Houart et al. 1999), that showed a significant downregulation after flow exposure. As a transcription factor, HHEX modulates the expression of genes that are involved in cell proliferation and cell migration of different cell types (Uchiumi 2018). Previous studies in HHEX knock-out mice showed defective cardiovascular development, suggesting that HHEX is likely to contribute critically to normal cardiovascular development by suppressing VEGFA (Hallaq, Pinter et al. 2004). Topisirovic et al. have studied the effect of HHEX on cells of the hematopoietic system and found that HHEX inhibits cell proliferation and promotes apoptosis (Topisirovic, Culjkovic et al. 2003). Contrasting to the findings in ECs, are the study results of (Li, Liu et al. 2016). In this study, VSMCs were transfected with HHEX and the proliferation rate was subsequently compared with the proliferation rate of cells without HHEX transfection. A higher proliferation rate was observed in the HHEX transfected cells. Based on these results, it was assumed that HHEX promotes the proliferation of VSMCs. Furthermore, it was shown that more cells transitioned from G to S phase after overexpression of HHEX, thus HHEX might have an inhibitory effect on apoptotic processes in VSCMs (Li, Liu et al. 2016). Similar effects of HHEX on SMC proliferation have been described by (Hallaq, Pinter et al. 2004), as HHEX knockout mice exhibited a defect in vasculogenesis caused by reduced or absent VSMC formation. The altered expression in our sequencing data cannot be properly explained by the function of the gene. An opposite effect, i.e., overexpression of HHEX in response to flow exposure, would have been expected on the basis of the function of the gene.

5.3.1.7. KEGG-pathway analysis

The most enriched KEGG pathway was the cytokine-cytokine pathway. Cytokines are an inhomogeneous group of soluble proteins that regulate important cellular processes (Leonard and Lin 2000). These include cell differentiation, cell growth, cellular defense, repair mechanisms, cell death, and angiogenesis. The strong enrichment of the pathway after exposure to flow indicates that the ECs are in an active, stimulus-triggered state. Among those genes upregulated within the pathway is growth differentiation factor (GDF)-5, which stimulates angiogenesis via increased expression of VEGF (Yamashita, Shimizu et al. 1997), (Zeng, Li et al. 2007). The second most enriched KEGG pathway was the TGF beta signaling pathway with the following associated genes: CDKN2B, GDF5, ID2, INHBA and SMAD7. TGF beta itself

is interconnected into a variety of complex signaling pathways, including those regulating cellular growth (Clark and Coker 1998). The expression of the associated gene CDKN2B is promoted by TGF beta, which is why CDKN2B is considered to play a cellular growth inducing role (NCBI n.d.). A contrary effect is seen on the SMAD7 gene, suggesting that SMAD7 acts as a negative feedback loop to prevent excessive growth (Nakao, Afrakhte et al. 1997). The enrichment of this pathway reinforces the previously postulated hypothesis that ECs respond with cellular growth to the stimulus flow and the accompanying wall shear stress. The genes associated with the Hippo signaling pathway, which was also found to be enriched, were largely overlapping with those mentioned above in the context of the TGF beta signaling pathway. Another highly enriched pathway is the chemokine signaling pathway. Chemokines are chemotactic mediators that maintain a directional function in cell migration (Zernecke and Weber 2014). This function is particularly important for an adequate immune response of the organism. Furthermore, they are involved in multiple processes such as homeostasis, cell activation and differentiation. The chemokines that are particularly up-regulated in the pathway control mainly homeostatic processes. These chemokines are the following: CCL16, CCL20, CCL23, CXCL12 and XCL1. CXCL12 exerts a limiting effect on atherosclerosis and increases plaque stability in the presence of atherosclerotic lesion (Zernecke, Bidzhekov et al. 2009). This vascular repair mechanism is achieved through the mobilization and recruitment of progenitor SMCs, which form a stable fibrous cap above the atherosclerotic plaque (Akhtar, Gremse et al. 2013). In addition, CXCL12 has an antiapoptotic effect on ECs and SMCs (Glass and Witztum 2001). Similarly, the chemokine CCL 20 shows an effect on vascular integrity by recruiting atheroprotective B cells (Doran, Lipinski et al. 2012).

The enrichment of the arginine biosynthesis pathway is also an interesting observation consistent with our hypothesis, since arginine is the precursor for the synthesis of the vasodilator nitrogen molecule nitric oxide (NO) (Marletta 1989). NO is secreted in response to altering blood pressures and, through its vasodilatory properties, contributes decisively in maintaining blood pressure at a constant level (Lowenstein, Dinerman et al. 1994). NO is considered to be an indicator for the integrity of the endothelium (Predescu, Predescu et al. 2005). This integrity is compromised in vascular diseases such as atherosclerosis. Accordingly, an intact NO release can be regarded as an indication of a healthy endothelium and thereby again strengthens the hypothesis that the selected wall shear stress of 10dyne/cm^2 exerts a protective effect on the endothelium. All together these pathways suggest that the applied shear stress has protective effects on the ECs.

The analysis of the DEGs showed a small number of significantly altered genes in the SMCs compared to the ECs. Making a KEGG-pathway analysis in SMCs meaningless. A larger sample size may increase the power of the DEGs and thus the KEGG pathways in the future.

5.3.1.8. Concluding remarks and outlook

The aim of our study was to provide an analysis of cell and gene changes in response to mechanical stimulation of the vessel wall performed using a model that better mimics physiological conditions. Combined with the utilized gene sequencing technologies, this allowed us to detect novel genes that are influenced by wall shear stress and thus may be relevant for the pathogenesis of major cardiovascular disease, such as atherosclerosis. Although the protective effect of wall shear stress on the endothelium is well known, the underlying complex molecular mechanisms remain insufficiently understood. In addition to known regulators of endothelial integrity and functionality such as KLF-2 and -4, which also showed significant upregulation in response to wall shear stress in our experimental series, we further identified significantly altered expression of two genes previously unknown in this context. Down-regulation of the gene LRG1, responsible for pathological neovascularization, and upregulation of the gene CRYAB, supporting cell differentiation, could be detected, leading to the assumption that these regulations exhibit a protective influence on the endothelium.

It can be foreseen to utilize the aorta-on-a-chip as a drug testing tool. A potential therapeutical agent can be transported directly to the cells via the circulating cell medium and thus the effect on the ECs can be analyzed. On the other hand, the co-cultivation and cell-cell communication and the diffusion ensured by the semi-permeable membrane offer the additional possibility to investigate the effect of the drug on the underlying SMCs. This enables an analysis of different beneficial effects as well as potential toxic effects. Such an influence on the system of the human body can be tested with the AoC model.

Obviously, the OoC technology holds an immense potential and, besides the application in experimental research, offers a broad applicability in clinical medicine: from diagnostics to direct drug testing and personalized medicine. Nevertheless, despite the rapidly growing use of these microfluidic devices, a general integration into experimental and personalized medicine is not yet achieved. Particularly with regard to the comparability and reproducibility of different experiments, a standardized chip model would be an important step for a more efficient use and a broader application of OoC technology. Whether this technology will soon be routinely used in clinical practice and in the increasingly important field of personalized medicine, depends crucially on how quickly quality assurance can be implemented in the form of standardization.

6. BIBLIOGRAPHY

Ahmed, I., Iqbal, H. M. & Akram, Z. (2018). Microfluidics engineering: recent trends, valorization, and applications. *Arabian Journal for Science and Engineering,* 43(1), 23-32.

Akhtar, S., Gremse, F., Kiessling, F., Weber, C. & Schober, A. (2013). CXCL12 promotes the stabilization of atherosclerotic lesions mediated by smooth muscle progenitor cells in Apoedeficient mice. *Arteriosclerosis, thrombosis, and vascular biology*, 33(4), 679-686.

Antoni, D., Burckel, H., Josset, E. & Noel, G. (2015). Three-dimensional cell culture: a breakthrough in vivo. *International Journal of Molecular Sciences*, 16(3), 5517-5527.

Aoki-Kinoshita, K. F. & Kanehisa, M. (2007). Gene annotation and pathway mapping in KEGG. *Methods In Molecular Biology,* 396, 71-91.

Armbrecht, M. & Eppendorf, A. (2013). Detection of contamination in DNA and protein samples by photometric measurements. *Application Note*, 279, 1-6.

Arnett, D. K., Blumenthal, R. S., Albert, M. A., Buroker, A. B., Goldberger, Z. D., Hahn, E. J., Himmelfarb, C.D., Khera, A., Lloyd-Jones, D., McEvoy, J. W., Michos, E. D., Miedema, M. D., Muñoz, D., Smith Jr, S.C., Virani, S.S., Williams Sr, K.A., Yeboah, J., Ziaeian, B. J (2019). 2019 ACC/AHA Guideline on the Primary Prevention of Cardiovascular Disease: A Report of the American College of Cardiology/American Heart Association Task Force on Clinical Practice Guidelines. *Circulation*, 140(11), 596-646.

atdbio. (n.d.). Next generation sequencing. Retrieved August 06, 2021, from https://www.atdbio.com/content/58/Next-generation-sequencing

Azizipour, N., Avazpour, R., Rosenzweig, D.H., Sawan, M. & Ajji, A. (2020). Evolution of Biochip Technology: A Review from Lab-on-a-Chip to Organ-on-a-Chip. *Micromachines,* 11(6), 599.

Bauer-Mehren, A., Furlong, L. I. & Sanz, F. (2009). Pathway databases and tools for their exploitation: benefits, current limitations and challenges. *Molecular Systems Biology*, 5(290), 1-13.

Baumann, F., Makaloski, V. & Diehm, N. (2013). Aortenaneurysma und -dissektion. *Der Internist*, 54, 535–542.

Bennett, M. R., Sinha, S., & Owens, G. K. (2016). Vascular Smooth Muscle Cells in Atherosclerosis. *Circulation research,* 118(4), 692–702.

Bhatia, S. N. & Ingber, D. E. (2014). Microfluidic organs-on-chips. *Nature biotechnology*, 32(8), 760-772.

Biasetti, J., Hussain, F. & Gasser, T. C. (2011). Blood flow and coherent vortices in the normal and aneurysmatic aortas: a fluid dynamical approach to intra-luminal thrombus formation. *Journal of The Royal Society Interface*, 8(63), 1449-1461.

Bicknell, C., Kiru, G., Falaschetti, E., Powell, J., & Poulter, N. (2016). An evaluation of the effect of an angiotensin-converting enzyme inhibitor on the growth rate of small abdominal aortic aneurysms: a randomised placebo-controlled trial. *European heart journal,* 37(42), 3213-3221.

Bieker, J. J. (2001). Kruppel-like factors: three fingers in many pies. *Journal Of Biological Chemistry*, 276(37), 34355-34358.

Bieker, J. J. (2001). Krüppel-like factors: three fingers in many pies. *Journal of Biological Chemistry*, 276(31), 34355-34358.

Bluhm, W. F., Martin, J. L., Mestril, R. & Dillmann, W. H. (1998). Specific heat shock proteins protect microtubules during simulated ischemia in cardiac myocytes. *American Journal Of Physiology*, 275(6), 2243-2249.

Brady, A. R., Thompson, S. G., Fowkes, F. G., Greenhalgh, R. M., Powell, J. T. & UK Small Aneurysm Trial Participants. (2004). Abdominal aortic aneurysm expansion: risk factors and time intervals for surveillance. *Circulation*, 110(1), 16-21.

Bragg, L. M., Stone, G., Butler, M. K., Hugenholtz, P. & Tyson, G. W. (2013). Shining a light on dark sequencing: characterising errors in Ion Torrent PGM data. *PLOS Computational Biology*, 9(4), 1-18.

Brown, L. C. & Powell, J. T. (1999). Risk factors for aneurysm rupture in patients kept under ultrasound surveillance. UK Small Aneurysm Trial Participants. *Annals Of Surgery*, 230(3), 289-296.

Bustin, S. A., Benes, V., Garson, J. A. G, Hellemans, J., Huggett, J., Kubista, M., Mueller, R., Nolan, T., Pfaffl, M. W., Shipley, G. L., Vandesompele, J. & Wittwer, C. T. (2009). The MIQE guidelines:minimum information for publication of quantitative real-time PCR experiments. *Clinical Chemistry,* 55(4), 611-622.

Cann, O. (2016, June 23). These are the top 10 emerging technologies of 2016. Retrieved from https://www.weforum.org/agenda/2016/06/top-10-emerging-technologies-2016/

Carlsson, R., Engvall, E., Freeman, A. & Ruoslahti, E. (1981). Laminin and fibronectin in cell adhesion: enhanced adhesion of cells from regenerating liver to laminin. *Proceeding of the National Academy Science of the USA,* 78(4), 2403-2406.

Carson, J. A. S., Lichtenstein, A.H., Anderson, C.A.M., Appel, L.J., Kris-Etherton, P.M., Meyer, K.A., Petersen, K., Polonsky, T. & Van Horn, L. (2019). Dietary Cholesterol and Cardiovascular Risk: A Science Advisory From the American Heart Association. *Circulation* 141, 3.

Childs, B. G., Baker, D. J., Wijshake, T., Conover, C. A., Campisi, J. & Deursen, van J. M. (2016). Senescent intimal foam cells are deleterious at all stages of atherosclerosis. *Science*, 354(6311), 472-477.

Cho, M. & Park, J. K. (2020). Fabrication of a Perfusable 3D In Vitro Artery-Mimicking Multichannel System for Artery Disease Models. *ACS Biomaterials Science & Engineering,* 6(9), 5326-5336.

Chowdhury, S. & Sarkar, R. R. (2015). Comparison of human cell signaling pathway databases-evolution, drawbacks and challenges. *The Journal of Biological Databases and Curation,* 2015.

Clark, D. A. & Coker, R. (1998). Transforming growth factor-beta (TGF-beta). *The International Journal Of Biochemistry & Cell Biology*, 30(3), 293-298.

Cornuz, J., Sidoti Pinto, C., Tevaearai, H., & Egger, M. (2004). Risk factors for asymptomatic abdominal aortic aneurysm: systematic review and meta-analysis of population-based screening studies. *European Journal Of Public Health*, 14(4), 343–349.

Davignon, J., Ganz, P. (2004). Role of Endothelial Dysfunction in Atherosclerosis. *Circulation,* 109(23), 27-32.

Davies, P. F. (1995). Flow-mediated endothelial mechanotransduction. *Physiological reviews*, 75(3), 519-560.

Deanfield, J. E., Halcox, J. P. & Rabelink, T. J. (2007). Endothelial function and dysfunction: testing and clinical relevance. *Circulation*, 115(10), 1285-1295.

Debus, E. (2018). *S3-Leitlinie zum Screening, Diagnostik Therapie und Nachsorge des Bauchaortenaneurysmas*. New York: Springer.

Dekker, R. J., van Soest, S., Fontijn, R. D., Salamanca, S., de Groot, P. G., van Bavel, E., Pannekoek, H. & Horrevoets, A. J. (2002). Prolonged fluid shear stress induces a distinct set of endothelial cell genes, most specifically lung Kruppel-like factor (KLF2). *Blood*, 100(5), 1689-1698.

DeLisser, H. M., Newman, P. J. & Albelda, S. M. (1994). Molecular and functional aspects of PECAM-1/CD31. *Immunology Today*, 15(10), 490-495.

Desjardins, P. & Conklin, D. (2010). NanoDrop microvolume quantitation of nucleic acids. *Journal of Visualized Experiments*, (45), 2565.

Diehl, F., Li, M., He, Y., Kinzler, K. W., Vogelstein, B. & Dressman, D. (2006). BEAMing: single-molecule PCR on microparticles in water-in-oil emulsions. *Nature methods*, 3(7), 551559.

Dimauro, I., Antonioni, A., Mercatelli, N. & Caporossi, D. (2018). The role of αB-crystallin in skeletal and cardiac muscle tissues. *Cell Stress and Chaperones*, 23(4), 491-505.

Dimberg, A., Rylova, S., Dieterich, L. C., Olsson, A. K., Schiller, P., Wikner, C., Bohman, S., Botling, J., Lukinius, A., Wawrousek, E. F. & Claesson-Welsh, L. (2008). alphaB-crystallin promotes tumor angiogenesis by increasing vascular survival during tube morphogenesis. *Blood*, 111(4), 2015-2023.

Doran, A. C., Lipinski, M. J., Oldham, S. N., Garmey, J. C., Campbell, K. A., Skaflen, M. D., Cutchins, A., Lee, D. J., Glover, D. K. & Kelly, K. A. (2012). B-cell aortic homing and atheroprotection depend on Id3. *Circulation research*, 110(1), 1-12.

Du, J., Li, M., Yuan, Z., Guo, M., Song, J., Xie, X. & Chen, Y. (2016). A decision analysis model for KEGG pathway analysis. *BMC Bioinformatics*, 17(1), 407.

Duffy, D. C., McDonald, J. C., Schueller, O. J. & Whitesides, G. M. (1998). Rapid Prototyping of Microfluidic Systems in Poly(dimethylsiloxane). *Analytical Chemistry*, 70(23), 4974-4984.

Ekblom, R. and Galindo, J. (2011). Applications of next generation sequencing in molecular ecology of non-model organisms. *Heredity,* 107(1), 1-15.

Endemann, D. H. & Schiffrin, E. L. (2004). Endothelial dysfunction. *Journal of the American Society of Nephrology*, 15(8), 1983-1992.

Erbel, R., Aboyans, V., Boileau, C., Bossone, E., Di Bartolomeo, R., Eggebrecht, H., Evangelista, A., Falk, V., Frank, H., Gaemperli, O., Grabenwoger, M., Haverich, A., Iung, B., John Manolis, A., Meijboom, F., Nienaber, C. A., Roffi, M., Rousseau, H., Sechtem, U., Sirnes, P. A., von Allmen, R. S. & Vrints, C. J. (2015). Corrigendum to: 2014 ESC Guidelines on the diagnosis and treatment of aortic diseases. *European Heart Journal*, 36(41), 2779.

Falk, E. (2006). Pathogenesis of atherosclerosis. *Journal of the American College of Cardiology*, 47(8), 7-13.

Federici, A. B. (2003). The factor VIII/von Willebrand factor complex: basic and clinical issues. *Haematologica*, 88(6), EREP02.

Fezoulidis, N., Assadian, A., Zandieh, S. & Werner, M. (2019). Das abdominelle Aorten-aneurysma. *Wiener klinische Wochenschrift Education,* 14, 19–27.

Gawenda, M. B. (2012). Ruptured Abdominal Aortic Aneurysm. *Deutsches Ärzteblatt International,* 109(43), 727-732.

Giddens, D. P., Zarins, C. K. & Glagov, S. (1993). The role of fluid mechanics in the localization and detection of atherosclerosis. *Journal Of Biomechanical Engineering,* 115, 588-594.

Glass, C. K. & Witztum, J. L. (2001). Atherosclerosis. the road ahead. *Cell*, 104(4), 503-516.

Glass, C. K., Witztum, J.L. (2001). Atherosclerosis. *Cell,* 104(4), 503-516.

Goodwin, S., McPherson, J. D. & McCombie, W. R. (2016). Coming of age: ten years of next-generation sequencing technologies. *Nature Reviews Genetics,* 17(6), 336, https://www.nature.com/articles/nrg.2016.49

Gordon, J. R. & Bernfield, M. R. (1980). The basal lamina of the postnatal mammary epithelium contains glycosaminoglycans in a precise ultrastructural organization. *Developmental Biology,* 74(1), 118-135.

Gordon, P. B., Levitt, M. A., Jenkins, C. S. & Hatcher, V. B. (1984). The effect of the extracellular matrix on the detachment of human endothelial cells. *Journal Of Cellular Physiology,* 121(3), 467-475.

Goumans, M. J., Valdimarsdottir, G., Itoh, S., Rosendahl, A., Sideras, P. & Dijke, P. (2002). Balancing the activation state of the endothelium via two distinct TGF-beta type I receptors. *EMBO Journal*, 21(7), 1743-1753.

Gravesen, P., Branebjerg, J. & Jensen, O. S. (1993). Microfluidics-a review. *Journal of micromechanics and microengineering,* 3(4), 168.

Gunther, A., Yasotharan, S., Vagaon, A., Lochovsky, C., Pinto, S., Yang, J., Lau, C., Voigtlaender-Bolz, J. & Bolz, S. S. (2010). A microfluidic platform for probing small artery structure and function. *Lab on a Chip*, 10(18), 2341-2349.

Hadi, H. A., Carr, C. S. & Al Suwaidi, J. (2005). Endothelial dysfunction: cardiovascular risk factors, therapy, and outcome. *Vascular health and risk management*, 1(3), 183.

Hahn, D. A., Ragland, G. J., Shoemaker, D. D. & Denlinger, D. L. (2009). Gene discovery using massively parallel pyrosequencing to develop ESTs for the flesh fly Sarcophaga crassipalpis. *BMC Genomics,* 10(1), 234.

Hallaq, H., Pinter, E., Enciso, J., McGrath, J., Zeiss, C., Brueckner, M., Madri, J., Jacobs, H. C., Wilson, C. M., Vasavada, H., Jiang, X. & Bogue, C. W. (2004). A null mutation of Hhex results in abnormal cardiac development, defective vasculogenesis and elevated Vegfa levels. *Development*, 131(20), 5197-5209.

He, M., Huang, T. S., Li, S., Hong, H. C., Chen, Z., Martin, M., Zhou, X., Huang, H. Y., Su, S. H., Zhang, J., Wang, W. T., Kang, J., Huang, H. D., Zhang, J., Chien, S. & Shyy, J. Y. (2019). Atheroprotective Flow Upregulates ITPR3 (Inositol 1,4,5-Trisphosphate Receptor 3) in Vascular Endothelium via KLF4 (Kruppel-Like Factor 4)-Mediated Histone Modifications.

Arteriosclerosis Thrombosis, and Vascular Biology, 39(5), 902-914.

Heiss, M., Hellstrom, M., Kalen, M., May, T., Weber, H., Hecker, M., Augustin, H. G. & Korff, T. (2015). Endothelial cell spheroids as a versatile tool to study angiogenesis in vitro. *FASEB Journal*, 29(7), 3076-3084.

Helmlinger, G., Geiger, R. V., Schreck, S. & Nerem, R. M. (1991). Effects of pulsatile flow on cultured vascular endothelial cell morphology. *Journal Of Biomechanical Engineering,* 113(2), 123-131.

Hirama, H., Satoh, T., Sugiura, S., Shin, K., Onuki-Nagasaki, R., Kanamori, T. & Inoue, T. (2019). Glass-based organ-on-a-chip device for restricting small molecular absorption. *Journal Of Bioscience Bioengineering,* 127(5), 641-646.

Ho, C. M., Ng, K, S. H.. Li, H. & Yoon, Y. J. (2015). 3D printed microfluidics for biological applications. *Lab on a Chip*, 15(18), 3627-3637.

Ho, C. Y., Houart, C., Wilson, S. W. & Stainier, D. Y. (1999). A role for the extraembryonic yolk syncytial layer in patterning the zebrafish embryo suggested by properties of the hex gene. *Current Biology*, 9(19), 1131-1134.

Hoeng, J., D. Bovard and M. C. Peitsch (2019). Organ-on-a-chip: Engineered Microenvironments for Safety and Efficacy Testing. *Academic Press* (1st ed.), https://doi.org/10.1016/C2018-0-01892-7.

Hofer, M. & Lutolf, M. P. (2021). Engineering organoids. *Nature Reviews Materials*, 6(5), 402420.

Holdt, L. M. & Teupser, D. (2013). From genotype to phenotype in human atherosclerosis-recent findings. *Current Opinion in Lipidology*, 24(5), 410-418.

Howard, B. E., Hu, Q., Babaoglu, A. C., Chandra, M., Borghi, M., Tan, X., He, L., WinterSederoff, H., Gassmann, W., Veronese, P. & Heber, S. (2013). High-throughput RNA sequencing of pseudomonas-infected Arabidopsis reveals hidden transcriptome complexity and novel splice variants. *Public Library of Science One,* 8(10), e74183.

Huh, D., Torisawa, Y.-s., Hamilton, G. A., Kim, H. J. & Ingber, D. E. (2012). Microengineered physiological biomimicry: organs-on-chips. *Lab on a Chip,* 12(12), 21562164.

Ilan, N. & Madri, J. A. (2003). PECAM-1: old friend, new partners. *Current Opinion in Cell Biology,* 15(5), 515-524.

Insull, W. (2009). The pathology of atherosclerosis: plaque development and plaque responses to medical treatment. *American Journal of Medicine*, 122, 3-14.

Jackson, E. L. & Lu, H. (2016). Three-dimensional models for studying development and disease: moving on from organisms to organs-on-a-chip and organoids. *Integrative Biology,* 8(6), 672-683.

Jensen, C. & Teng, Y. (2020). Is It Time to Start Transitioning From 2D to 3D Cell Culture? *Frontiers in molecular biosciences,* 7, 33.

Juonala, M., Viikari, J. S., Laitinen, T., Marniemi, J., Helenius, H., Rönnemaa, T. & Raitakari, O. T. (2004). Interrelations between brachial endothelial function and carotid intima-media thickness in young adults: the cardiovascular risk in young Finns study. *Circulation,* 110(18), 2918-2923.

Kanagal-Shamanna, R. (2016). *Emulsion PCR: techniques and applications. Clinical Applications of PCR.* New York: Springer.

Kanehisa, M., Goto, S., Sato, Y., Furumichi, M. & Tanabe, M. (2012). KEGG for integration and interpretation of large-scale molecular data sets. *Nucleic Acids Research*, 40, 109-114.

Kanehisa, M. & Sato, Y. (2020). KEGG Mapper for inferring cellular functions from protein sequences. *Protein Science,* 29(1), 28-35.

Kanehisa, M., Sato, Y. & Morishima, K. (2016). BlastKOALA and GhostKOALA: KEGG Tools for Functional Characterization of Genome and Metagenome Sequences. *Journal of Molecular Biology*, 428(4), 726-731.

Karsenty, G. & de Crombrugghe, B. (1991). Conservation of binding sites for regulatory factors in the coordinately expressed alpha 1 (I) and alpha 2 (I) collagen promoters. *Biochemical and Biophysical Research Communications*, 177(1), 538-544.

Kase, S., He, S., Sonoda, S., Kitamura, M., Spee, C., Wawrousek, E., Ryan, S. J., Kannan, R. & Hinton, D. R. (2010). alphaB-crystallin regulation of angiogenesis by modulation of VEGF. *Blood*, 115(16), 3398-3406.

Kasper, D. L., Fauci, A.S., Hauser, S.L., Longo, D.L., Jameson, J.L. & Loscalzo, J. (2015). Harrison's Principles of Internal Medicine. McGraw Hill Education.

Kefalides, N. A. (1978). Biology and chemistry of basement membranes. International Symposium on the Biology and Chemistry of Basement Membranes 1976, Philadelphia: *Academic Press.*

Kent, K. C. (2014). Clinical practice. Abdominal aortic aneurysms. *The New England journal of medicine*, 371, 2101–2108.

Kim, S., Lee, H., Chung, M. & Jeon, N. L. (2013). Engineering of functional, perfusable 3D microvascular networks on a chip. *Lab on a Chip*, 13(8), 1489-1500.

Klak, M., Bryniarski, T., Kowalska, P., Gomolka, M., Tymicki, G., Kosowska, K., Cywoniuk, P., Dobrzanski, T., Turowski, P. & Wszola, M. (2020). Novel Strategies in Artificial Organ Development: What Is the Future of Medicine? *Micromachines,* 11(7), 646.

Klemenz, R., Frohli, E., Steiger, R. H., Schafer, R. & Aoyama, A. (1991). Alpha B-crystallin is a small heat shock protein. *Proceedings of the National Academy of Science of the United States of America,* 88(9), 3652-3656.

Kotera, M., Hirakawa, M., Tokimatsu, T., Goto, S. & Kanehisa, M. (2012). The KEGG databases and tools facilitating omics analysis: latest developments involving human diseases and pharmaceuticals. *Methods in Molecular Biology,* 802, 19-39.

Kuivaniemi, H. & Tromp, G. (2019). Type III collagen (COL3A1): Gene and protein structure, tissue distribution, and associated diseases. *Gene*, 707, 151-171.

Kuo, C. T., Veselits, M. L., Barton, K. P., Lu, M. M., Clendenin, C. & Leiden, J. M. (1997). The LKLF transcription factor is required for normal tunica media formation and blood vessel stabilization during murine embryogenesis. *Genes & Development*, 11(22), 2996-3006.

Lederle, F. A., Johnson, G. R., Wilson, S. E., Ballard, D. J., Jordan, W. D., J, Jr., Blebea, F. Littooy, N., Freischlag, J. A., Bandyk, D., Rapp, J. H., Salam, A. A. & Veterans Affairs Cooperative Study. (2002). Rupture rate of large abdominal aortic aneurysms in patients refusing or unfit for elective repair. *Journal of American Medical Association*, 287(22), 29682972.

Lederle, F. A. W., Johnson, G. R. Reinke, D. B., Littooy, F. N., Acher, C. W., Ballard, D. J., Messina, L. M., Gordon, I. L., Chute, E. P., Krupski, W. C., Busuttil, S. J., Barone, G. W., Sparks, S., Graham, L. M., Rapp, J. H., Makaroun, M. S., Moneta, G. L., Cambria, R. A., Makhoul, R. G. … (2002). Aneurysm Detection and Management Veterans Affairs Cooperative Study Group. Immediate repair compared with surveillance of small abdominal aortic aneurysms. *The New England journal of medicine,* 346(19), 1437–1444.

Ledford, H. (2011). Translational research: 4 ways to fix the clinical trial. *Nature*, 477(7366), 526-528.

Lee, S. H., & Sung, J. H. (2017). Microtechnology-Based Multi-Organ Models. *Bioengineering*, 4(2), 46.

Leonard, W. J. & Lin, J. X. (2000). Cytokine receptor signaling pathways. *Journal of Allergy and Clinical Immunology,* 105(5), 877-888.

Levesque, M., Sprague, E. A., Schwartz, C. & Nerem, R. (1989). The influence of shear stress on cultured vascular endothelial cells: The stress response of an anchorage-dependent mammalian cell. *Biotechnology progress*, 5(1), 1-8.

Li, L., Liu, M., Kang, L., Li, Y., Dai, Z., Wang, B., Liu, S., Chen, L., Tan, Y. & Wu, G.

(2016). HHEX: A Crosstalker between HCMV Infection and Proliferation of VSMCs. *Frontiers in Cellular and Infection Microbiology*, 6, 169.

Libby, P. (2002). Inflammation in atherosclerosis. *Nature*, 420, 868–874.

Libby, P., Buring, J.E., Badimon, L., Hansson, G.K., Deanfield, J., Bittencourt, M.S., Tokgözoğlu, L. & Lewis, E.F. (2019). Atherosclerosis. *Nature review*, 5, 56.

Libby, P., Ridker, P. M. & Hansson, G. K. (2011). Progress and challenges in translating the biology of atherosclerosis. *Nature*, 473(7347), 317-325.

Lin, Z., Kumar, A., SenBanerjee, S., Staniszewski, K., Parmar, K., Vaughan, D. E., Gimbrone, M. A., Balasubramanian, V., García-Cardeña, G., Jain, M. K. (2005). Kruppel-like factor 2 (KLF2) regulates endothelial thrombotic function. *Circulation research*, 96(5), 48–57.

Liu, L., Li, Y., Li, S., Hu, N., He, Y., Pong, R., Lin, D., Lu, L. & Law, M. (2012). Comparison of next-generation sequencing systems. *Journal of Biomedicine and Biotechnology,* 2012.

Lowenstein, C. J., Dinerman, J. L. & Snyder, S. H. (1994). Nitric oxide: a physiologic messenger. *Annals of internal medicine*, 120(3), 227-237.

Lozano, R., Naghavi, M., Foreman, K., Lim, S., Shibuya, K., Aboyans, V., Abraham, J., Adair, A., Aggarwal, R., Ahn, S. Y., Alvarado, M., Anderson, H. R., Anderson, L. M., Andrews, K. G., Atkinson, C., Baddour, L. M., Barker-Collo, S., Bartels, D. H., Bell, M. L., Benjamin, E. J. … (2012). Global and regional mortality from 235 causes of death for 20 age groups in 1990 and 2010: a systematic analysis for the Global Burden of Disease Study 2010. *Lancet*, 380(9859), 2095-2128.

Lusis, A. J. (2000). Atherosclerosis. *Nature*, 507(6801), 233-241.

Luxembourg, B., Krause, M. & Lindhoff-Last, E. (2007). Basiswissen Gerinnungslabor. *Deutsches Ärzteblatt,* 104(21), 1489-1498.

Maciag, T., Hoover, G. A., Stemerman, M. B. & Weinstein, R. (1981). Serial propagation of human endothelial cells in vitro. *Journal of Cell Biology,* 91, 420-426.

Mak, I. W., Evaniew, N., Ghert, M. (2014). Lost in translation: animal models and clinical trials in cancer treatment. *American journal of translational research,* 6(2), 114-118.

Mammoto, T., Mammoto, A. & Ingber, D. E. (2013). Mechanobiology and developmental control. *Annual review of cell and developmental biology,* 29, 27-61.

Mannucci, P. M. (1998). Von Willebrand factor: a marker of endothelial damage? *Arteriosclerosis, thrombosis, and vascular biology*, 18(9), 1359–1362.

Manson, J. E., Greenland, P., LaCroix, A. Z., Stefanick, M. L., Mouton, C. P., Oberman, A., Perri, M. G., Sheps, D. S., Pettinger, M. B. & Siscovick, D. S. (2002). Walking compared with vigorous exercise for the prevention of cardiovascular events in women. *New England Journal of Medicine*, 347(10), 716-725.

Mantione, K. J., Kream, R. M., Kuzelova, H., Ptacek, R., Raboch, J., Samuel, J. M. & Stefano, G. B. (2014). Comparing bioinformatic gene expression profiling methods: microarray and RNA-Seq. *Medical Science Monitor Basic Research*, 20, 138-142.

Marine, R. L., Magana, L. C., Castro, C. J., Zhao, K., Montmayeur, A. M., Schmidt, A., DiezValcarce, M., Ng, T. F. F., Vinje, J., Burns, C. C., Nix, W. A., Rota, P. A. & Oberste, M. S. (2020). Comparison of Illumina MiSeq and the Ion Torrent PGM and S5 platforms for wholegenome sequencing of picornaviruses and caliciviruses. *Journal of Virological Methods,* 280, 113865.

Marletta, M. A. (1989). Nitric oxide: biosynthesis and biological significance. *Trends in biochemical sciences,* 14(12), 488-492.

Martinsried, M. (n.d.). Next Generation Sequencing (NGS). Retrieved August 07, 2021, from https://www.medizinische-genetik.de/diagnostik/allgemeine-informationen/methoden/nextgeneration-sequencing

Mastrangeli, M., Millet, S., Orchid Partners, T. & Van den Eijnden-van Raaij, J. (2019). Organ-on-chip in development: Towards a roadmap for organs-on-chip. *Alternatives to Animal Experimentation,* 36(4), 650-668.

Medina-Leyte, D. J., Domínguez-Pérez, M., Mercado, I., Villarreal-Molina, M. T. & JacoboAlbavera, L. (2020). Use of human umbilical vein endothelial cells (HUVEC) as a model to study cardiovascular disease: A review. *Applied Sciences,* 10(3), 938.

Meng, H., Song, Y., Zhu, J., Liu, Q., Lu, P., Ye, N., Zhang, Z., Pang, Y., Qi, J. & Wu, H. (2016). LRG1 promotes angiogenesis through upregulating the TGFbeta1 pathway in ischemic rat brain. *Molecular Medicine Reports*, 14(6), 5535-5543.

Merriman, B., Team, I. T. D & Rothberg, J. M. (2012). Progress in ion torrent semiconductor chip based sequencing. *Electrophoresis*, 33(23), 3397-3417.

Meyer, D., Pietu, G., Fressinaud, E. & Girma, J. P. (1991). von Willebrand factor: structure and function. *Mayo Clinic Proceedings*, 66(5), 516-523.

Micronit GmbH. (n.d.). Organ-on-a-chip. Retrieved August 09, 2021, from https://store.micronit.com/media/productattach/f/c/fc_pro_ooc_manual_v0.2.pdf

Miller, E. J. & Gay, S. (1987). The collagens: an overview and update. *Methods in Enzymology,* 144, 3-41.

Mills, E. J., Rachlis, B., Wu, P., Devereaux, P. J., Arora, P. & Perri, D. (2008). Primary prevention of cardiovascular mortality and events with statin treatments: a network metaanalysis involving more than 65,000 patients. *Journal of the American College of Cardiology,* 52(22), 1769-1781.

Moll, F. L. P., Fraedrich, G., Verzini, F., Haulon, S., Waltham, M., van Herwaarden, J.A., Holt, P.J.E., van Keulen, J.W., Rantner, B., Schlösser, F. J.V., Setacci, F., Ricco, J.-B. (2011). Management of abdominal aortic aneurysms clinical practice guidelines of the European society for vascular surgery. *European Journal of Vascular and Endovascular Surgery*, 41, 158.

Morrison, L. E., Hoover, H. E., Thuerauf, D. J. & Glembotski, C. C. (2003). Mimicking phosphorylation of alphaB-crystallin on serine-59 is necessary and sufficient to provide maximal protection of cardiac myocytes from apoptosis. *Circulation Research,* 92(2), 203211.

Nakano, T., Tominaga, R., Nagano, I., Okabe, H. & Yasui, H. (2000). Pulsatile flow enhances endothelium-derived nitric oxide release in the peripheral vasculature. *American Journal of Physiology- Heart and Circulatory Physiology*, 278(4), 1098-1104.

Nakao, A., Afrakhte, M., Morn, A., Nakayama, T., Christian, J. L., Heuchel, R., Itoh, S., Kawabata, M., Heldin, N.-E., Heldin, C.-H. & Dijke, P. t. (1997). Identification of Smad7, a TGFβ-inducible antagonist of TGF-β signalling. *Nature*, 389(6651), 631-635.

National Institue of Health. (n.d.). Abdominal aortic aneurysm. Retrieved August 08, 2021, from https://medlineplus.gov/ency/article/000162.htm

NCBI. (n.d.). CDKN2B. Retrieved August 02, 2021, from https://www.ncbi.nlm.nih.gov/gene?cmd=search&term=txid9606%5Borgn%5D+AND+CDKN2B%5Bsym%5D

NCBI. (n.d.). SMTN smoothelin. Retrieved August 10, 2021, from https://www.ncbi.nlm.nih.gov/gene?Db=gene&Cmd=DetailsSearch&Term=6525

Newman, P. J. (1997). The biology of PECAM-1. *Journal of Clinical Investigation,* 100, 2529.

Ohnesorge, N., Viemann, D., Schmidt, N., Czymai, T., Spiering, D., Schmolke, M., Ludwig, S., Roth, J., Goebeler, M. & Schmidt, M. (2010). Erk5 activation elicits a vasoprotective endothelial phenotype via induction of Kruppel-like factor 4 (KLF4). *Journal of Biological Chemistry*, 285(34), 26199-26210.

Oshinski, J. N., Curtin, J. L. & Loth, F. (2006). Mean-average wall shear stress measurements in the common carotid artery. *Journal of Cardiovascular Magnetic Resonance,* 8(5), 717-722.

Oshinski, J. N., Ku, D. N., Mukundan, S., Loth, Jr., F. & Pettigrew, R. I. (1995). Determination of wall shear stress in the aorta with the use of MR phase velocity mapping. *Journal of Magnetic Resonance Imaging,* 5(6), 640-647.

Ota, T., Fujii, M., Sugizaki, T., Ishii, M., Miyazawa, K., Aburatani, H. & Miyazono, K. (2002). Targets of transcriptional regulation by two distinct type I receptors for transforming growth factor-beta in human umbilical vein endothelial cells. *J Cell Physiol,* 193(3), 299-318.

Paloschi, V., Sabater-Lleal, M., Middelkamp, H., Vivas, A., Johansson, S., van der Meer, A., Tenje, M. & Maegdefessel, L. (2021). Organ-on-a-chip technology: a novel approach to investigate cardiovascular diseases. *Cardiovascular Research,* 117(14), 2742-2754.

Palotie, A., Tryggvason, K., Peltonen, L. & Seppa, H. (1983). Components of subendothelial aorta basement membrane. Immunohistochemical localization and role in cell attachment. *Laboratory Investigation*, 49(3), 362-370.

Pammolli, F., Magazzini, L., Riccaboni, M. (2011). The productivity crisis in pharmaceutical R&D. *Nature reviews. Drug discovery*, 10(6), 428–438.

Pan, X., Chen, Z., Huang, R., Yao, Y., & Ma, G. (2013). Transforming growth factor β1 induces the expression of collagen type I by DNA methylation in cardiac fibroblasts. *Public Library of Science One,* 8(4), e60335.

Papaioannou, T. G. & Stefanadis, C. (2005). Vascular wall shear stress: basic principles and methods. *Hellenic Journal of Cardiology*, 46(1), 9-15.

Perestrelo, A. R., Águas, A. C., Rainer, A. & Forte, G. (2015). Microfluidic Organ/Body-ona-Chip Devices at the Convergence of Biology and Microengineering. *Sensors,* 15(12), 31142-31170.

Peskin, C. S. (1977). Numerical analysis of blood flow in the heart. *Journal of computational physics*, 25(3), 220-252.

Piper, W. (2013*). Krankheiten des Herz-Kreislauf-Systems*. *Innere Medizin,* Berlin Heidelberg: Springer.

Ponticos, M., Partridge, T., Black, C. M., Abraham, D. J. & Bou-Gharios, G. (2004). Regulation of collagen type I in vascular smooth muscle cells by competition between Nkx2.5 and deltaEF1/ZEB1. *Molecular and Cellular Biology*, 24(14), 6151-6161.

Predescu, D., Predescu, S., Shimizu, J., Miyawaki-Shimizu, K. & Malik, A. B. (2005). Constitutive eNOS-derived nitric oxide is a determinant of endothelial junctional integrity. *American Journal of Physiology-Lung Cellular and Molecular Physiology,* 289(3), 371-381.

Quail, M. A., Smith, M., Coupland, P., Otto, T. D., Harris, S. R., Connor, T. R., Bertoni, A., Swerdlow, H. P. & Gu, Y. (2012). A tale of three next generation sequencing platforms: comparison of Ion Torrent, Pacific Biosciences and Illumina MiSeq sequencers. *BMC Genomics,* 13, 341.

Rafieian-Kopaei, M., Setorki, M., Doudi, M., Baradaran, A., & Nasri, H. (2014). Atherosclerosis: process, indicators, risk factors and new hopes. *International journal of preventive medicine,* 5(8), 927-946.

Ramadan, Q., Gourikutty, S. B. N. & Zhang, Q. X. (2020). OOCHIP: Compartmentalized Microfluidic Perfusion System with Porous Barriers for Enhanced Cell-Cell Crosstalk in Organ-on-a-Chip. *Micromachines, 11*(6), 565.

Ramadan, Q. & Zourob, M. (2020). Organ-on-a-chip engineering: Toward bridging the gap between lab and industry. *Biomicrofluidics*, 14(4), 041501.

Ramalanjaona, G., Kempczinski, R. F., Rosenman, J. E., Douville, E. C. & Silberstein, E. B. (1986). The effect of fibronectin coating on endothelial cell kinetics in polytetrafluoroethylene grafts. *Journal of Vascular Surgery*, 3(2), 264-272.

Ravi, M., Paramesh, V., Kaviya, S., Anuradha, E. & Solomon, F. P. (2015). 3D cell culture systems: advantages and applications. *Journal of cellular physiology,* 230(1), 16-26.

Ross, R. (1993). The pathogenesis of atherosclerosis: a perspective for the 1990s. *Nature,* 362(6423), 801-809.

Ross, R. (1999). Atherosclerosis—an inflammatory disease. *New England journal of medicine*, 340(2), 115-126.

Rothberg, J. M., Hinz, W., Rearick, T. M., Schultz, J., Mileski, W., Davey, M., Leamon, J. H., Johnson, K., Milgrew, M. J., Edwards, M., Hoon, J., Simons, J. F., Marran, D., Myers, J. W., Davidson, J. F., Branting, A., Nobile, J. R., Puc, B. P., Light, D., Clark, T. A., Huber, M. … (2011). An integrated semiconductor device enabling non-optical genome sequencing. *Nature*, 475(7356), 348-352.

Rughani, G., Robertson, L. & Clarke, M. (2012). Medical treatment for small abdominal aortic aneurysms. *The Cochrane database of systematic reviews,* (9), CD009536.

Sakakura, K., Nakano, M., Otsuka, F., Ladich, E., Kolodgie, F. D. & Virmani, R. (2013). Pathophysiology of atherosclerosis plaque progression. *Heart Lung Circulation*, 22(6), 399411.

Sakalihasan, N., Limet, R. & Defawe, O. D. (2005). Abdominal aortic aneurysm. *Lancet,* 365(9470), 1577-1589.

Sato, K. & Sato, K. (2018). Recent Progress in the Development of Microfluidic Vascular Models. *Analytic Science, 34*(7), 755-764.

Scannell, J. W., Blanckley, A., Boldon, H. & Warrington, B. (2012). Diagnosing the decline in pharmaceutical R&D efficiency. *Nature reviews. Drug discovery*, 11(2), 191-200.

Schefe, J. H., Lehmann, K. E., Buschmann, I. R., Unger, T. & Funke-Kaiser, H. (2006). Quantitative real-time RT-PCR data analysis: current concepts and the novel gene expression's C T difference formula. *Journal of molecular medicine,* 84(11), 901-910.

Schmitz-Rixen, T., Debus, S. E. & Grundmann, R. T. (2017). Epidemiologie und ScreeningStrategien des abdominellen Aortenaneurysmas. Gefässchirurgie, 22(1), 31-40.

Schroeder, A., Mueller, O., Stocker, S., Salowsky, R., Leiber, M., Gassmann, M., Lightfoot, S., Menzel, W., Granzow, M. & Ragg, T. (2006). The RIN: an RNA integrity number for assigning integrity values to RNA measurements. *BMC Molecular Biology,* 7(3), 1-14.

Singh, R. B., Mengi, S.A., Xu, Y.J., Ameja, A.S. & Dhalla, N.S. (2003). Pathogenesis of atherosclerosis: A multifactorial process. *Experimental and clinical cardiology*, 7, 40-53.

Siqueira, J. F., Fouad, A. F. & Rocas, I. N. (2012). Pyrosequencing as a tool for better understanding of human microbiomes. *Journal of Oral Microbiology*, 4, 10743.

Song, K., Li, G., Zu, X., Du, Z., Liu, L. & Hu, Z. (2020). The Fabrication and Application Mechanism of Microfluidic Systems for High Throughput Biomedical Screening: A Review. *Micromachines,* 11(3), 297.

Song, P., Fang, Z., Wang, H., Cai, Y., Rahimi, K., Zhu, Y., Fowkes, F. G. R., Fowkes, F. J. I. & Rudan, I. (2020). Global and regional prevalence, burden, and risk factors for carotid atherosclerosis: a systematic review, meta-analysis, and modelling study. *Lancet Glob Health,* 8(5), 721-729.

Song, W. & Wang, X. (2015). The role of TGFbeta1 and LRG1 in cardiac remodelling and heart failure. *Biophysical Reviews,* 7(1), 91-104.

Stahlberg, A., Aman, P., Ridell, B., Mostad, P. & Kubista, M. (2003). Quantitative real-time PCR method for detection of B-lymphocyte monoclonality by comparison of kappa and lambda immunoglobulin light chain expression. *Clinical Chemistry*, 49(1), 51-59.

Stern-Straeter, J., Bonaterra, G. A., Hormann, K., Kinscherf, R. & Goessler, U. R. (2009). Identification of valid reference genes during the differentiation of human myoblasts. *BMC Molecular Biology*, 10(66).

Sugiura, S., Hattori, K. and Kanamori, T. (2010). Microfluidic serial dilution cell-based assay for analyzing drug dose response over a wide concentration range. *Analtical Chemistry,* 82(19), 8278-8282.

Sweeting, M. J., Thompson, S.G., Brown, L.C. & Powell, J.T. (2012). Meta-analysis of individual patient data to examine factors affecting growth and rupture of small abdominal aortic aneurysms. *British journal of surgery,* 56(5).

Tabas, I. & Bornfeldt, K. E. (2016). Macrophage Phenotype and Function in Different Stages of Atherosclerosis. *Circulation Research,* 118(4), 653-667.

Tago, K., Ohta, S., Kashiwada, M., Funakoshi-Tago, M., Matsugi, J., Tominaga, S.-i. & Yanagisawa, K. (2017). ST2 gene products critically contribute to cellular transformation caused by an oncogenic Ras mutant. *Heliyon,* 3(10), e00436.

Takebe, T. and Wells, J. M. (2019). Organoids by design. *Science,* 364(6444), 956-959.

Tedgui, A. & Mallat, Z. (2006). Cytokines in Atherosclerosis: Pathogenic and Regulatory Pathways. *Physiological Reviews*, 86(2), 515-581.

Tharp, D. L., Wamhoff, B. R., Turk, J. R. & Bowles, D. K. (2006). Upregulation of intermediate-conductance Ca2+-activated K+ channel (IKCa1) mediates phenotypic modulation of coronary smooth muscle. *American Journal of Physiology- Heart and Circulatory Physiology,* 291(5), 2493-2503.

Thermo Fisher. (n.d.). Transcriptome Sequencing by Ion Torrent Next-Generation Sequencing. Retrieved August 06, 2021, from https://www.thermofisher.com/de/de/home/life-science/sequencing/rna-sequencing/transcriptome-sequencing/transcriptome-sequencing-ion-torrent-next-generationsequencing.html

Topisirovic, I., Culjkovic, B., Cohen, N., Perez, J. M., Skrabanek, L. & Borden, K. L. (2003). The proline-rich homeodomain protein, PRH, is a tissue-specific inhibitor of eIF4E-dependent cyclin D1 mRNA transport and growth. *EMBO Journal*, 22(3), 689-703.

Tovar-Lopez, F. J., Rosengarten, G., Westein, E., Khoshmanesh, K., Jackson S. P., Mitchell, A. & Nesbitt, W. S. (2010). A microfluidics device to monitor platelet aggregation dynamics in response to strain rate micro-gradients in flowing blood. *Lab on a Chip,* 10(3), 291-302.

Uchiumi, F. (2018). *Gene Expression and Regulation in Mammalian Cells: Transcription Toward the Establishment of Novel Therapeutics*. London: IntechOpen.

Van Dijk, E. L., Auger, H., Jaszczyszyn, Y. & Thermes, C. (2014). Ten years of nextgeneration sequencing technology. *Trends in genetics,* 30(9), 418-426.

van Eys, G. J., Niessen, P. M. & Rensen, S. S. (2007). Smoothelin in vascular smooth muscle cells. *Trends Cardiovascular Medicine,* 17(1), 26-30.

Vardulaki, K. A., Walker, N. M., Day, N. E., Duffy, S. W., Ashton, H. A., & Scott, R. A. (2000). Quantifying the risks of hypertension, age, sex and smoking in patients with abdominal aortic aneurysm. *British journal of surgery,* 87, 195-200.

Vaziri, N. D. (2008). Mechanisms of lead-induced hypertension and cardiovascular disease. *American Journal of Physiology- Heart and Circulatory Physiology,* 295(2), 454-465.

Verhamme, P., Quarck, R., Hao, H., Knaapen, M., Dymarkowski, S., Bernar, H., Van Cleemput, J., Janssens, S., Vermylen, J., Gabbiani, G., Kockx, M. & Holvoet, P. (2002).

Dietary cholesterol withdrawal reduces vascular inflammation and induces coronary plaque stabilization inminiature pigs. *Cardiovascular Research,* 56(1), 135-144.

Villarreal, G., Zhang, Y., Larman, H. B., Gracia-Sancho, J., Koo, A. & Garcia-Cardena, G. (2010). Defining the regulation of KLF4 expression and its downstream transcriptional targets in vascular endothelial cells. *Biochemical and Biophysical Research Communications,* 391(1), 984-989.

Vining, K. H. & Mooney, D. J. (2017). Mechanical forces direct stem cell behaviour in development and regeneration. *Nature Reviews Molecular Cell Biology*, 18(12), 728-742.

Wagenseil, J. E. & Mecham, R. P. (2009). Vascular extracellular matrix and arterial mechanics. *Physiological Reviews*, 89(3), 957-989.

Wang, J. H. & Li, B. (2010). Mechanics rules cell biology. *BMC Sports Science, Medicine and Rehabilitation*, 2(1), 1-7.

Wang, X., Abraham, S., McKenzie, J. A. G., Jeffs, N., Swire, M., Tripathi, V. B., Luhmann, U. F. O., Lange, C. A. K., Zhai, Z., Arthur, H. M., Bainbridge, J., Moss, S. E. & Greenwood, J. (2013). LRG1 promotes angiogenesis by modulating endothelial TGF-beta signalling. *Nature,* 499(7458), 306-311.

Wanhainen, A., Verzini, F., Van Herzeele, I., Allaire, E., Bown, M., Cohnert, T., Dick, F., van Herwaarden, J., Karkos, C., Koelemay, M., Kolbel, T., Loftus, I., Mani, K., Melissano, G., Powell, J., Szeberin, Z., Esvs Guidelines, C., de Borst, G. J., Chakfe, N., Debus, S., Hinchliffe, R. … (2019). Editor's Choice - European Society for Vascular Surgery (ESVS) 2019 Clinical Practice Guidelines on the Management of Abdominal Aorto-iliac Artery Aneurysms. *European Journal of Vascular & Endovascular Surgery*, 57(1), 8-93.

Westein, E., van der Meer, A. D., Kuijpers, M. J., Frimat, J. P., van den Berg, A. & Heemskerk, J. W. (2013). Atherosclerotic geometries exacerbate pathological thrombus formation poststenosis in a von Willebrand factor-dependent manner. *Proceedings of the National Academy of Science of the United States of America*, 110(4), 1357-1362.

White, S. J., Hayes, E. M., Lehoux, S., Jeremy, J. Y., Horrevoets, A. J. & Newby, A. C. (2011). Characterization of the differential response of endothelial cells exposed to normal and elevated laminar shear stress. *Journal of Cellular Physiology*, 226(11), 2841-2848.

WHO. (2021, June 11). Cardiovascular diseases (CVDs) Fact Sheet. Retrieved from https://www.who.int/news-room/fact-sheets/detail/cardiovascular-diseases-(cvds)

WHO. (2018). Cardiovascular disease: Global Hearts Initiative. Retrieved from https://www.cdc.gov/globalhealth/healthprotection/resources/infographics/world-heartday.html

WHO. (2020). About cardiovascular diseases. Retrieved from https://www.who.int/cardiovascular_diseases/about_cvd/en/

Woodfin, A., Voisin, M. B. & Nourshargh, S. (2007). PECAM-1: a multi-functional molecule in inflammation and vascular biology. *Arteriosclerosis, Thrombosis, and Vascular Biology,* 27(12), 2514-2523.

Wu, Q., Liu, J., Wang, X., Feng, L., Wu, J., Zhu, X., Wen, W. & Gong, X. (2020). Organ-on-a-chip: recent breakthroughs and future prospects. *Biomed Eng Online,* 19(1), 9.

Xu, M. Y., Aragon, A. D., Mascarenas, M. R., Torrez-Martinez, N. & Edwards, J. S. (2010). Dual primer emulsion PCR for next-generation DNA sequencing. *Biotechniques*, 48(5), 409412.

Yamashita, H., Shimizu, A., Kato, M., Nishitoh, H., Ichijo, H., Hanyu, A., Morita, I., Kimura, M., Makishima, F. & Miyazono, K. (1997). Growth/differentiation factor-5 induces angiogenesisin vivo. *Experimental cell research,* 235(1), 218-226.

Yin, X., Mead, B. E., Safaee, H., Langer, R., Karp, J. M. & Levy, O. (2016). Engineering Stem Cell Organoids. *Cell Stem Cell,* 18(1), 25-38.

Young, E. W. (2013). Advances in microfluidic cell culture systems for studying angiogenesis. *Journal of Laboratory Automation,* 18(6), 427-436.

Zanetta, L., Marcus, S. G., Vasile, J., Dobryansky, M., Cohen, H., Eng, K., Shamamian, P. & Mignatti, P. (2000). Expression of Von Willebrand factor, an endothelial cell marker, is upregulated by angiogenesis factors: a potential method for objective assessment of tumor angiogenesis. *International Journal of Cancer*, 85(2), 281-288.

Zeng, Q., Li, X., Beck, G., Balian, G. & Shen, F. H. (2007). Growth and differentiation factor-5 (GDF-5) stimulates osteogenic differentiation and increases vascular endothelial growth factor (VEGF) levels in fat-derived stromal cells in vitro. *Bone*, 40(2), 374-381.

Zernecke, A., Bidzhekov, K., Noels, H., Shagdarsuren, E., Gan, L., Denecke, B., Hristov, M., Köppel, T., Jahantigh, M. N. & Lutgens, E. (2009). Delivery of microRNA-126 by apoptotic bodies induces CXCL12-dependent vascular protection. *Science signaling*, 2(100), 81.

Zernecke, A. & Weber, C. (2014). Chemokines in atherosclerosis: proceedings resumed. *Arteriosclerosis, Thrombosis and Vascular Biology*, 34(4), 742-750.

Zhang, J., Zhu, L., Fang, J., Ge, Z. & Li, X. (2016). LRG1 modulates epithelial-mesenchymal transition and angiogenesis in colorectal cancer via HIF-1alpha activation. *Journal of Experimental & Clinical Cancer Research*, 35, 29.

Zhao, S., Fung-Leung, W. P., Bittner, A., Ngo, K. & Liu, X. (2014). Comparison of RNA-Seq and microarray in transcriptome profiling of activated T cells. *Public Library of Science One*, 9(1), e78644.

Zheng, Y., Chen, J., Craven, M., Choi, N. W., Totorica, S., Diaz-Santana, A., Kermani, P., Hempstead, B., Fischbach-Teschl, C., Lopez, J. A. & Stroock, A. D. (2012). In vitro

microvessels for the study of angiogenesis and thrombosis. *Proceedings of the National Academy of Science of the United States of America*, 109(24), 9342-9347.

Zhou, J., Li, Y. S., & Chien, S. (2014). Shear stress-initiated signaling and ist regulation of endothelial function. *Arteriosclerosis, thrombosis, and vascular biology,*34(10), 2191-2198.

Zhulidov, P. A., Bogdanova, E. A., Shcheglov, A. S., Vagner, L. L., Khaspekov, G. L., Kozhemyako, V. B., Matz, M. V., Meleshkevitch, E., Moroz, L. L., Lukyanov, S. A. & Shagin, D. A. (2004). Simple cDNA normalization using kamchatka crab duplex-specific nuclease. *Nucleic Acids Research,* 32(3), 37.

Zylka-Menhorn, V. (2018). Bauchaortenaneurysma: Lieber aktiv als „passiv“ screenen. *Deutsches Ärzteblatt*, 115, 19.

7. ACKNOWLEDGEMENTS

At this point, I would like to thank everyone who made my studies and the completion of my PhD possible:

First of all, my special thanks goes to my thesis supervisor, Prof. Dr. med. Lars Mägdefessel, Head of the Experimental Vascular Surgery and Medicine at the University of Munich, who gave me the opportunity to pursue this work under his guidance. The always friendly help and support, as well as the constructive exchange and the regular discussions on a professional and personal level, were of great help and enrichment to me.

I would like to thank Dr. Valentina Paloschi for the excellent supervision and the constant willingness to discuss and help. I am grateful for learning from your wide knowledge in science and life. Thank you for your friendship and for all the inspiration you have been to me. I would also like to express my sincere thanks for the painstaking work of proofreading. I couldn't have asked for better supervision.

I would also like to especially thank Nadiya Glukha, for your patience in introducing me to the methods, as well as for your unstinting support in conducting the experiments. Your positive energy and activism was a great asset for everyone and made it consistently enjoyable and fun to work together.

Special thanks also to the entire working group for welcoming me with open arms and immediatley made me feel part of the group. I appreciated the friendly working atmosphere, many valuable suggestions and constant helpfulness, which contributed substantially to the success of this work.

I would like to express my special thanks to my parents, siblings as well as my boyfriend for their unrestricted, loving and versatile support during the writing of this thesis and throughout all of my studies.

For the financial support I would like to thank the IRTG (SFB1123).